Analysis of Power Transistor Behavioural Modeling Techniques Suitable for Narrow-band Power Amplifier Design

by

Amir-Reza Amini

A thesis
presented to the University of Waterloo
in fulfillment of the
thesis requirement for the degree of
Master of Applied Science
in
Electrical and Computer Engineering

Waterloo, Ontario, Canada, 2012

Author's Declaration

I hereby declare that I am the sole author of this thesis. This is a true copy of the thesis, including any required final revisions, as accepted by my examiners.

I understand that my thesis may be made electronically available to the public.

Amir-Reza Amini

Abstract

The design of power amplifiers within a circuit simulator requires a good non-linear model that accurately predicts the electormagnetic behaviour of the power transistor. In recent years, a certain class of large signal frequency-dependent black-box behavioural modeling techniques known as Poly-Harmonic Distortion (PHD) models has been devised to mimic the non-linear unmatched RF transistor. These models promise a good prediction of the device behaviour under multi-harmonic periodic continuous wave inputs. This thesis describes the capabilities of the PHD modeling framework and the theoretical type of behaviour that it is capable of predicting. Specifically, the PHD framework cannot necessarily predict the response of a broadband aperiodic signal. This analysis will be performed by deriving the PHD modeling framework as a simplification of the Volterra series kernel functions under the assumption that the power transistor is operating under continuous periodic multi-harmonic voltage and current signals in a stable circuit. A PHD model will be seen as a set of describing functions that predict the response of the DUT for any given non-linear periodic continuous-wave inputs that have a specific fundamental frequency.

Two popular implementations of PHD models that can be found in the literature are the X-parameter and Cardiff models. Each model formulates the describing functions of the general PHD model differently. The mathematical formulation of the X-parameter and Cardiff models will be discussed in order to provide a theoretical ground for comparing their robustness. The X-parameter model will be seen as the first-order Taylor series approximation of the PHD model describing functions around a Large Signal Operating Point (LSOP) of the device under test. The Cardiff large-signal model uses Fourier series coefficient functions that vary with the magnitude of the large signal(s) as the PHD model describing functions.

This thesis will provide a breakdown of the measurement procedure required for the extraction of these models, the challenges involved in the measurement, as well as the mathematical extraction of the model coefficients from measurement data.

As each of these models contain have extended versions that enhance the predictive capability of the model under stronger nonlinear modes of operation, a comparison is used to represent the cost of increasing model accuracy as a function of the increasing model complexity for each model. The order of complexity of each model can manifest itself in terms of the mathematical formulation, the number of parameters required and the measurement time that is required to extract each model for a given DUT. This comparison will fairly assess the relative strengths and weaknesses of each model.

Acknowledgements

I would like to take this opportunity to express my sincere gratitude to my supervisor, Professor Slim Boumaiza, for his valuable guidance, encouragement and support throughout my graduate studies. Also, I am grateful to Professor Shreyas Sundaram and Professor Christopher Nielsen for reading my thesis and providing me with valuable comments.

I would like to also thank all my friends who have provided me with joy and warmth through these years. Last but not least, I would like to thank my parents and my family for their continued love, support and understanding.

Contents

List of Figures

List of Tables

Chapter 1

Introduction

1.1 Motivation

Wireless communication has been becoming a major part of the lifestyle of most people around the world. In 2001, it was estimated that there were around 5.6 billion mobile phones in use globally [2]. In addition, wireless communication protocols like Wi-Fi and Bluetooth are becoming quite common in many consumer appliances.

There are always two parties involved in any communication: the sender and the receiver of the message. To enable the sender to communicate over-the-air, there needs to be a wireless transmitter architecture for the sending party and similarly, the receiver needs a wireless receiver architecture. Since most wireless communication is a two-way communication, a wireless transmitter circuit is required in the vast majority of wireless-capable devices.

Power amplifiers are the most power consuming element of any wireless transmitter circuit and thus efficient power amplifier designs are gaining ground and attention. A wireless communication signal is the encoding of a message into an electromagnetic wave. Before the electromagnetic wave can be propagated over the antenna through the medium of free space (or air), it needs to have sufficient power to reach its intended receiver that could be far away. In the case of mobile phone communication, this distance is as long as the coverage area for the closest mobile network provider's base station. To achieve this goal, there is a need to amplify the power of the communication signal without losing its signal integrity. This is the raison d'être of the power amplifier.

The power amplifier is the component that consumes the most amount of power in the wireless transmitter circuit. Improving the power efficiency of power amplifiers has become a very important challenge for power amplifier designers. The classic trade-off in power amplifier design exists between the linearity of its performance and its power efficiency.

The typical example of this in power amplifier design is the class F and F^{-1} modes of operation that make use of the non-linearity to achieve better power efficiency than more linear classes of operation like class A or B [3]. It is becoming quite common to design amplifiers that are non-linear but have been optimized for power efficiency and to use a linearization technique to tackle the distortion caused by the non-linearity.

The process of designing a power amplifier typically involves the choice of a power transistor, setting DC bias conditions and the design of the input and output matching networks (that expose the power transistor to specific impedances at frequencies of interest). If the power amplifier designer has access to a good model of the power transistor, she can use CAD simulation approaches to design the power amplifier matching networks in simulation before implementing it in a microstrip printed circuit board (which is a costly process). Because of this, proper simulation of the behaviour of power transistors within power amplifier circuits can become very important to the power amplifier design process.

This thesis will explore an emerging power transistor black-box behavioural modeling framework popularly known as poly-harmonic distortion (PHD) modeling [4]. There are a few proposed models based on this framework that will be analyzed, implemented in simulation and compared to one another. The relative strengths and weaknesses of these PHD models are discussed and conclusions are made about the region of applicability of each model.

1.2 Thesis Organization

Chapter 2 reviews the various techniques that have been developed to model the electromagnetic behaviour of a power transistor in simulation. The most common transistor modeling and simulation approaches are discussed in this chapter. Chapter 3 starts the analysis of the power transistor by using the Volterra framework as a means of modeling its behaviour. The PHD modeling framework is derived and introduced in detail from the assumption that the power transistor is in a stable circuit excited with a periodic signal. Two popular PHD modeling techniques, the X-parameter model and the Cardiff PHD formulation are derived and their modeling capabilities are discussed. Chapter 4 discusses the important measurement considerations involved in extracting these PHD behavioural models from a power transistor. The measurement requirements of a PHD model are clearly outlined and common impedance-pull techniques are discussed. The challenges involved in the extraction of the models derived in chapter 3 are presented in this chapter. Chapter 5 discusses the extraction and implementation of these PHD models within a harmonic balance simulator. Three different behavioural models will be extracted from the same

non-linearity and their performances are compared to each other in this chapter. Chapter 6 concludes the thesis with a discussion of the applicability of the different PHD model formulations and the challenges and limitations involved. Also, possible future work related to improving the modeling capabilities of future PHD models are presented here.

Chapter 2

Background: Power Amplifier Circuit Simulation

In this chapter, the idea of power transistor modeling will be introduced and various different approaches to this problem will be discussed. Each modeling approach has its strengths and limitations and some are more useful for some applications than others. Since the power transistor is mainly used to design a power amplifier circuit, the choice of the circuit simulator also becomes important in the design process. The common time-domain and frequency-domain non-linear simulation techniques are discussed here.

2.1 The Power Transistor Model

Electrical engineering is usually said to be at the intersection of applied science and applied mathematics, but at least in the case of transistor modeling, it can be said that it also intersects with applied epistemology. An important question that should be asked when confronted with any proposed transistor model is this: Is this transistor model valid or invalid and why?

As empiricists, we like to believe that the "proof is in the pudding", meaning that empirical observation (measurement) should be the basis of our judgment of models. A good transistor model is a model that accurately represents what is happening in the physical transistor, and if we do not make any mistakes in our measurement of the physical behaviour of the device, a good transistor model is one that matches the measurement well.

The author of this thesis agrees with the caution of noted essayist and applied epistemologist Nassim Nicholas Taleb against naïve empiricism. Taleb argues that since positive evidence supporting a model (or theory) can never fully prove that the model is correct, negative empiricism becomes an important tool in tackling the question of validity of mod-

els. He sums up the idea of negative empiricism by arguing that "*you know what is wrong with a lot more confidence than you know what is right*" [5]. In the same spirit, in the absence of glaring measurement error or faulty equipment, a mismatch between a transistor model and measurement is strong evidence proving the invalidity of the model. So instead of worrying about the validity of models, we should see where and under what circumstances can a model be *useful*. It is not simply enough to have a model that is mathematically consistent, the assumptions and underlying axioms of the theorems used must be somehow related back to the transistor and how we know it behaves from our understanding of physics.

Here we will discuss a few transistor modeling approaches and their usefulness.

2.1.1 Physics-based Transistor Modeling

The idea behind a physics-based model is to accurately describe the physical geometry, material properties, surface chemistry, and manufacturing details of a transistor in CAD software and use physics solvers to model the device characteristics. The type of physical relations used are partial differential equations that require specific boundary conditions for their solution. The solver uses relationships that are based on the quantum theory of matter, electrodynamics, and non-equilibrium thermodynamics. Creating these physics base models requires a profound knowledge of the material system [6].

These models when simulated in an electromagnetic solver result in a very accurate prediction of the behaviour of the transistor at the cost of an exceptionally long and complex simulation. This makes them unfeasible for use in simulating an entire power amplifier circuit when the objective is to design for matching network parameters. While physics based models might not be used by power amplifier designers because of their slow simulation, they provide valuable insight to transistor design engineers that want to find the optimal transistor dimensions that yield desired performance.

2.1.2 Compact Modeling

Unlike physics-based transistor models that focus on modeling the transistor itself independently, there are other models that are suitable for modeling the transistor within the context of its operating circuit that makes them suitable for power amplifier design. This class of transistor models that are based on circuit theory abstractions of the electromagnetic material are known as compact models [7]. A circuit description of the transistor will allow for fast simulation without the overhead necessary for computing the material physics.

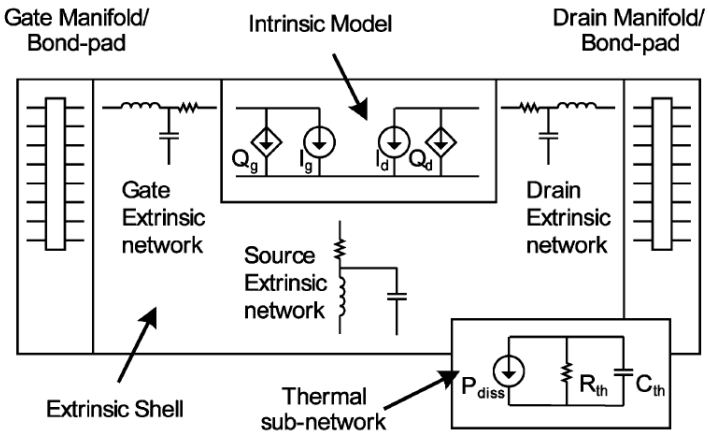

Figure 2.1: Block diagram of a typical transistor compact model architecture[1]

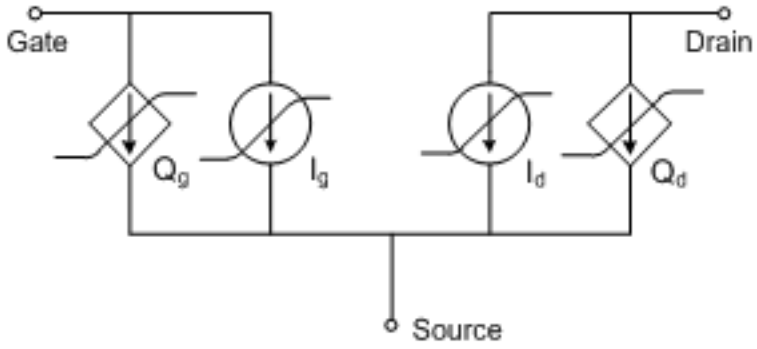

Figure 2.2: Intrinsic transistor model

Figure 2.1 describes the overall architecture of a typical compact model. A compact model like the one shown in this figure tries to describe the phenomenon of FET operation through the use of circuit components. This is why these compact models are referred to as *phenomenological models* [7]. The transistor is seen here in different layers. There is an intrinsic transistor within the compact model that will describe the non-linear relationship between the voltage and current. This intrinsic transistor is not really accessible through direct measurement of the transistor die. This intrinsic model is surrounded by passive linear extrinsic networks at each of the transistor terminals. Since power transistors usually come packaged and have their currents directed from the transistor die through bond-wires, the compact model can include models for these outer layers as well. In addition to the electrical modeling described, some compact models even perform thermal based modeling to vary the compact model circuit parameters based on varying substrate temperatures.

The intrinsic transistor is the main non-linear component of the transistor compact model, since it holds both the conduction current and the displacement current non-

linearity. Figure 2.2 shows the intrinsic model non-linear circuit components. Non-linear voltage controlled current sources are used to model the conduction current non-linearity and non-linear voltage controlled charge sources are used to model the displacement current non-linearity. An intrinsic model of this form will have the following state equations where the instantaneous voltages at both the gate and the drain and their first time derivatives are the states of the intrinsic system:

$$i_{drain}(t) = I_d(V_{gs}(t), V_{ds}(t)) + \frac{d}{dt}Q_d(V_{gs}(t), V_{ds}(t)) \tag{2.1}$$

$$i_{gate}(t) = I_g(V_{gs}(t), V_{ds}(t)) + \frac{d}{dt}Q_g(V_{gs}(t), V_{ds}(t)) \tag{2.2}$$

Equations 2.1 and 2.2 describe the intrinsic transistor of a compact model using non-linear differential equations that describe the dynamic non-linear behaviour of the device. There have been further developments recently to complicate these equations further by making the non-linear functions I_d, I_g, Q_d and Q_g also as a function of the junction temperature T_j and trap states of the device that would model the so-called trapping effects of the power transistor [8].

The modeling capability of the power transistor is based on an in-depth knowledge of the transistor technology that is used. The parameters of the compact models are extracted from characterization and the model will then use its phenomenological constitutive equations to predict the behaviour of the power transistor under signals that are of interest to power amplifier designers.

2.1.3 Behavioural Modeling

If a compact model fails to accurately predict the behaviour of the transistor in measurement, it could be because there are effects that are outside of the model. Instead of trying to fully understand how the transistor works, the opposite approach assumes very little about the transistor and is purely based on the measured behaviour of the transistor. This behavioural modeling approach views the transistor as a black-box (unlike compact models that try to fully describe what's inside the box), meaning that only the electromagnetic behaviour of the power transistor at its interface to the rest of the world matters. Here, unlike in the compact modeling approach, one does not need to have any insight into the specific transistor technology used.

The behavioural modeling approach has been quite popular among RF engineers to even model linear systems. In fact, it's quite common to perform an S-parameter measurement on a passive RF component and use these measured black-box relations instead of using

a circuit model. The motivation for using behavioural models for transistors follows this same reasoning. Behavioural models are useful when we have access to measurement of the device but no theory of its operation.

A behavioural model will use mathematical relationships to describe the behaviour of the power transistor. This means that the model will have less detail compared to the compact circuit model. However this also means that behavioural models will perform better in simulation. A common mathematical framework for modeling deterministic time-invariant non-linear systems is the Volterra series framework [9]. In chapter 3, we will discuss this framework and other behavioural modeling approaches based on this framework in great detail.

2.2 Circuit Simulation

Regardless of the type of transistor model used, these models are not useful for circuit design unless they are a part of a circuit simulation. The two common non-linear circuit simulation approaches are time-domain simulation and frequency-domain simulation techniques [10].

2.2.1 Time-domain Simulation

In time domain simulation, the circuit simulator uses a time-domain differential equation representation of each circuit element. The simulator steps slowly in time and solves for the voltage and current at each node and branch of the circuit that satisfy the time-domain relationships imposed by the circuit elements [10]. The main disadvantage of time-domain simulation is the relative slowness of it compared to frequency-domain simulation techniques. Finding the circuit response for high frequency multi-tone (or modulated signals) can take an extremely long time and would not be appropriate for a power amplifier designer that wants to sweep many different matching network parameters and see the response of the transistor to them.

2.2.2 Frequency-domain Simulation

Frequency-domain simulation techniques are faster than time-domain simulation since they can focus the simulation only at frequencies of interest. Harmonic Balance simulation is a very useful frequency-domain simulation technique that is suitable for non-linear circuits and designing power amplifiers [10].

In Harmonic Balance simulation, it is assumed that the voltage at every node and the current in every branch of the circuit is a periodic multi-harmonic signal. The solution to a Harmonic Balance simulation is the set of the voltages and currents at every node and branch respectively that satisfies the linear and non-linear equations of the circuit. The linear circuit elements behave as they regularly would in linear simulators, except now they are evaluated in the frequency domain at DC, the fundamental frequency of the simulation and the harmonic frequencies (up to a certain threshold of the simulator). The non-linear element of the circuit (which in the context of power amplifier design would be the power transistor) will behave as a frequency-mixing element (which is a result of its non-linearity). The simulator tries to converge to a solution that satisfies both the linear equations (at all frequencies) and the non-linear cross-frequency equations.

An extension of the Harmonic Balance simulator has been proposed in recent years known as Envelope Transient simulation. This extends the usefulness of Harmonic Balance simulation to modulated signals with a time-varying envelope. This type of simulation works as a type of hybrid between frequency-domain and time-domain simulations as the carrier frequency of the modulated signal is simulated with Harmonic Balance simulation while the envelope is simulated with time-domain integration techniques [11].

Chapter 3

Narrow-band Behavioural Modeling of a Power Transistor

This chapter is focused on the methods used for describing the electrical behaviour of a power transistor. The assumptions about the physical behaviour of power transistors are clearly stated, and the use of a Volterra framework as a basis for the nonlinear analysis of the power transistor is justified. The poly-harmonic distortion (PHD) framework is introduced and the various models based on this framework (namely the X-parameter PHD model and the Cardiff PHD model) are discussed and their limitations clearly stated.

3.1 The Power Transistor as a System

The first question that should be asked when one wants to approach the behavioural modeling of a power transistor is this: What type of behaviour of the power transistor is important to us? As power amplifier designers, we use the power transistor within the context of an electrical circuit, and so naturally we are interested in its electromagnetic behaviour. This behaviour is captured by the voltage and current at the terminals of the power transistor.

Since the power transistor is a three-terminal device, we can take the electrical potential at one of the terminals (namely the source terminal for FET devices) as a reference and treat the potential difference between the other two terminals (the gate and the drain) relative to the potential reference (the source) as the two variables that define the voltage state of the device. In terms of the current behaviour, we take the current flowing in through the gate and drain terminals as the two variables defining the current state of the device (the current flowing out of the source terminal is the sum of these two currents).

To view the power transistor of figure 3.1 as a two-port system, we take the gate and

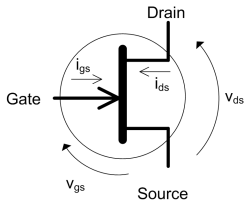

Figure 3.1: The three-port transistor as a two-port system

the drain as the two ports of the transistor and the electromagnetic behaviour will be described using these four voltage and current variables: v_{gs}, v_{ds}, i_{gs}, and i_{ds} (or v_1, v_2, i_1, and i_2 respectively).

Of the time-varying variables (or signals) that define the electromagnetic state of the power transistor, we can naturally pick the voltage variables as our input (stimulus) signals and the current variables as our output (response) signals. This voltage controlled current source view of the transistor is quite common among circuit designers. It allows us to think about the voltage at both ports as what we subject our system to and the current measured at the ports as how our device responds to this stimulus. Even though this view of the transistor intuitively implies that the current is *caused* by the voltage, it should be noted however that from elementary electromagnetics we know there is no causal link here between the current and voltage which are related to the magnetic and electric field respectively [12]. It is not appropriate to say that the voltage causes the current but rather that we are using a voltage-controlled current source description of the relationship between them. We could theoretically provide the same relationship using a current-controlled voltage source description even though this is not common at all for transistor descriptions.

Even though for a power amplifier we are mostly interested in how the input signal at the input port is amplified at the output port, a simple unilateral description of the device does not capture all the electrical behaviour of interest. We empirically know that the matching networks connected to both the source side and the load side of a power transistor has a significant effect on the behaviour of the power transistor [3]. This is why a complete two-port description of the power transistor is necessary for power amplifier design.

With this view of a power transistor as a *two-port system* with the voltage at each port as the input signals and the current at each port as the output signals, we can write:

$$i_1 = f_1(v_1, v_2) \tag{3.1}$$

$$i_2 = f_2(v_1, v_2) \tag{3.2}$$

The power transistor is a *non-linear* device and this means that the functions in equations 3.1 and 3.2 are non-linear functions. The power transistor is however much more complicated than a static nonlinear function. This means that the instantaneous output of the transistor is not simply just a function of the instantaneous input of the transistor. Thus we will assume that the power transistor a *dynamic* non-linear system. The dynamic non-linearity of the FET can be seen as the result of the reactive components that constitute the transistor. These reactive components can be generally non-linear in their behaviour (the non-linear gate capacitance in GaN FETs and the non-linear drain capacitance in LDMOS devices can be used as an example of this sort of non-linear dynamic behaviour).

The power transistor, being a physical device following physical laws is best described assuming that it is a *causal* system. This is intuitively the correct way of looking at this device as we don't expect the output current at either port to be a function of anything other than the voltage at the current instance in time and the past. Any dependency on a future input would be unphysical (since the device would anticipate future inputs and become a non-causal system).

We are also only interested in viewing the power FET as a *deterministic* system. This assumption means that the behavioural model should determine the exact output signal coming from the device given the past behaviour of the input stimulus. If the behaviour of the power transistor is too random, then it wouldn't be suitable for use to design a power amplifier. Any probabilistic deviation from this deterministic prediction is seen as undesirable noise. Even though the noise performance of a transistor is important, we will ignore the effect of noise and focus our modeling on the deterministic signal behaviour of the power transistor. Noise considerations however are important when measuring the behaviour of the transistor and dynamic range issues can be significant for non-linear measurement.

Finally, we'd like to assume that the power transistor as a *time-invariant* system with *fading memory*. Time-invariance implies that given the same input stimulus to the system, we should get the same output response regardless of what time of the day it is. This is a behaviour that we expect for most circuit components of interest, including power transistors. Another empirical behaviour that is of interest to us with regard to power FETs is that they have fading memory. This means that even though the behaviour of the transistor is a function of its past input, the effect of the past is fading such that we can begin to ignore the distant past in our modeling. This assumption significantly simplifies

the modeling of the dynamic behaviour of the power FET.

3.2 The Volterra Series

In section 3.1 we argued that we can view the power transistor as a dynamic, non-linear, time-invariant, causal and deterministic two-port system. If we also assume that the power transistor is an *equicontinuous* and *uniformly bounded* system then according to the Arzela-Ascoli theorem and Fréchet's approximation theorem [13], this system can be approximated uniformly to an arbitrary degree of precision by a sufficiently high finite order Volterra series [14, 15, 16].

The uniformly bounded assumption is quite valid for a power transistor in a stable circuit. Since we are making the assumption that the transistor is not unstable, then any model that comes out of this formulation will not be able to predict instability. The equicontinuous assumption is also valid for most physically realizable systems [14, 15] and should be a valid assumption for the case of a power transistor. This means that we can theoretically approximate the electromagnetic behaviour of a stable power transistor arbitrarily closely with a sufficiently high finite order Volterra series.

We can write the general infinite order causal two-port Volterra series for each of the output variables of the system as follows [9]:

$$i_1(t) = \sum_{n=0}^{\infty}\sum_{m=0}^{\infty}\int_{-\infty}^{0}\cdots\int_{-\infty}^{0} h_{1nm}(\tau_{11},\ldots,\tau_{1n},\tau_{21},\ldots,\tau_{2m}) \\ v_1(t+\tau_{11})\ldots v_1(t+\tau_{1n})v_2(t+\tau_{21})\ldots v_2(t+\tau_{2m})d\tau_{11}\ldots d\tau_{1n}d\tau_{21}\ldots d\tau_{2m} \quad (3.3)$$

$$i_2(t) = \sum_{n=0}^{\infty}\sum_{m=0}^{\infty}\int_{-\infty}^{0}\cdots\int_{-\infty}^{0} h_{2nm}(\tau_{11},\ldots,\tau_{1n},\tau_{21},\ldots,\tau_{2m}) \\ v_1(t+\tau_{11})\ldots v_1(t+\tau_{1n})v_2(t+\tau_{21})\ldots v_2(t+\tau_{2m})d\tau_{11}\ldots d\tau_{1n}d\tau_{21}\ldots d\tau_{2m} \quad (3.4)$$

The Volterra series expressions in equations 3.3 and 3.4 give the current response of the transistor for any two $\mathbb{R}^{\infty}$ voltage signals at each port of the device. The functions h_{1nm} and h_{2nm} are the two-port Volterra series kernel functions (where $k = n + m$ is the order of the kernel function) that hold the non-linear dynamics of the system at different orders. Taking the Fourier transform of these expressions gives:

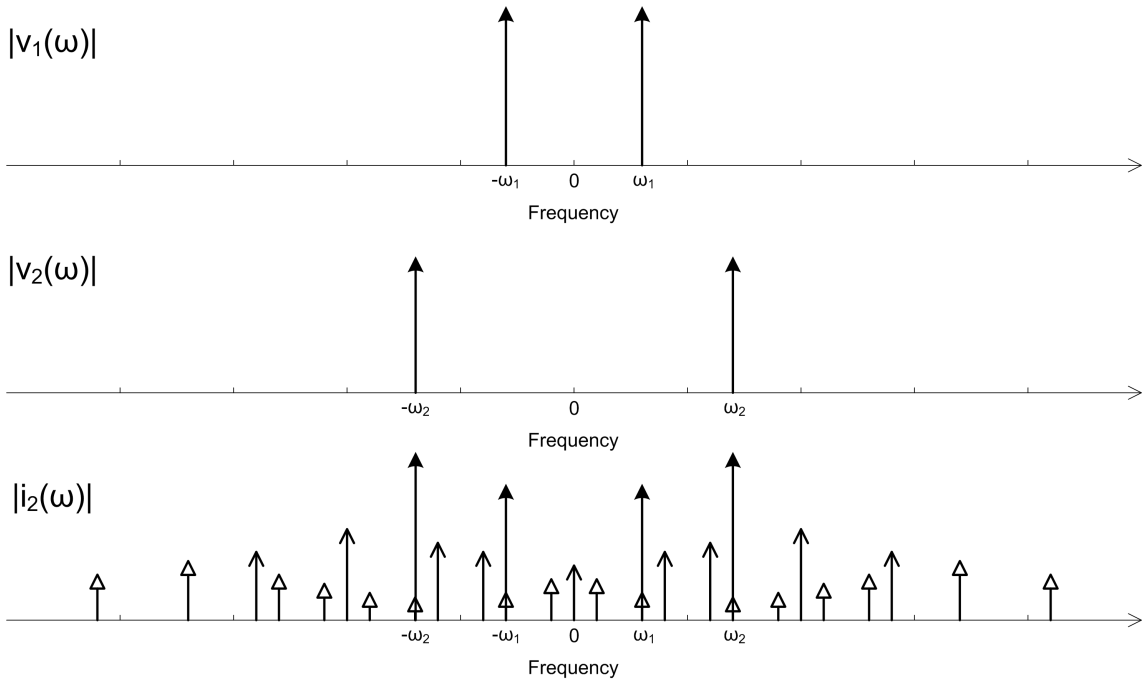

Figure 3.2: Frequency mixing products of a Volterra system (up to the third order)

$$I_1(\omega) = \sum_{n=0}^{\infty}\sum_{m=0}^{\infty}\int_{-\infty}^{\infty}\cdots\int_{-\infty}^{\infty} H_{1nm}(\omega_{11},\ldots,\omega_{1n},\omega_{21},\ldots,\omega_{2m})$$
$$V_1(\omega+\omega_{11})\ldots V_1(\omega+\omega_{1n})V_2(\omega+\omega_{21})\ldots V_2(\omega+\omega_{2m})d\omega_{11}\ldots d\omega_{1n}d\omega_{21}\ldots d\omega_{2m} \quad (3.5)$$

$$I_2(\omega) = \sum_{n=0}^{\infty}\sum_{m=0}^{\infty}\int_{-\infty}^{\infty}\cdots\int_{-\infty}^{\infty} H_{2nm}(\omega_{11},\ldots,\omega_{1n},\omega_{21},\ldots,\omega_{2m})$$
$$V_1(\omega+\omega_{11})\ldots V_1(\omega+\omega_{1n})V_2(\omega+\omega_{21})\ldots V_2(\omega+\omega_{2m})d\omega_{11}\ldots d\omega_{1n}d\omega_{21}\ldots d\omega_{2m} \quad (3.6)$$

It is apparent from the frequency domain Volterra series expressions (equations 3.5 and 3.6) that the output spectral components are only a result of a mixing of all the input spectral components. Figure 3.2 shows the first, second and third mixing products produced at the output of the system if both the inputs of the system are stimulated with simple sinusoidals at different frequencies. The first order mixing products (shown with solid arrowheads in the figure) are at the same frequencies as the inputs. These are generated by the first order Volterra series kernel functions. The second order mixing products (shown with open arrowheads in the figure) are located at the frequency addition

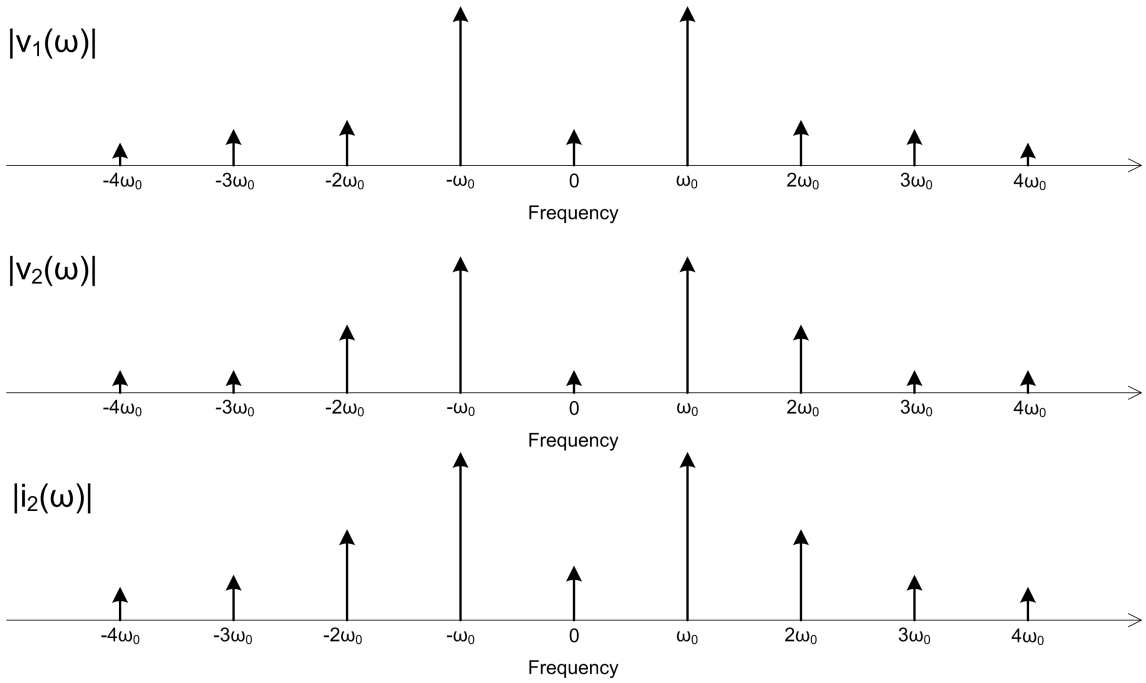

Figure 3.3: Volterra system under non-linear CW stimulus signals

of both the positive and negative frequency components of the input on the frequency spectrum of the output. These are generated by the second order Volterra series kernel functions. Note that there is a frequency component generated at DC by the second order kernels. The third order mixing products, generated by the third order Volterra series kernel functions (shown with triangular arrowheads in the figure) are then located at the third order frequency addition of the input frequency components.

3.3 Poly-Harmonic Distortion Modeling

In section 3.2, the frequency domain formulation of the Volterra series (equations 3.5 and 3.6) was used to describe the output signals of the power transistor system as a function of its input signals.

To simplify the problem, instead of focusing on the response of the Volterra system to any two arbitrary $\mathbb{R}^\infty$ voltage signals, we will restrict our two inputs to periodic multi-harmonic signals with the same fundamental frequency (see figure 3.3). These signals are also called non-linear continuous wave (CW) signals. This means that the frequency spectrum for both of the inputs ($V_1(\omega)$ and $V_2(\omega)$) are only non-zero for values of $\omega_0 = 2\pi n f_0$ for $\forall n \in \mathbb{Z}$, where f_0 is the fundamental frequency. By a quick observation of the frequency domain Volterra series in equations 3.5 and 3.6, it becomes apparent that the

output frequency spectrums ($I_1(\omega)$ and $I_2(\omega)$) only have non-zero components at $\omega_0 = 2\pi n f_0$ for $\forall n \in \mathbb{Z}$. The time domain exponential expression for the real periodic multi-harmonic (non-linear CW) input and output signals are as follows:

$$v_1(t) = v_{10} + v_{11}e^{j\omega_0 t} + v_{11}^* e^{-j\omega_0 t} + v_{12}e^{j2\omega_0 t} + v_{12}^* e^{-j2\omega_0 t} + v_{13}e^{j3\omega_0 t} + v_{13}^* e^{-j3\omega_0 t} + \dots \quad (3.7)$$

$$v_2(t) = v_{20} + v_{21}e^{j\omega_0 t} + v_{21}^* e^{-j\omega_0 t} + v_{22}e^{j2\omega_0 t} + v_{22}^* e^{-j2\omega_0 t} + v_{23}e^{j3\omega_0 t} + v_{23}^* e^{-j3\omega_0 t} + \dots \quad (3.8)$$

$$i_1(t) = i_{10} + i_{11}e^{j\omega_0 t} + i_{11}^* e^{-j\omega_0 t} + i_{12}e^{j2\omega_0 t} + i_{12}^* e^{-j2\omega_0 t} + i_{13}e^{j3\omega_0 t} + i_{13}^* e^{-j3\omega_0 t} + \dots \quad (3.9)$$

$$i_2(t) = i_{20} + i_{21}e^{j\omega_0 t} + i_{21}^* e^{-j\omega_0 t} + i_{22}e^{j2\omega_0 t} + i_{22}^* e^{-j2\omega_0 t} + i_{23}e^{j3\omega_0 t} + i_{23}^* e^{-j3\omega_0 t} + \dots \quad (3.10)$$

In equations 3.7 to 3.10, $\omega_0 = 2\pi f_0$ and v_{10}, v_{20}, i_{10}, and i_{20} are real numbers that represent the DC component of each signal and the other variables v_{ph} and i_{ph} are complex numbers representing the spectral component at port p and harmonic index h.

Since all of the input and output signals are real signals, we have that the negative frequency components of the frequency spectrum are the complex conjugate of the positive frequency components. This means that to identify the output signal completely, we need to only find the relations describing the positive frequency components (i_{20}, i_{21}, i_{22}, i_{23}, etc.) and the negative frequency components will just be the complex conjugate of these values. However from the Volterra series formulation we know that each one of these output frequency components is a function of *both* the negative and positive frequency components of the inputs. So generally we can write for each output component i_{ph}:

$$i_{ph} = f_{ph}(v_{10}, v_{20}, v_{11}, v_{11}^*, v_{21}, v_{21}^*, v_{12}, v_{12}^*, v_{22}, v_{22}^*, \dots) \quad (3.11)$$

Note that the functions f_{ph} in equation 3.11 emerge from the Volterra series formulation of equations 3.5 and 3.6 and since the Volterra series is an analytic expression, these functions are also analytic. The analyticity of the describing functions becomes important when we want to approximate such a function using a Taylor series [17]. If we were to write the expression of equation 3.11 in the following form (ignoring the conjugate, negative

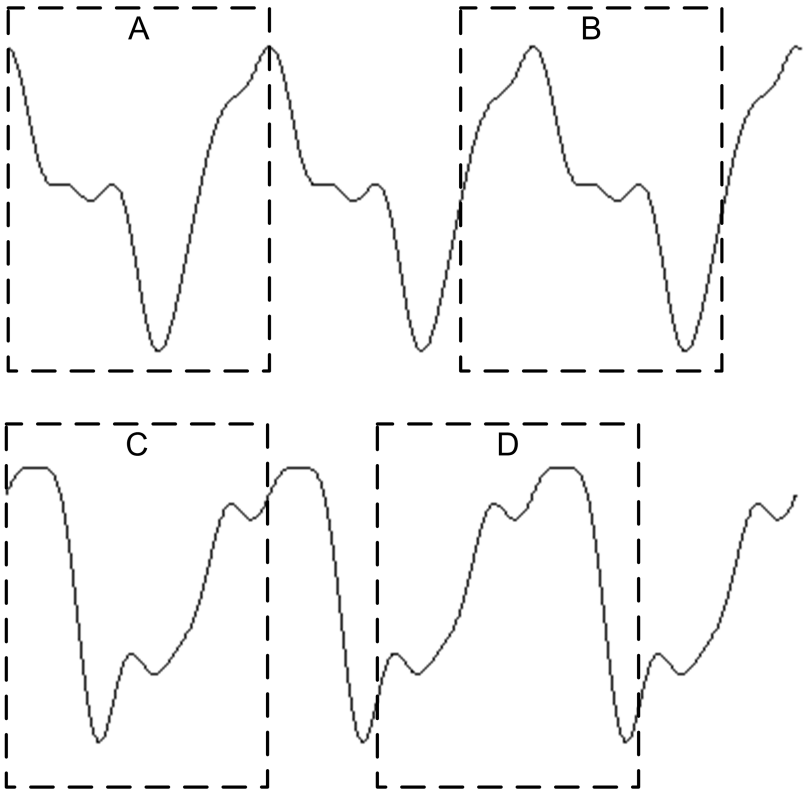

Figure 3.4: Non-linear periodic continuous waves in the time domain

frequency terms), it would generally be non-analytic:

$$i_{ph} = \hat{f_{ph}}(v_{10}, v_{20}, |v_{11}|, v_{21}, v_{12}, v_{22}, \ldots) \tag{3.12}$$

We can simplify equation 3.11 further by adding a phase reference to our periodic signals. Since we have already assumed that the power transistor is a time-invariant system, this means that only the relative phase of the output and input frequency components matter and so we set the phase of v_{11} to zero and normalize the phase of all the complex components by using the transformation $\tilde{v}_{ph} = v_{ph}P^{-h}$ and $\tilde{i}_{ph} = i_{ph}P^{-h}$, where $P = v_{11}/|v_{11}|$. This time-invariance principle further simplifies the expression of equation 3.11 to:

$$\tilde{i}_{ph} = \tilde{f}_{ph}(v_{10}, v_{20}, |v_{11}|, \tilde{v}_{21}, \tilde{v}^*_{21}, \tilde{v}_{12}, \tilde{v}^*_{12}, \tilde{v}_{22}, \tilde{v}^*_{22}, \ldots) \tag{3.13}$$

The functions $\tilde{f}_{ph}$ in equation 3.13 for each port p and harmonic index h define the poly-harmonic distortion (PHD) model for the system at a single fundamental frequency f_0.

The PHD model can also be understood by looking at the time-domain waveforms of

equations 3.7 through 3.10. Figure 3.4 shows two examples of non-linear continuous wave signals with the same fundamental frequency that could represent either the current or voltage at either port of the power transistor. The windows A, B, C and D have the length of the fundamental period of each of the two periodic non-linear CW tones. The windows A and C are the reference windows for each of the two signals (since they line up with the phase of the fundamental frequency component of the Fourier series of both waveforms). The idea here is that even though frame A and B hold one period of the same periodic signal, their Fourier series coefficients are different. To make the PHD model account for this time-invariance effect, we will always represent the periodic signal with a known reference signal.

As long as the currents and voltages at both ports of the power transistor are continuous periodic waveforms with the same fundamental frequency, these waveforms can be fully described by a high enough order Fourier series decomposition. The PHD model then effectively maps the Fourier series coefficients of both inputs to the Fourier series coefficients at both outputs. The window used for each of these Fourier series coefficient sets is the one that corresponds to the phase reference of the fundamental frequency component input at the first port of the system. Using the time-invariant property of the system, we can find these phase-normalized Fourier series coefficients using either of the following transformations:

$$\tilde{v}_{ph} = v_{ph} P^{-h} \tag{3.14}$$

$$\tilde{i}_{ph} = i_{ph} P^{-h} \tag{3.15}$$

where $P = v_{11}/|v_{11}|$.

Even though the time-domain Volterra series formulations of equation 3.3 and 3.4 can be used in a time-domain simulation of a circuit, the PHD model lends itself well to a type of frequency-domain non-linear circuit simulation called Harmonic Balance simulation (discussed in section 2.2.2). The cross-frequency equations used by the Harmonic Balance simulator in the context of a PHD model are simply the $\tilde{f}_{ph}$ functions defined in equation 3.13.

3.3.1 Equivalent PHD Model Mappings

The PHD model expressed by the functions $\tilde{f}_{ph}$ of equation 3.13 can be equivalently expressed in other ways. Here we will discuss these equivalent PHD model mappings.

3.3.1.1 The Power-wave defined PHD Model

A popular method for representing the behaviour of linear RF systems is the use of S-parameters [18]. In the S-parameter framework, the reflected power-wave at each port is written as a linear combination of the incident power-waves at all of the ports of the system. Incident and reflected power-waves at a port (and a defined frequency) are defined as follows:

$$a = \frac{v + Z_0 i}{2} \tag{3.16}$$

$$b = \frac{v - Z_0 i}{2} \tag{3.17}$$

where Z_0 is a reference impedance (usually 50Ω for RF applications).

The incident wave at each port is usually represented by the letter a and the reflected wave by the letter b. These define pseudowaves and are not physical. They are mathematical artifacts of an arbitrarily chosen reference impedance. They are mainly used because they have convenient properties [19]. As can be seen from equations 3.16 and 3.17, the power-waves at each port are a function of both the voltage and current at each port. In the behavioural models we have discussed up to this point, the current was seen as an output and the voltage as the input. We can equivalently describe the the reflected power-waves at each port as a function of the incident power-waves at each port. This is similar to the equivalence between Y-parameters and S-parameters for linear electromagnetic multi-port systems after a simple transformation [18].

Unlike voltage and current which describe a physical aspect of the behaviour of the power transistor (where the voltage and current are directly related to the electric and magnetic field respectively), the power-wave definitions described in equations 3.16 and 3.17 only refer to a physical parameter (energy transfer rate), that is the power flowing in or out of a port, when the port has an output impedance of Z_0. This means that if the port of the device at the corresponding frequency has an output impedance different from Z_0, then the a and b waves are simply a function of the voltage and current at the port and cannot be directly related to the physics of the device. By convention RF engineers usually use $Z_0 = 50\Omega$ as the reference characteristic impedance. The power transistor will normally provide different output impedances at both ports at the fundamental and harmonic frequencies of interest and this output impedance is subject to variation throughout the range of its non-linearity and different operating states.

Traditionally however, RF engineers popularized the use of frequency-dependent S-parameters which uses power-waves in its definition (as opposed to Z or Y-parameters)

because the behaviour of linear systems are easier to measure using S-parameters when using a Voltage Network Analyzer (VNA).

The reason for the equivalence of the power-wave definition of a non-linear systems to its voltage-current definition in the presence of periodic multi-harmonic signals stems from the fact that once the Harmonic Balance simulator has converged to a solution with either method of defining the system, one can convert the state of the circuit from one representation to another. This means that having the incident and reflected wave at a port gives us the current and voltage information as well and vice versa. This can be seen from the following relationships:

$$v = a + b \tag{3.18}$$

$$i = \frac{a - b}{Z_c} \tag{3.19}$$

The implication of this equivalence in the context of PHD models is that we can write the PHD model relations of equation 3.13 in the following form:

$$\tilde{b}_{ph} = \tilde{f}_{ph}^{(p)}(v_{10}, v_{20}, |a_{11}|, \tilde{a}_{21}, \tilde{a}_{21}^*, \tilde{a}_{12}, \tilde{a}_{12}^*, \tilde{a}_{22}, \tilde{a}_{22}^*, \ldots) \tag{3.20}$$

where $\tilde{b}_{ph} = b_{ph}P^{-h}$ and $\tilde{a}_{ph} = a_{ph}P^{-h}$, where $P = a_{11}/|a_{11}|$.

This form of the PHD model formulation described in equation 3.20 is used in the X-Parameter PHD formulation described in section 3.3.2.

3.3.1.2 The Polar PHD Model

The describing functions in the PHD model formulations of equations 3.13 or 3.20 can maintain their analyticity if they are instead a function of the magnitudes and phases of the complex inputs as opposed to being a function of the complex variables and their conjugates. This is because you need two real parameters to equivalently describe a complex variable and its complex conjugate. In this case the two real parameters are the magnitude and phase of the complex number. For example, a function of complex variables c and c^* can be written in terms of the two real variables $|c|$ and $\angle c$ by rewriting $c = |c|e^{j\omega\angle c}$ and $c^* = |c|e^{-j\omega\angle c}$. This means that we can rewrite equations 3.13 and 3.20 as follows:

$$\tilde{i}_{ph} = \tilde{f}_{ph_{polar}}(v_{10}, v_{20}, |v_{11}|, |v_{21}|, \angle v_{21}, |v_{12}|, \angle v_{12}, |v_{22}|, \angle v_{22}, \ldots) \tag{3.21}$$

$$\tilde{b}_{ph} = \tilde{f}_{ph_{polar}}^{(p)}(v_{10}, v_{20}, |a_{11}|, |a_{21}|, \angle a_{21}, |a_{12}|, \angle a_{12}, |a_{22}|, \angle a_{22}, \ldots) \tag{3.22}$$

The form of the PHD model formulation described in equation 3.22 is used in the Cardiff PHD formulation described in section 3.3.3.

3.3.1.3 The Reflection Coefficient PHD Model

For every point in the power-wave defined PHD model mapping of equation 3.20, we can use the transformations:

$$\Gamma_{ph} = \frac{\tilde{a}_{ph}}{\tilde{b}_{ph}} \tag{3.23}$$

$$\tilde{a}_{ph} = \Gamma_{ph}\tilde{b}_{ph} \tag{3.24}$$

to get the following equivalent PHD model mapping (expressed in the polar form described in section 3.3.1.2):

$$\tilde{b}_{ph} = \tilde{f}_{ph}^{(p)}(v_{10}, v_{20}, |a_{11}|, \Gamma_{21}, \angle\Gamma_{21}, \Gamma_{12}, \angle\Gamma_{12}, \Gamma_{22}, \angle\Gamma_{22}, \ldots)$$

3.3.1.4 The Rectangular PHD Model

In a similar line of reasoning as the one used in section 3.3.1.2, we can say that the PHD model formulations of equation 3.13 or 3.20 can maintain their analyticity if the real and imaginary parts of the input complex numbers are used as the inputs to the describing functions. This is because a function of complex variables c and c^* can be written in terms of the two real variables $Re\{c\}$ and $Im\{c\}$ by rewriting $c = Re\{c\} + jIm\{c\}$ and $c^* = Re\{c\} - jIm\{c\}$. This means we can also write the PHD model equations as follows:

$$\tilde{i}_{ph} = \tilde{f}_{ph_{rect}}(v_{10}, v_{20}, |\tilde{v}_{11}|, Re\{\tilde{v}_{21}\}, Im\{\tilde{v}_{21}\}, Re\{\tilde{v}_{12}\}, Im\{\tilde{v}_{12}\}, Re\{\tilde{v}_{22}\}, Im\{\tilde{v}_{22}\}, \ldots) \tag{3.25}$$

$$\tilde{b}_{ph} = \tilde{f}_{ph_{rect}}^{(p)}(v_{10}, v_{20}, |\tilde{a}_{11}|, Re\{\tilde{a}_{21}\}, Im\{\tilde{a}_{21}\}, Re\{\tilde{a}_{12}\}, Im\{\tilde{a}_{12}\}, Re\{\tilde{a}_{22}\}, Im\{\tilde{a}_{22}\}, \ldots) \tag{3.26}$$

3.3.2 The X-Parameter PHD Model

The X-Parameter PHD model [4], uses a first order multi-variable Taylor series approximation for the analytic functions $\tilde{f}_{ph}^{(p)}$ described in equation 3.20. Note that these functions are complex functions so in order to perform calculus on these functions, we need to use a definition of a derivative that is defined for complex functions. The Wirtinger derivative is a derivative defined for complex functions. It is in fact a derivative from the abstract algebra point of view and can be used in exactly the same places that ordinary real derivatives are used. The Wirtinger derivative with respect to the complex variable $z = x + jy$ where $x, y \in \mathbb{R}$ is defined as follows [20]:

$$\frac{\partial}{\partial z} = \frac{1}{2}(\frac{\partial}{\partial x} - j\frac{\partial}{\partial y}) \tag{3.27}$$

$$\frac{\partial}{\partial z^*} = \frac{1}{2}(\frac{\partial}{\partial x} + j\frac{\partial}{\partial y}) \tag{3.28}$$

Using the definition of the Wirtinger derivative, we can define the multi-variable Taylor series for complex functions the same way we define them for real functions.

The Taylor series approximation linearizes the function $\tilde{f}_{ph}^{(p)}$ with respect to its input variables around a certain point in the input space. We will call the point in the input space of function $\tilde{f}_{ph}^{(p)}$ that we linearize around the Large Signal Operating Point (henceforth referred to as the LSOP). In the X-Parameter PHD model, we fix the port DC voltage biases ($v_{10} = v_{10}^p$ and $v_{20} = v_{20}^p$) and the magnitude of the fundamental input port incidental power-wave ($|a_{11}| = |a_{11}^p|$). The value of the rest of the input variables ($\tilde{a}_{21}, \tilde{a}_{21}^*, \tilde{a}_{12}, \tilde{a}_{12}^*, \tilde{a}_{22}, \tilde{a}_{22}^*, \ldots$) are set to be zero since they represent the small signals of the system. The first-order Taylor series approximation will be as follows:

$$\tilde{b}_{ph} = \tilde{f}_{ph}^{(p)}(v_{10}, v_{20}, |a_{11}|, \tilde{a}_{21}, \tilde{a}_{21}^*, \tilde{a}_{12}, \tilde{a}_{12}^*, \tilde{a}_{22}, \tilde{a}_{22}^*, \ldots) \tag{3.29}$$

$$\begin{aligned}\tilde{b}_{ph} = \tilde{f}_{ph}^{(p)}(v_{10}^p, v_{20}^p, |a_{11}^p|, 0, 0, 0, 0, 0, 0, \ldots) \\ + (v_{10} - v_{10}^p)\frac{\partial \tilde{f}_{ph}^{(p)}}{\partial v_{10}} + (v_{20} - v_{20}^p)\frac{\partial \tilde{f}_{ph}^{(p)}}{\partial v_{20}} + (|a_{11}| - |a_{11}^p|)\frac{\partial \tilde{f}_{ph}^{(p)}}{\partial |a_{11}|} \\ + \tilde{a}_{21}\frac{\partial \tilde{f}_{ph}^{(p)}}{\partial \tilde{a}_{21}} + \tilde{a}_{21}^*\frac{\partial \tilde{f}_{ph}^{(p)}}{\partial \tilde{a}_{21}^*} + \tilde{a}_{12}\frac{\partial \tilde{f}_{ph}^{(p)}}{\partial \tilde{a}_{12}} + \tilde{a}_{12}^*\frac{\partial \tilde{f}_{ph}^{(p)}}{\partial \tilde{a}_{12}^*} + \tilde{a}_{22}\frac{\partial \tilde{f}_{ph}^{(p)}}{\partial \tilde{a}_{22}} + \tilde{a}_{22}^*\frac{\partial \tilde{f}_{ph}^{(p)}}{\partial \tilde{a}_{21}^*} + \ldots\end{aligned} \tag{3.30}$$

To simplify equation 3.30 further, we make all our model parameters (the partial deriva-

tives with respect to the small signal inputs) a function of the LSOP variables. This way we never linearize around the LSOP variables (v_{10}, v_{20} and $|a_{11}|$) and thus the corresponding linearization terms can be removed from the first-order Taylor series approximation:

$$\begin{aligned}\tilde{b}_{ph} = {} & \tilde{f}_{ph}^{(p)}(v_{10}^p, v_{20}^p, |a_{11}^p|, 0, 0, 0, 0, 0, 0, \ldots) \\ & + \tilde{a}_{21}\frac{\partial \tilde{f}_{ph}^{(p)}}{\partial \tilde{a}_{21}}(v_{10}, v_{20}, |a_{11}|) + \tilde{a}_{21}^*\frac{\partial \tilde{f}_{ph}^{(p)}}{\partial \tilde{a}_{21}^*}(v_{10}, v_{20}, |a_{11}|) + \tilde{a}_{12}\frac{\partial \tilde{f}_{ph}^{(p)}}{\partial \tilde{a}_{12}}(v_{10}, v_{20}, |a_{11}|) \\ & + \tilde{a}_{12}^*\frac{\partial \tilde{f}_{ph}^{(p)}}{\partial \tilde{a}_{12}^*}(v_{10}, v_{20}, |a_{11}|) + \tilde{a}_{22}\frac{\partial \tilde{f}_{ph}^{(p)}}{\partial \tilde{a}_{22}}(v_{10}, v_{20}, |a_{11}|) + \tilde{a}_{22}^*\frac{\partial \tilde{f}_{ph}^{(p)}}{\partial \tilde{a}_{21}^*}(v_{10}, v_{20}, |a_{11}|) + \ldots \end{aligned} \tag{3.31}$$

Using the notation popularized as X-parameters, we can define:

$$X_{ph}^{(F)}(v_{10}, v_{20}, |a_{11}|) := \tilde{f}_{ph}^{(p)}(v_{10}^p, v_{20}^p, |a_{11}^p|, 0, 0, 0, 0, 0, 0, \ldots) \tag{3.32}$$

$$X_{ph,qi}^{(S)}(v_{10}, v_{20}, |a_{11}|) := \frac{\partial \tilde{f}_{ph}^{(p)}}{\partial \tilde{a}_{qi}}(v_{10}, v_{20}, |a_{11}|) \tag{3.33}$$

$$X_{ph,qi}^{(T)}(v_{10}, v_{20}, |a_{11}|) := \frac{\partial \tilde{f}_{ph}^{(p)}}{\partial \tilde{a}_{qi}^*}(v_{10}, v_{20}, |a_{11}|) \tag{3.34}$$

Thus we can re-write equation 3.31 as:

$$\tilde{b}_{ph} = X_{ph}^{(F)}(v_{10}, v_{20}, |a_{11}|) + \sum_{q,i}(X_{ph,qi}^{(S)}(v_{10}, v_{20}, |a_{11}|)\tilde{a}_{qi} + X_{ph,qi}^{(T)}(v_{10}, v_{20}, |a_{11}|)\tilde{a}_{qi}^*) \tag{3.35}$$

where $\{q, i\} \notin \{\{1, 1\}\}$.

To get a feel for the individual role of the $X_{ph}^{(F)}$, $X_{ph,qi}^{(S)}$ and $X_{ph,qi}^{(T)}$ terms in equation 3.35 see figure 3.5. In this figure we clearly see that the $X_{ph}^{(F)}$ term is the output $\tilde{b}_{ph}$ at the LSOP when all small signal inputs $\tilde{a}_{qi}$ are zero. If one of the small signals is varied (as in the case of the figure), we see that variations of constant magnitude for $\tilde{a}_{qi}$ (each one of the circles in the left graph of figure 3.5) correspond to variations on an ellipse at the output. The elliptical shape is the result of the $X_{ph,qi}^{(S)}$ and $X_{ph,qi}^{(T)}$ terms (and in fact varying the $X_{ph,qi}^{(S)}$ and $X_{ph,qi}^{(T)}$ will always result in elliptical variation of $\tilde{b}_{ph}$ for circular variations of $\tilde{a}_{qi}$). We can also see that scaling the magnitude of the circles in the $\tilde{a}_{qi}$, also scales the output ellipses by the same factor. This is because the X-parameter formulation of equation 3.35 is linear with respect to the small signal partial derivative terms $X_{ph,qi}^{(S)}$ and $X_{ph,qi}^{(T)}$. The

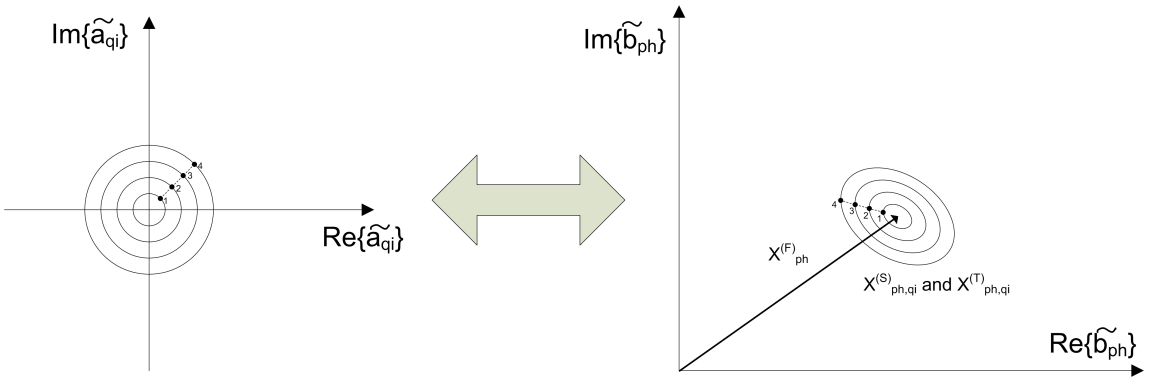

Figure 3.5: Visual representation of the $X^{(F)}_{ph}$, $X^{(S)}_{ph,qi}$ and $X^{(T)}_{ph,qi}$ X-parameters

result of the variation of multiple $\tilde{a}_{qi}$ inputs (for different values of q and i) will be taken in superposition. This linear approximation of the small signal effects is called the *harmonic superposition approximation* which is another way of saying that we are using a linear first order Taylor series approximation for the harmonic content.

Equation 3.35 defines the X-Parameter PHD model for the reflected power-waves at each port and harmonic frequency. To make this a complete PHD model, we also need to model how the DC current varies when the input signal has changed. Agilent introduced two other X-parameters to linearize for the DC current output. We will use the relation 3.26 for the DC current and use a first order Taylor approximation to get:

$$i_{p0} = \tilde{f}^{(p)}_{ph_{rect}}(v_{10}, v_{20}, |\tilde{a}_{11}|, Re\{\tilde{a}_{21}\}, Im\{\tilde{a}_{21}\}, Re\{\tilde{a}_{12}\}, Im\{\tilde{a}_{12}\}, Re\{\tilde{a}_{22}\}, Im\{\tilde{a}_{22}\}, \ldots) \tag{3.36}$$

$$\begin{aligned} i_{p0} = \tilde{f}^{(p)}_{p0}(v^p_{10}, v^p_{20}, |a^p_{11}|, 0, 0, 0, 0, 0, 0, \ldots) \\ + Re\{\tilde{a}_{21}\}\frac{\partial \tilde{f}^{(p)}_{p0}}{\partial Re\{\tilde{a}_{21}\}}(v_{10}, v_{20}, |a_{11}|) + Im\{\tilde{a}_{21}\}\frac{\partial \tilde{f}^{(p)}_{p0}}{\partial Im\{\tilde{a}_{21}\}}(v_{10}, v_{20}, |a_{11}|) \\ + \partial Re\{\tilde{a}_{12}\}\frac{\partial \tilde{f}^{(p)}_{p0}}{\partial Re\{\tilde{a}_{12}\}}(v_{10}, v_{20}, |a_{11}|) + Im\{\tilde{a}_{12}\}\frac{\partial \tilde{f}^{(p)}_{p0}}{\partial Im\{\tilde{a}_{12}\}}(v_{10}, v_{20}, |a_{11}|) \\ + Re\{\tilde{a}_{22}\}\frac{\partial \tilde{f}^{(p)}_{p0}}{\partial Re\{\tilde{a}_{22}\}}(v_{10}, v_{20}, |a_{11}|) + Im\{\tilde{a}_{22}\}\frac{\partial \tilde{f}^{(p)}_{p0}}{\partial Im\{\tilde{a}_{22}\}}(v_{10}, v_{20}, |a_{11}|) + \ldots \end{aligned} \tag{3.37}$$

We define:

$$X^{(I)}_p(v_{10}, v_{20}, |a_{11}|) := \tilde{f}^{(p)}_{p0}(v^p_{10}, v^p_{20}, |a^p_{11}|, 0, 0, 0, 0, 0, 0, \ldots) \tag{3.38}$$

$$X_{p,qi}^{(Y,r)}(v_{10}, v_{20}, |a_{11}|) := \frac{\partial \tilde{f}_{p0}^{(p)}}{\partial Re\{\tilde{a}_{qi}\}}(v_{10}, v_{20}, |a_{11}|) \tag{3.39}$$

$$X_{p,qi}^{(Y,i)}(v_{10}, v_{20}, |a_{11}|) := \frac{\partial \tilde{f}_{p0}^{(p)}}{\partial Im\{\tilde{a}_{qi}\}}(v_{10}, v_{20}, |a_{11}|) \tag{3.40}$$

Thus we have:

$$i_{p0} = X_p^{(I)}(v_{10}, v_{20}, |a_{11}|) + \sum_{q,i}(X_{p,qi}^{(Y,r)}(v_{10}, v_{20}, |a_{11}|)Re\{\tilde{a}_{qi}\} + X_{p,qi}^{(Y,i)}(v_{10}, v_{20}, |a_{11}|)Im\{\tilde{a}_{qi}\}) \tag{3.41}$$

where $\{q, i\} \notin \{\{1, 1\}\}$ and $X_p^{(I)}$, $X_{p,qi}^{(Y,r)}$ and $X_{p,qi}^{(Y,i)}$ are all real valued for the real valued DC current at port p (i_{p0}). Define $X_{p,qi}^{(Y)} := X_{p,qi}^{(Y,r)} - jX_{p,qi}^{(Y,i)}$; we have:

$$i_{p0} = X_p^{(I)}(v_{10}, v_{20}, |a_{11}|) + \sum_{q,i} Re(X_{p,qi}^{(Y)}(v_{10}, v_{20}, |a_{11}|)\tilde{a}_{qi}) \tag{3.42}$$

where $\{q, i\} \notin \{\{1, 1\}\}$.

The X-parameters used in equation 3.42 are the parameters used by Agilent Technologies in their implementation of the X-Parameter PHD model. Note that the $X_p^{(I)}$ and $X_{p,qi}^{(Y)}$ parameters are a function of the LSOP (including the DC bias voltage of the power transistor). In the context of the PHD model being used in Harmonic Balance simulation, it is important to note that DC current contribution resulting from the exposure of the RF signal to the non-linearity in return varies the DC bias voltage away from the value set by the DC bias circuit. Varying the fundamental input power ($|a_{11}|$) for a given DC supply voltage pair (V_{GG} and V_{DD}) will also vary the DC bias voltage at the FET device (v_{10} and v_{20}). Since we cannot fix v_{10} and v_{20} under various input power conditions, in order to make the extraction of the X-parameter model possible, we can consider making the X-parameters as a function of V_{GG} and V_{DD} (which we can fix), instead of v_{10} and v_{20}.

3.3.2.1 LSOP Expansion for Highly Non-linear Devices

The region of validity of equation 3.31 is the same as the region of validity of a first-order Taylor series. This means that if the value of the reflection power wave at load side or the harmonic input powers at both ports gets significant (which is the case of the operation of the power transistor in highly non-linear classes of operation), a simple first order Taylor-series where the LSOP is defined with only v_{10}, v_{20} and $|a_{11}|$ would not provide a sufficient approximation of the poly-harmonic behaviour of the power-transistor. A way

to alleviate this problem is to expand the number of variables of the LSOP to include the most significant variables of the non-linearity and linearize the rest of the PHD model variables (which are assumed to be less significant and thus modeled with a first-order linear approximation).

For a typical power-transistor device, these extra LSOP variables from the polar form of the PHD model input variable space (refer to equation 3.22) can typically include all or some of these variables: $|a_{21}|$, $\angle a_{21}$, $|a_{12}|$, $\angle a_{12}$, $|a_{22}|$ and $\angle a_{22}$. These variables become significant for highly non-linear classes of power amplifier operation due to the passive reflection coefficient provided by the matching networks on both the load and source side of the power transistor. Since the reflection coefficient of the passive matching network is reflecting back some of the reflected power-wave from the power transistor back into the transistor (e.g. $a_{ph} = \Gamma_{ph} b_{ph}$), we can make the X-parameters as a function of the LSOP defined by v_{10}, v_{20}, $|a_{11}|$ and also as a function of the additional passive reflection coefficients Γ_{21}, Γ_{12} and Γ_{22} (using the reflection coefficient defined PHD model of section 3.3.1.3). For the simple LSOP extension where we only make the X-parameters as a function of Γ_{21}, we have:

$$\begin{aligned}\tilde{b}_{ph} &= X_{ph}^{(F)}(v_{10}, v_{20}, |a_{11}|, |\Gamma_{21}|, \angle\Gamma_{21}) \\ &\quad + \sum_{q,i} (X_{ph,qi}^{(S)}(v_{10}, v_{20}, |a_{11}|, |\Gamma_{21}|, \angle\Gamma_{21})\tilde{a}_{qi} + X_{ph,qi}^{(T)}(v_{10}, v_{20}, |a_{11}|, |\Gamma_{21}|, \angle\Gamma_{21})\tilde{a}_{qi}^{*}) \quad (3.43)\end{aligned}$$

where $\{q, i\} \notin \{\{1, 1\}, \{2, 1\}\}$.

To extract the parameters in equation 3.43 in measurement, we need to vary the fundamental load and measure the partial derivative parameter dependencies for each load condition. A measurement setup similar to a typical load-pull measurement is needed for the extraction of a model described by this equation [18].

If passive impedance tuners are used for measurement, a further extension of the LSOP to include reflection coefficients at harmonic frequencies at the source or the load side of the power transistor will require at least two multi-harmonic impedance tuners. In addition it quickly becomes apparent that the more the number of LSOP variables grows, the measurement space complexity for the extraction of the X-parameter model grows exponentially.

There is a trade-off here that should also be considered, the more variables are added to the LSOP, the more of the non-linearity is described solely by the $X_{ph}^{(F)}$ function (which unlike the $X_{ph,qi}^{(S)}$ and $X_{ph,qi}^{(T)}$ functions has no modeling capability and is only the scalar

coefficient in the first-order Taylor series approximation). Agilent has used an interpolation of a look-up table (indexed for different values of the LSOP variables) as an implementation of the $X_{ph}^{(F)}$, $X_{ph,qi}^{(S)}$ and $X_{ph,qi}^{(T)}$ functions.

3.3.3 The Cardiff PHD Model

In the Cardiff PHD model formulation developed at Cardiff University, a multidimensional Fourier series function is used as a basis to approximate the PHD function of equation 3.22 ($\tilde{f}_{ph_{polar}}^{(p)}$) [21]. The insight here is that the PHD model function described in polar form is periodic with respect to the angle variables ($\angle a_{21}$, $\angle a_{21}$, $\angle a_{22}$ and so on). This means that by fixing the values of the magnitude variables (v_{10}, v_{20}, $|a_{11}|$, $|a_{21}|$, $|a_{22}|$ and so on), we can fit a multidimensional Fourier series to the PHD function for each value of the magnitude variables. The parameters representing the Cardiff PHD model are then simply these multidimensional Fourier series coefficients as a function of the magnitude variables.

As an example, in the simplified case where the reflected power-waves of the Cardiff PHD model is only a function of $|a_{11}|$, $|a_{21}|$, $\angle a_{21}$, $|a_{22}|$ and $\angle a_{22}$; for a fixed DC bias voltage v_{10} and v_{20} we have:

$$\tilde{b}_{ph} = \tilde{f}_{ph_{polar}}^{(p)}(v_{10}, v_{20}, |a_{11}|, |a_{21}|, \angle a_{21}, |a_{22}|, \angle a_{22}) \tag{3.44}$$

$$\tilde{b}_{ph} = \sum_{n}\sum_{r} G_{ph,n,r}(|a_{11}|, |a_{21}|, |a_{22}|)e^{j(n\angle a_{21} + r\angle a_{22})} \tag{3.45}$$

The functions $G_{ph,n,r}$ in equation 3.45 are functions of the magnitude variables. These functions define the Cardiff model. A multi-variate polynomial (that is a function of theses magnitude variables) can be used to fit these $G_{ph,n,r}$ functions. It is apparent that the number of functions required by the Cardiff model increases when the order of the Fourier series (signified by the letters n and r in equation 3.45) increases and the model complexity also increases. The solution provided by the Cardiff group is to prune these functions and only include the most significant Fourier series coefficient functions in the final model. This is done by looking at the relative magnitude of $G_{ph,n,r}$ functions and only including the most significant ones in the model.

For a simple two variable Cardiff PHD model with only a_{11} and a_{21} as the large signals, we have:

$$\tilde{b}_{ph} = \sum_{n} G_{ph,n}(|a_{11}|, |a_{21}|)e^{j(n\angle a_{21})} \tag{3.46}$$

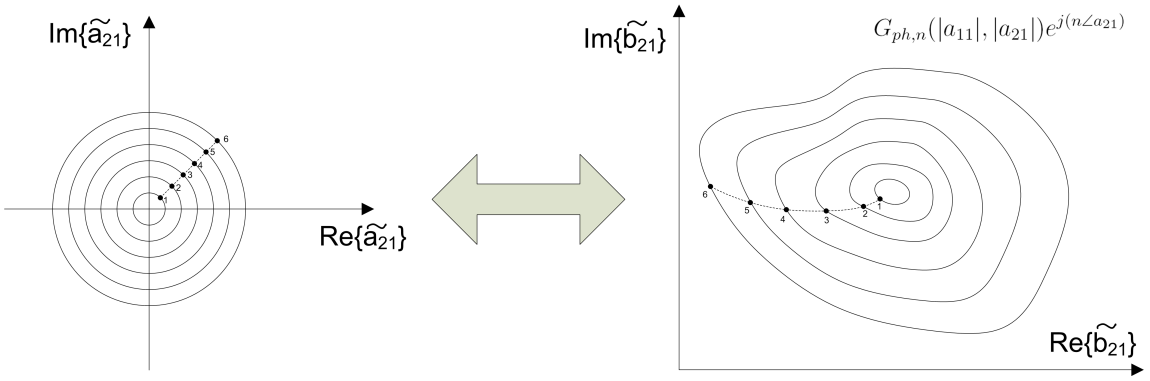

Figure 3.6: Change in b_{21} with constant $|a_{11}|$ and a polar sweep of a_{21}

For the simple case described by equation 3.46, figure 3.6 shows an example variation of the b_{21} power-wave when the input fundamental power-wave magnitude $|a_{11}|$ is held constant and for each magnitude of the output port incident power-wave ($|a_{21}|$), its phase ($\angle a_{21}$) is swept. Each contour of variation of a_{21} (any one of the concentric circles on the left graph) in this figure corresponds to a contour of variation in b_{21}. Each contour in the graph of b_{21} shown in figure 3.6 is described by its Fourier series coefficients $G_{ph,n}$ for the fixed value of $|a_{11}|$ and $|a_{21}|$ that represents the contour. The numbered line in the figure corresponds to a constant phase $\angle a_{21}$ and increasing magnitude $|a_{21}|$.

A limitation of the Cardiff PHD model compared to the X-Parameter PHD model described in section 3.3.2 is that the effects of the higher harmonic input power-waves cannot be included without blowing up the number of Fourier series functions needed to describe the model. This is why most Cardiff PHD models are truncated up to the effects of the second harmonic only [21].

3.4 What are Poly-Harmonic Distortion Models Good For?

From the beginning of section 3.3 where PHD models introduced based on the Volterra framework, the assumption was made that the voltage and current waveforms are non-linear CW signals (described by equations 3.7 through 3.10). Since power amplifiers are used to amplify vector modulated signals and not CW signals, we should note that the PHD model is not necessarily correct for modeling the power transistor behaviour under arbitrary modulated signals. In fact, wide-band modulated signals exhibit long-term memory effects that cannot be modeled by a PHD model that can only model quasi-static (non-linear CW) responses.

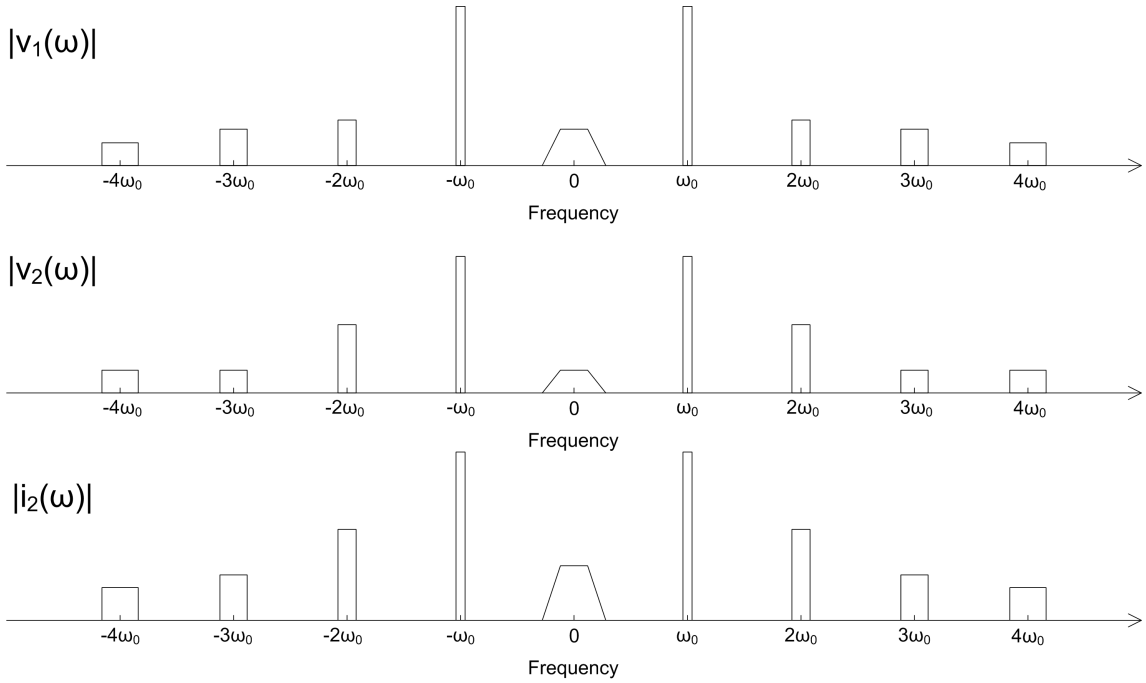

Figure 3.7: Narrow-band modulated signals in a Volterra system

The class of modulated signals that approach CW signal behaviour are narrow-band modulated signals. Figure 3.7 shows how the spectrum of the voltage and current signals would look for a Volterra system under the stimulus of a narrow-band modulated signal. It seems apparent as the bandwidth of the modulation decreases, the envelope of the signal around each harmonic frequency approaches constant tone behaviour (that is, figure 3.7 approaches figure 3.3). This means that the time-domain waveform for a narrow-band modulated signal looks like a slowly varying version of the non-linear CW signals of figure 3.4. If the window of the Short Term Fourier Transform (STFT) is small enough to be on the order of magnitude of the period of the centre frequency of modulation, then the STFT of the narrow-band modulated signal will look like the non-linear CW tone used to derive the PHD model.

For power-amplifiers stimulated with narrow-band modulated signals, the long term memory effects are not significant and the time-domain shape of the modulated signal is close to the shape of non-linear CW signals. PHD models are thus suitable for designing the matching networks of narrow-band power amplifiers for desired behaviour.

Chapter 4

Narrow-band Non-linear Measurement of a Power Transistor

In chapter 3 the power transistor was described as a two-port Volterra system and various PHD models were derived to describe the behaviour of the power transistor that is useful for the design of narrow-band power amplifiers. The PHD models described can only become useful if their parameters are extracted from a physical power amplifier device.

In this chapter, we will discuss the measurement approaches used to extract PHD model parameters. This includes a discussion of the necessary measurement equipment and the methods involved in exciting the power transistor to a state required by each model.

4.1 The PHD Model Measurement Requirements

The set of periodic signals described by equations 3.7 through 3.10 represent the behaviour of the voltage and current signals at either port of the power transistor when it is excited by a poly-harmonic periodic signal with a fundamental frequency of $\omega_0 = 2\pi f_0$. This quasi-static periodic behaviour of the power transistor represents a single point in the PHD model space. To be able to extract a PHD model, we need to be able to traverse this space by exciting the power transistor with different poly-harmonic inputs and measuring its poly-harmonic response.

Figure 4.1 shows the variables that should be set and the variables that should be measured at each port in order to extract a PHD model. The DC voltage at each port of the transistor (v_{10} and v_{20}) can be set via a DC bias circuit connected to each side of the transistor. The DC currents (i_{10} and i_{20}) can then be measured at each port with DC current meters.

The following sections will describe how we can excite the power transistor with specific

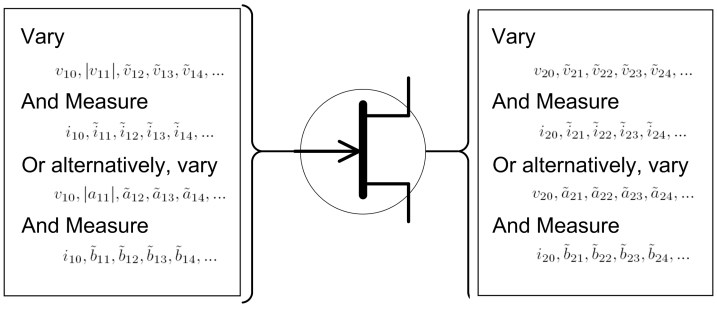

Figure 4.1: PHD model measurement procedure at each port

periodic CW tones (with control over the magnitude and phase of the harmonic frequencies as well as the fundamental) and how to measure the periodic current and voltage response at fundamental and harmonic frequencies at either port of the power transistor.

4.2 Non-linear Continuous Wave Signal Measurement Instruments

There are two main types of measurement devices that allow us to measure the spectral contents (both magnitude and relative phase) of a periodic signal at a specific frequency and its harmonics. These two devices are the Large Signal Network Analyzer (LSNA) and the Non-linear Vector Network Analyzer (NVNA) [22]. In terms of their measurement capability to capture the measurement data necessary to generate a PHD model, both technologies result in the same measurement. That is, both devices measure the voltage and current spectral contents at both ports of the power transistor with the relative phase information.

The main difference between these RF non-linear measurement instruments is that LSNAs are sampler-based while NVNAs are mixer-based instruments. Both techniques are competitive for the measurement of PHD models.

An LSNA uses samplers to perform the down conversion of the high-frequency signals to the IF spectrum by using harmonic sampling [23]. With an LSNA the whole spectrum of the voltage and current is measured at once. To get an accurate relative phase reading on an LSNA, a phase calibration needs to be performed against a phase reference element.

An NVNA on the other hand uses the heterodyne principle to down-convert the RF signals to the IF spectrum [24]. The NVNA needs to extract each spectral component separately. In order to measure the relative phase of the spectral components with respect to each other, the NVNA uses a harmonic phase reference during measurement. When

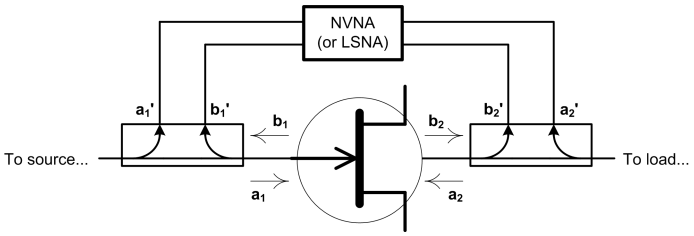

Figure 4.2: NVNA (or LSNA) measurement of the non-linear CW signal using dual directional couplers

calibrating the phase measurement of the NVNA, another harmonic phase reference is needed to perform the calibration.

By targeting only a specific fundamental frequency and its harmonics, both instruments are capable of reconstructing the non-linear continuous wave voltage and current at both ports. The NVNA (or LSNA) usually interfaces with the power transistor through two dual-directional couplers (one at each port). These couplers allow for a sampling of both the forward traveling and backward traveling power-waves at the interfaces of the power transistor. Using couplers allow us to measure the waves at the power transistor with minimal interference with the signal itself. Figure 4.2 shows the non-linear measurement ($a_1^{'}$, $b_1^{'}$, $a_2^{'}$ and $b_2^{'}$) is a low-power sampled version of the actual non-linear power-waves at the interface of the power amplifier (a_1, b_2, a_2 and b_2). From these measured power-waves (and knowing the attenuation factor of the directional couplers), the NVNA (or LSNA) can deduce the time-domain voltage and current waveforms through the use of equations 3.18 and 3.19 and the inverse Fourier transform [22].

4.3 Multi-harmonic Load and Source Pull

In section 4.2, the method used to measure the non-linear CW tones at each port was described. Now it is necessary to consider the equipment necessary to force a specific non-linear CW tone at the port of a transistor. A multi-harmonic load pull measurement setup can help us vary the RF components on the right hand side of figure 4.1, while a multi-harmonic source pull measurement setup can help us vary the RF components on the left hand side of the figure.

The concept of a load pull measurement was introduced by RF engineers who wanted to map out various performance measurements of interest produced by the power transistor for varying loading impedance conditions. This way they are able to find an optimal load matching network that allows for either maximum output power, maximum gain or maximum efficiency [3]. A varying load effectively imposes a voltage on the output port

of the device based on what current is produced at that port. Meaning, that if we have a load impedance of Z_{21} at the fundamental frequency presenting itself at the output port, we will have:

$$v_{21} = Z_{21} i_{21} \tag{4.1}$$

$$a_{21} = \Gamma_{21} b_{21} \tag{4.2}$$

where $a_{21} = \frac{v_{21}+Z_0 i_{21}}{2}$, $b_{21} = \frac{v_{21}-Z_0 i_{21}}{2}$ and $\Gamma_{21} = \frac{Z_0-Z_{21}}{Z_0+Z_{21}}$. Note that Γ_{21} is the reflection coefficient (at reference impedance Z_0) presented to the power transistor at the load. Simple algebra shows that equations 4.1 and 4.2 are equivalent. We can now see that the effect of the load pull measurement is to re-introduce an input signal back at the load side of the transistor (either a voltage or an incident power wave depending on the modeling framework being used). We can extend this idea of presenting impedances to all the harmonic frequencies as well as on both sides of the power transistor (meaning that we control the Z_{ph} impedances presented at port p and harmonic index h). This is what is meant by a multi-harmonic load and source pull system. By varying these impedances, we vary the non-linear CW signal that is being presented to each port of the power transistor.

There are many highly-efficient but non-linear emerging PA classes of operation that can be defined by their matching network design space. This means that the set of impedances that the input and output matching networks provide to the power transistor will determine the class of operation of the PA. If we can steer our PHD model measurements into load and source conditions that are highly non-linear but provide good power efficiency, we can design PAs for these classes of operation using CAD tools.

There are different ways to synthesize the impedances at the load and source of the power transistor device. In sections 4.3.1 through 4.3.2 we will discuss them.

4.3.1 Passive Load and Source Pull

If we use passive impedances to reflect back voltages (or incident power-waves) into the power transistor at both ports and the frequencies of interest, then we have a passive load and source pull system. Generally passive multi-harmonic impedance tuners are used on each side of the transistor. These impedance tuners are mechanical devices that reconfigure themselves to tune for requested impedances at a fundamental frequency and multiple harmonics (generally up to the 3rd harmonic). Figure 4.3 shows the multi-harmonic passive load and source pull measurement setup.

The only active part of the transistor excitation comes from the fundamental frequency

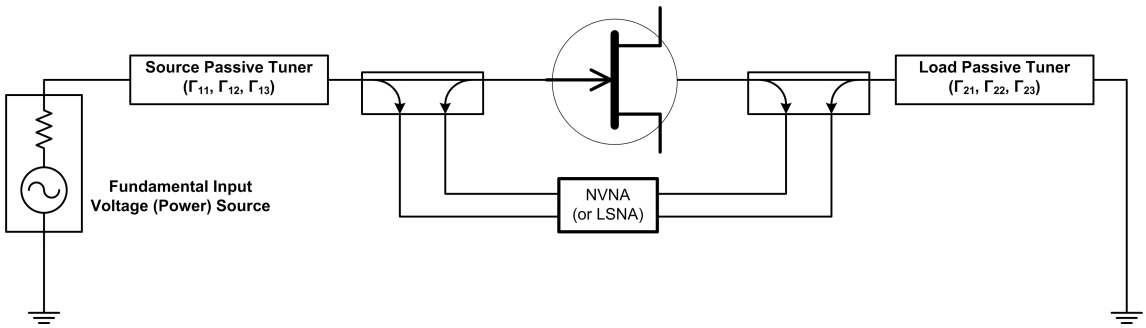

Figure 4.3: Passive load and source pull measurement setup (with the passive tuners outside)

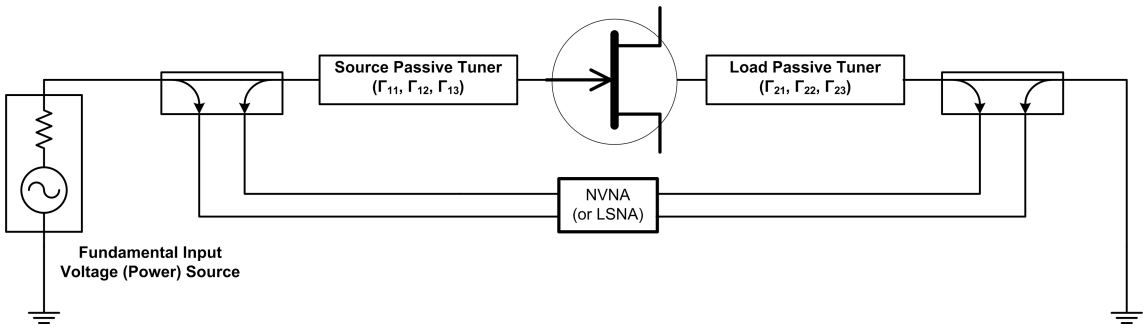

Figure 4.4: Passive load and source pull measurement setup (with the passive tuners inside)

signal source at the input (which provides $|v_{11}|$ or $|a_{11}|$). This is similar to the condition that the power transistor will be in when it is operated as a power amplifier. The main signal to be amplified will be inserted at the fundamental frequency at the source and the matching networks provide static impedances at either side. It should be noted that passive tuners can only provide passive reflection coefficients ($|\Gamma| < 1$). For single PAs designed with passive matching networks (with no cascading of PAs), the reflection coefficients seen at the transistor ports will always be passive as a result (a passive-element matching network can never provide a $|\Gamma| > 1$). Thus a PHD model derived from a passive load and source pull measurement setup will span the PA matching network design space.

Passive tuners have certain physical limitations in terms of the impedances they can produce. Usually there is a hard limit in terms of the maximum number of harmonic impedances you can control. The values of the higher harmonic impedances can be measured by the tuner but setting them is not possible.

Not all impedances can be produced by the passive tuners. For example, a perfect short or a perfect open circuit impedance can never be physically provided at a given frequency. Typically, the value of the reflection coefficient that can be synthesized is limited to a magnitude of 0.9 in a $Z_0 = 50\Omega$ Smith chart.

The directional couplers can either be inside the passive tuners (as they are in the figure 4.3) or outside of them (as in figure 4.4). In the case where the couplers are on the inside, the reflection coefficient provided at the passive tuner needs to be de-embedded through the coupler to get the reflection coefficient that the power transistor is seeing. However if the coupled signal at the power transistor is already small, it might go below the noise floor when it propagates through the tuner. This is why for measuring low signals, it is better to put the couplers in between the tuners and the power transistor.

If the couplers are put after the passive tuners, then the reflection coefficient synthesized by the tuner will be exactly at the power transistor interface. However now the measurement at the coupler needs to be de-embedded through the tuner in order for the measurement to be at the transistor port plane. This is why having a good linear model of the couplers and the passive tuners is necessary for an accurate measurement of the power transistor behaviour.

A drawback of using passive tuners for load and source pull purposes is that since they are mechanical devices, they take some time to reconfigure to change between impedance settings. This means that if the RF measurement engineer wants to sweep many impedance conditions, the total time needed for measurement can be very long.

The load-dependent X-parameter formulation developed in section 3.3.2.1 is well suited to be extracted using the passive source and load pull measurement system described here. For every passive load and source condition that is swept, an X-parameter model can be extracted by sweeping the input power magnitude and injecting an extraction tone at each input power level that will allow us to extract the partial derivative parameters of the X-parameter model. We will discuss this extraction tone concept in more detail in section 4.4.

Since the X-parameter model uses the power-wave defined PHD model (refer to section 3.3.1.1), we can take advantage of the fact that the reflected power-wave back into a transistor is zero if the impedance seen is the same as reference impedance used to define the power-wave. This means that if we are using 50Ω defined power-waves, there is no reflection back into the power transistor from the load if the load is also at 50Ω.

4.3.2 Active Load and Source Pull

In the active load and source pull technique, the incident power-waves presented to the power transistor at each port and harmonic index is not the result of reflection off a passive impedance at the source or load side of the transistor. Instead the reflected power-wave from the transistor is absorbed and another power-wave generated by another source is

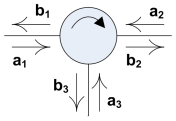

Figure 4.5: The ideal circulator

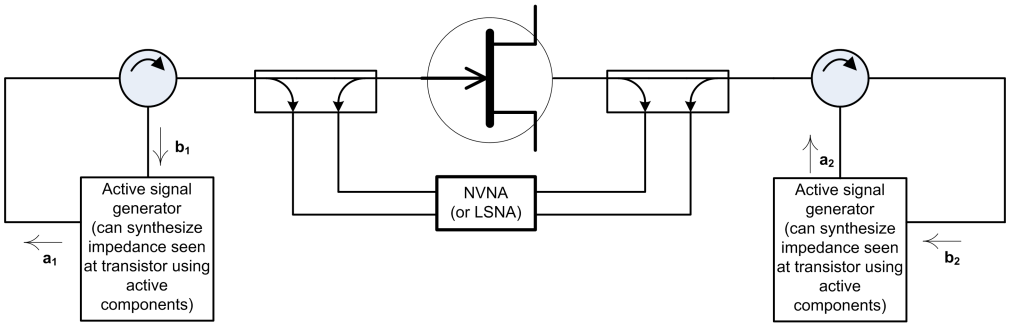

Figure 4.6: Active load and source pull measurement setup

injected back into the power transistor. This active source presents an effective impedance at the interface of the device. A measurement setup that presents active impedances to both sides of the transistor at the fundamental frequency and its harmonic frequencies is called a multi-harmonic active load and source pull measurement setup.

To be able to absorb the reflected power-wave from the transistor and to inject our own desired incident power-wave back into the transistor, we can use a three-port microwave device known as a circulator (shown in figure 4.5). For an ideal circulator we have:

$$b_1 = a_3 \tag{4.3}$$

$$b_2 = a_1 \tag{4.4}$$

$$b_3 = a_2 \tag{4.5}$$

Figure 4.6 shows the active load and source pull measurement setup required to extract a PHD model. We can see from this figure that any power-wave reflected from the power transistor is detected so the appropriate incident power-wave can be re-injected back into the transistor through the circulator. The RF signals that need to be varied at each port of the power transistor (see figure 4.1) are then generated by either multiple tone generators at the fundamental and harmonic frequencies (that are synchronized for phase coherence) or a single high-power arbitrary waveform generator. Regardless of how the non-linear CW signal is generated, it is injected back into the power transistor to steer us where we want

in the PHD model space.

Since active devices are used to generate the injected signal, we can produce active reflection coefficients ($\Gamma > 1$) which correspond to negative resistance values. While these operating conditions for the power transistor under a non-linear CW signal do not occur when the transistor is used in a single power transistor PA with passive matching networks, circuits with multiple transistors can have one transistor load another and produce an active impedance at the interface of the other transistor. The Doherty PA configuration is an example of a case where one PA is actively loading another PA [3].

Since in active load and source pull we avoid the use of mechanical passive tuners, measurement is quite faster in comparison to passive load and source pull. However unlike the passive measurement where only a single frequency power source is needed, a much more involved active waveform generation scheme is required by active loading measurement systems.

To achieve high magnitudes of reflection coefficient at the load (primarily for the fundamental load reflection coefficient Γ_{21}), we need to inject a significantly high-power incident power-wave. This is because $\Gamma_{21} = a_{21}/b_{21}$, and since b_{21} is large (it is after all the amplified signal so it is the most significant signal in the circuit), we need to inject a very high power a_{21} to get a high reflection coefficient. This is why the linearity and high-power performance of the active sources becomes important. This puts a requirement on the capabilities of our active sources if we are to achieve these points in the PHD model space.

The Cardiff PHD model (discussed in section 3.3.3) has been developed and validated using an active source and load pull measurement setup [21]. Since for the Cardiff model one needs to vary multiple large signals relative to each other, it becomes apparent why an active measurement setup is a lot more convenient than a passive measurement setup for the extraction of this model.

4.3.3 Hybrid Load and Source Pull

In section 4.3.1 we mentioned that the there is a limit to what reflection coefficients the passive tuners can provide (and sometimes for designing PAs, we need to put a reflection coefficient right at the edge of the Smith chart). In section 4.3.2 we saw that to have a high synthetic reflection coefficient, we sometimes need to inject back high magnitude power-wave signals which requires very linear high power drivers. The hybrid load and source pull techniques is a "best of both worlds" approach to the problem [25]. The idea here is to use a passive impedance to reflect back as much of the power-wave as the passive tuners allow us to and then inject the rest of the power needed to reach the impedance of

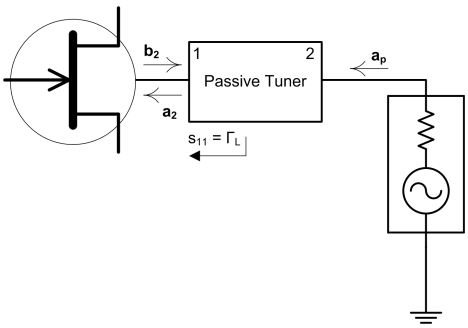

Figure 4.7: Hybrid power transistor loading technique

interest using an active signal.

Figure 4.7 shows the hybrid load and source pull concept. When the active power source is off ($a_p = 0$ in figure 4.7), we have:

$$a_2 = b_2 s_{11} = b_2 \Gamma_L \tag{4.6}$$

where s_{11} is an S-parameter of the two-port passive tuner (which is the same as the passive reflection coefficient Γ_L). When the active power source is on ($a_p \neq 0$), we get:

$$a_2 = b_2 s_{11} + a_p s_{12} = b_2 \Gamma_L + a_p s_{12} \tag{4.7}$$

where s_{11} and s_{12} are S-parameters of the two-port passive tuner and Γ_L is the passive reflection coefficient. We can see that the incident power wave a_2 in equation 4.7 is the result of both the reflection from the passive tuner and the active injected signal. This increases the magnitude of the effective reflection coefficient at the power transistor load interface. The effective reflection coefficient is thus:

$$\Gamma_{L_{eff}} = \frac{a_2}{b_2} = \Gamma_L + \frac{a_p s_{12}}{b_2} \tag{4.8}$$

This technique will allow us to reach impedance terminations that are at the edge of the Smith chart without using very high-power linear drivers.

4.4 The Extraction Tone Concept in the X-parameter Model

While the multi-harmonic load and source pull concepts discussed in section 4.3 provide enough measurement capability to extract a Cardiff PHD model (formulated in section 3.3.3), an X-parameter model (formulated in section 3.3.2) requires an extra stimulus signal

known as an extraction tone in order to extract the partial derivative terms associated with the model.

Since the X-parameter model is a first-order Taylor series linearization of the PHD model space around an LSOP, we will first need to bring the power transistor to this LSOP and perform slight deviations around this point in the PHD model space to extract the partial derivative terms. One (or a few) secondary sources can be used to inject the extraction tone at either side of the power transistor at the appropriate harmonic frequencies.

In order to extract all the partial derivative terms of the X-parameter model (the $X^{(S)}$ and $X^{(T)}$ terms of equations 3.35 or 3.43), we need to make sure that each of the small signal input variables of the PHD model (basically the input variables that are not LSOP variables) varies slightly and the effect on all the outputs of the PHD model is measured.

The non-linear CW voltage and current signals at either port of the power transistor for every single extraction tone insertion should be recorded and grouped together for a single LSOP point. The partial derivative parameters will then be extracted from this set of measurements as a function of the LSOP.

Injecting an extraction tone is basically the same as performing a small active loading at the frequency where the extraction tone is injected. If the LSOP includes a specific value for a load (or source) reflection coefficient, it is important that no extraction tones are injected at that port and harmonic index. This causes the effective reflection coefficient seen by the transistor to vary because of the hybrid loading effect seen in equation 4.8. Since we do not wish to change the LSOP variables when extracting the partial derivative terms, it is important not to inject the extraction tone at incident power-wave locations that we are not linearizing around.

Figure 4.8 shows the passive multi-harmonic load and source pull measurement setup with two phase coherent power sources to extract an X-parameter PHD model. One power source will sweep the fundamental frequency power at the source side of the transistor. The other power source will be used to inject a small signal tone at either side of the transistor and at one of the frequencies of interest (f_0, $2f_0$, $3f_0$, ...). If the four switches in figure 4.8 are set to position 1, the extraction tone will inject a signal a small signal extraction tone at the source side of the transistor, while if the switches are at position 2, the extraction tone will be injected at the load side of the transistor.

We will now study the effect of using an extraction tone in the measurement of various X-parameter models.

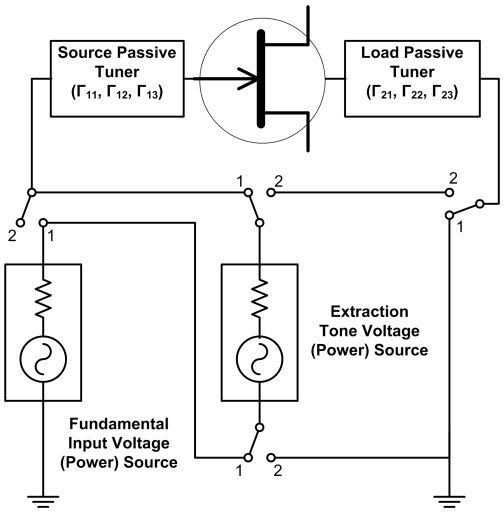

Figure 4.8: Extraction tone injection using switches and two power sources

4.4.1 Extraction Tone Injection in 50Ω-matched Conditions

To study the effect of the injection of an extraction tone, we will take as a case study the example of a power transistor that is conjugately matched at the fundamental frequency at the input port (to ensure optimal power transfer from the power source to the power transistor) and the impedance is set to 50Ω at all port p and harmonic index h (where $\{p,h\} \notin \{\{1,1\}\}$).

Here we will be using the power-wave defined PHD model (defined by equation 3.20). This is a simple case where the LSOP is only defined by the magnitude of the fundamental input power $|a_{11}|$. In this example, Γ_{11} in figure 4.8 is set to provide good power transfer from the fundamental input power source to the transistor while all other reflections coefficients set by the passive tuners (Γ_{12}, Γ_{13}, Γ_{21}, Γ_{22}, Γ_{23}) are all set to zero. If using power-wave definitions with a reference impedance of $Z_0 = 50\Omega$ (see equations 3.16 and 3.17), this is easily done by setting the impedances of the tuner to $Z_{12} = Z_{13} = Z_{21} = Z_{22} = Z_{23} = 50\Omega$.

When the fundamental input power source is turned on (while the extraction tone source is off), the transistor will generally scatter power at both ports and at the fundamental frequency and its harmonics. That is, generally in the PHD model space, the reflected power-wave at port p and harmonic index h, b_{ph} is non-zero (for $\{p,h\} \notin \{\{1,1\}\}$). Here, the reflection coefficients set to zero above will result in the incident power-wave at port p and harmonic index h, a_{ph} is zero (for $\{p,h\} \notin \{\{1,1\}\}$) *by definition*. This is because:

$$a_{ph} = \Gamma_{ph} b_{ph} \tag{4.9}$$

When the extraction tone source is turned on at a single port p' and set to harmonic frequency index h', the reflection coefficient seen by the transistor will vary away from zero. This is because of the hybrid-loading effect seen in equation 4.8. In this case $\Gamma_{p'h'} \neq 0$, and the small signal extraction tone $a_{p'h'}$ will be injected into the power transistor. However for all the incident power-waves at port p and harmonic index h, we have $a_{ph} = 0$ (where $\{p, h\} \notin \{\{1, 1\}, \{p', h'\}\}$). This results in the X-parameter formulation of equation 3.35 collapsing into the following form when each extraction tone is injected:

$$\tilde{b}_{ph} = X^{(F)}_{ph}(v_{10}, v_{20}, |a_{11}|) + X^{(S)}_{ph,p'h'}(v_{10}, v_{20}, |a_{11}|)a_{p'h'} + X^{(T)}_{ph,p'h'}(v_{10}, v_{20}, |a_{11}|)a^*_{p'h'} \quad (4.10)$$

The relationship of equation 4.10 shows that we can potentially individually extract the partial derivative X-parameter coefficients ($X^{(S)}$and $X^{(T)}$ parameters) by making sure the extraction tone is only injected at a single side of the transistor and only at one frequency. This can only be achieved if the device is matched to 50Ω impedances at all frequencies of interest.

To extract all the partial derivative parameters of the X-parameter model, we need to inject the extraction tone at all the port p and harmonic index h (where $\{p, h\} \notin \{\{1, 1\}\}$) in order to make sure that the device sees variation in all the inputs of the PHD model space. At each port and harmonic that the injection of an extraction tone is necessary, it is required to inject multiple different extraction tones with varying phases (with respect to the fundamental input phase reference) and measure the response of the device separately for each extraction tone injection. This will assure that we get a good permutation around the LSOP in the PHD model space in order to extract the partial derivatives of the non-linearity in this space.

4.4.2 Extraction Tone Injection in Unmatched Conditions

In a more general case than examined in section 4.4.1, all the impedances at all the harmonics cannot practically be realized at 50Ω. For example, if the passive tuners in figure 4.8 are set to provide 50Ω impedances up to the third harmonic, there is no guarantee that the impedance seen by the power transistor at the fourth and fifth harmonic frequencies are also 50Ω (in fact they generally aren't 50Ω). In addition, if we want to expand the LSOP of the X-parameter model to include the variation of the model parameters with respect to certain impedance variations at the load and/or source side of the transistor, then these reflection coefficients will also be non-zero.

In the most general unmatched condition of the device, none of the impedances at

either port of the device will be 50Ω at any of the frequencies of interest. In this most general case, the injection and variation of an extraction tone $a_{p'h'}$ at port p' and harmonic index h' will generally result in a variation of the reflected power-wave b_{ph} at all ports p and harmonic indices h. Since the reflection coefficient at ports p and harmonic indices h, Γ_{ph} is generally non-zero, then the incident power-wave a_{ph} at all ports p and harmonic indices h will also vary as a result. This means that the injection and variation of one extraction tone at one port p' and harmonic index h' results in the variation of the incident power-wave at all the ports p and harmonic indices h.

It should be noted that the hybrid-loading effect seen in equation 4.8 and discussed in section 4.3.3 only happens at the port and harmonic index where the extraction tone was injected. All the other reflection coefficients are set by the passive tuners. This means that as long as the extraction tone is not injected at the port and harmonic index corresponding to a reflection coefficient that is part of the LSOP, the LSOP does not vary as the extraction tones are injected.

Chapter 5

Extraction and Validation of Poly-Harmonic Distortion Models

In chapter 3 various poly-harmonic distortion models were derived based on the Volterra framework assumption for modeling the electromagnetic behaviour of a power transistor. Then in chapter 4 the measurement procedure required and the various techniques employed to extract these PHD models were discussed. In this chapter, we explore how the parameters of each of these models is extracted from the measurements and how these models are implemented within a commercial harmonic balance simulator. The performance of each model will be compared at various impedance matching conditions of the power transistor and the strengths and weaknesses of each model will be discussed.

5.1 Extraction of NVNA Measurements from Simulation of Compact Model

For the purpose of comparing the various PHD behaviour models discussed in this thesis, instead of measuring the behaviour of a power transistor on a lab bench using an NVNA (or LSNA) and a load and source pull measurement setup, the behaviour of the power transistor will be extracted from a known fairly accurate compact model (with periodic continuous wave stimulus) of the device under harmonic balance simulation (discussed in section 2.2.2). A compact model, as discussed in section 2.1.2, is a time-domain representation of the nonlinear behaviour of the power transistor (as seen in the time-domain intrinsic transistor relations of equations 2.1 and 2.2), while the PHD models that we plan to extract from this model will be defined solely in the frequency domain. This ensures that the comparison between the behavioural models is done based on the ability of each formulation to fit a

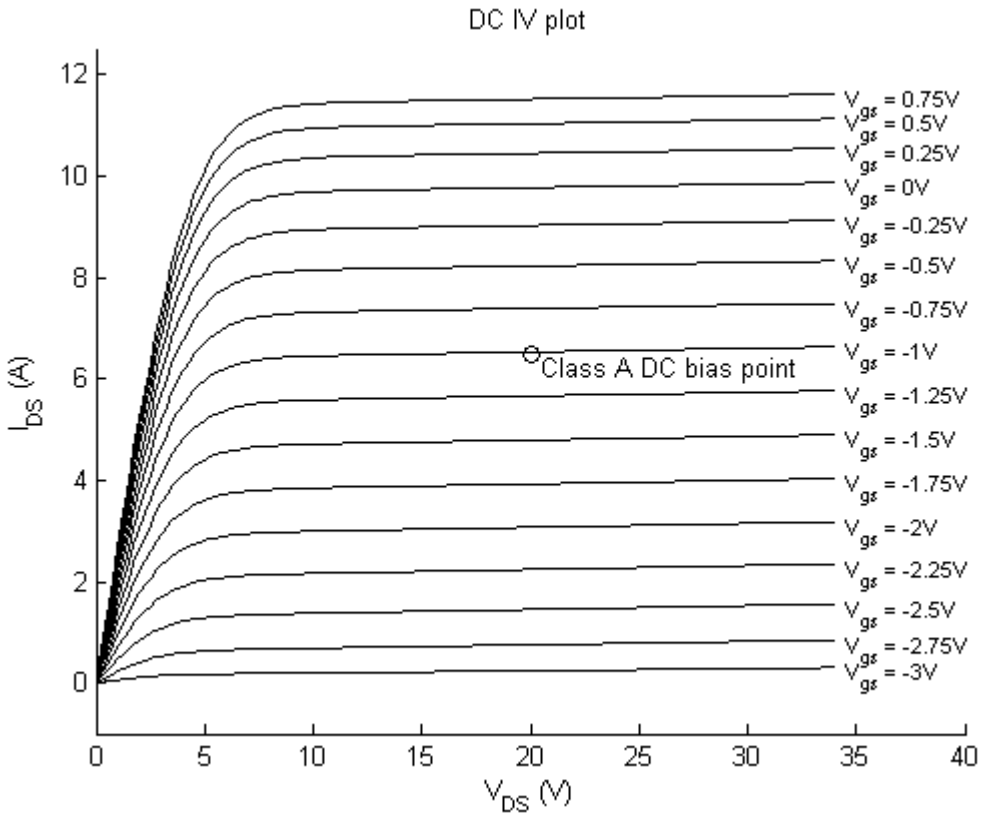

Figure 5.1: DC voltage and current characteristics of the $45W$ Cree transistor compact model

deterministic non-linear representation of the transistor that does not vary over time and is not susceptible to measurement, calibration or human error. For the purpose of the comparison here a manufacturer compact model of a $45W$ Cree transistor is used.

Figure 5.1 shows the variation of the drain DC current against the variation of the drain and gate DC voltages. All the behavioural models extracted will have to have the same DC bias conditions for a proper comparison between them. This is because all PHD models discussed in this thesis are dependent on the DC bias voltages (v_{10} and v_{20}). A typical class A power amplifier bias point is chosen for this comparison. For class A operation, the power amplifier will be mostly linear up to a certain input power threshold where after that point the non-linearity starts increasing [3]. From the DC analysis of the $45W$ Cree power transistor (figure 5.1), we choose a DC bias of $v_{10} = -1V$ and $v_{20} = 20V$.

Performing a harmonic balance simulation on the power transistor compact model under the stimulation of various power tones or impedance matching conditions will emulate the NVNA (or LSNA) measurement done on the lab bench. Here as long as the simulator does not fail to converge to a periodic solution for the voltages at the nodes of the circuit,

we do not have to worry about the accuracy of the power, vector and phase calibration of the NVNA or the correct measurement of the S-parameters of the various passive components or the accuracy of the passive (or active) impedance tuners at emulating the desired reflection coefficient. By performing the extraction of these PHD models in simulation, we avoid all these issues and instead focus on how well each formulation can match the typical electromagnetic behaviour of a power transistor.

In this chapter, we will compare the performance of the following frequency-domain PHD behavioural models extracted from the same compact model:

1. 50Ω-matched X-parameter model
2. Γ_L-dependent X-parameter model
3. 2-variable (a_{11} and a_{21}) Cardiff model

The following steps outline the extraction and validation process used for the comparison performed in this thesis:

1. Stimulate the power transistor compact model with the conditions required by each model and simulate it using a harmonic balance simulator.
2. Export the voltage and current waveforms (with all the necessary harmonic content) solved for by the harmonic balance simulator.
3. Use these simulated measurements to extract each model's parameters.
4. Implement each behavioural model within a harmonic balance simulator based on the model parameters extracted in the previous step.
5. Perform fundamental input power sweeps on each of the behavioural models under various load and source impedance matching conditions and compare the scattered power at both ports and harmonic frequencies with the behaviour of the compact model under the same stimulus conditions.

5.2 Simulated PHD Model Extraction Procedure

To extract the 50Ω-matched X-parameter, Γ_L-dependent and 2-variable Cardiff PHD models in simulation, the circuit of figure 5.2 was used in the commercial harmonic balance simulator of Agilent ADS [26]. The DC bias is fed to the power transistor compact model through ideal RF choke components and the RF signals at both sides of the power transistor are fed through ideal DC block (RF pass) components. Two 2-port equation based

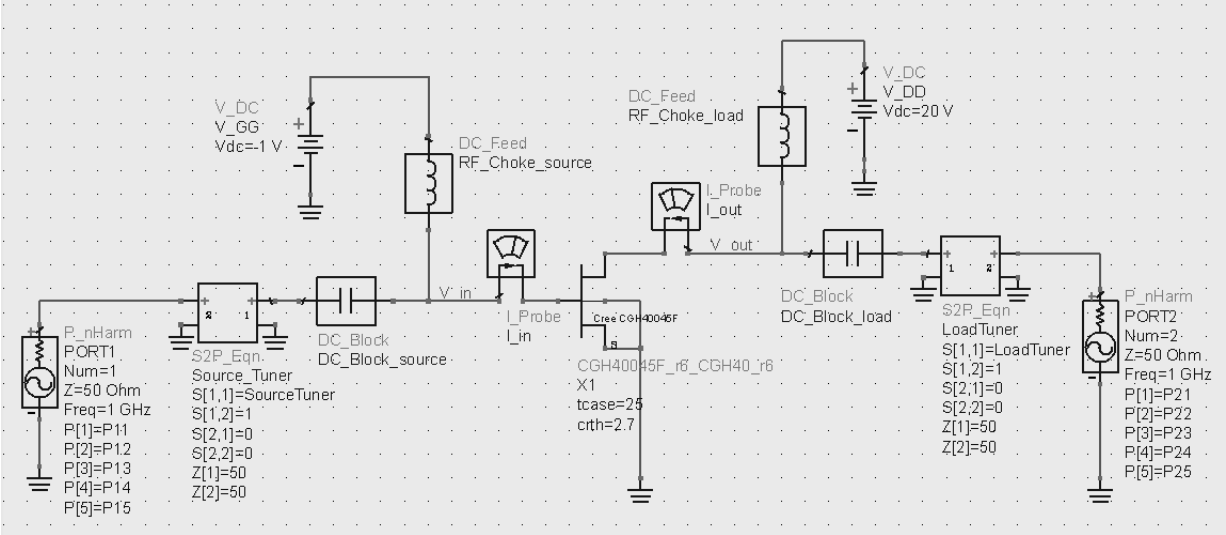

Figure 5.2: PHD model extraction simulation circuit

S-parameter blocks are used on either side of the simulated measurement circuit to emulate the effect of an arbitrarily set impedance (or more precisely the reflection coefficients with a 50Ω reference impedance) at all frequencies of interest. These passive tuner blocks are set up to fully let through the power injected through them by the power sources on either side of the power transistor. In this simulation circuit, power can arbitrarily be injected at either side of the power transistor at either the fundamental frequency (chosen to be $1GHz$ here) or its harmonic frequencies (set in the simulation circuit of figure 5.2 by setting the variables `P11`, `P12`, ..., `P21`, `P22`, ...).

The procedure used for extracting the behavioural models of interest here will be to sweep the powers and reflection coefficients (as required by each model) and perform a single harmonic balance simulation for each swept value. This means that the more swept variables we have to go through, the longer the entire simulation will take as there are more harmonic balance simulations that need to be performed.

All three of the PHD models compared here are dependent at least on the magnitude of the input fundamental frequency power-wave ($|a_{11}|$). This can be easily done in the simulation by sweeping the `P11` variable in the simulation circuit of figure 5.2. Since the power source labeled as `PORT1` has an input impedance of 50Ω, the value of `P11` determines power available from the power source (P_{avs}). This will be the power delivered to the source only if the impedance seen at the terminal input of the power transistor is 50Ω. By using the reference impedance of $Z_0 = 50\Omega$ to define the incident and reflected power-waves (described in equations 3.16 and 3.17) at the ports of the power transistor, we will have the following relationship between the power available from the 50Ω power source and the

50Ω-referenced fundamental input power-wave:

$$P_{avs} = \frac{|a_{11}|^2}{2Z_0} \tag{5.1}$$

The relationship of equation 5.1 holds since the input power-wave defined by equation 3.16 has a unit of Volts but the power available from source has a unit of Watts.

5.2.1 Simulated 50Ω-matched X-parameter Model Measurement

For the extraction of the 50Ω-matched X-parameter model in simulation, the following parameters are fixed:

1. The DC gate and drain bias voltages (v_{10} and v_{20}) are fixed to $-1V$ and $20V$ respectively (for class A power amplifier operation).

2. The impedances at the source and load side are set to 50Ω at all frequencies (to get a reflection coefficient of zero for a 50Ω referenced system).

3. The magnitude of the extraction tone power injected for this X-parameter model extraction is fixed to $0.1dBm$.

The variable sweep required for this extraction is performed in the following way:

1. Sweep the input fundamental frequency incident power-wave ($|a_{11}|$). For the purpose of this comparison, the input power is swept from $0W$ to $62W$ linearly with steps of $2W$, which results in 32 different power levels.

2. For each fundamental frequency incident power-wave magnitude, sweep the extraction tone injection port (the side of the transistor that the extraction tone will be injected in). Since this is a two-port system, there are two states for this swept parameter.

3. For each extraction tone input port, sweep the extraction tone injection frequency (the harmonic index that will have an extraction tone injected in). For the purpose of this comparison, we will have extraction tones injected up to the fifth harmonic so there will be five states for this swept parameter. The only point of caution is to not inject an extraction tone when the harmonic index is 1 and the injection port is 1 as we want to keep $|a_{11}|$ constant for each extraction tone injection.

4. For each extraction tone harmonic index, sweep the extraction tone phase. This ensures that partial derivative parameters are extracted with reference to the phase

variation of the small signal extraction tone. Even though we need a minimum of 3-phase variations to extract the parameters of equation 4.10, we will use eight swept extraction tone phases (spaced equally across 360°) to get a robust partial derivative extraction.

The parameter sweep described above will result in $32 \times 2 \times 4.5 \times 8 = 2304$ different harmonic balance simulations. For each of these simulations the current and voltage at DC and the frequencies of interested are extracted and indexed by their swept parameters. These measurements will be used to extract the 50Ω-matched X-parameter model.

5.2.2 Simulated Γ_L-dependent X-parameter Model Measurement

For the extraction of the Γ_L-dependent X-parameter model in simulation, the following parameters are fixed:

1. The DC gate and drain bias voltages (v_{10} and v_{20}) are fixed to $-1V$ and $20V$ respectively (for class A power amplifier operation).

2. The impedances at the source and load side are set to 50Ω at all frequencies except the fundamental frequency at the load side. We will refer to the fundamental frequency load side 50Ω-referenced reflection coefficient as Γ_L. The X-parameter parameters of this model will include this variable in its LSOP definition.

3. The magnitude of the extraction tone power injected for this X-parameter model extraction is fixed to $0.1dBm$.

The variable sweep required for this extraction is performed in the following way:

1. Sweep the magnitude and phase of the fundamental frequency load reflection coefficient Γ_L. For the purpose of this comparison, a polar sweep of the reflection coefficient is used with four different magnitudes (0.25, 0.5. 0.75 and 1) and eight phases (equally spaced from 45° to 360°) are swept for this complex parameter. In addition, the case of $\Gamma_L = 0$ is added into the measurements to get behaviour of the 50Ω-matched system. This results in a total of $4 \times 8 + 1 = 33$ different Γ_L values.

2. For each swept fundamental load reflection coefficient, sweep the input fundamental frequency incident power-wave (32 levels), extraction tone injection port (2 possible states), extraction tone injection frequency (from the second to fifth harmonic) and extraction tone phase (8 phases) exactly as was swept for the 50Ω-matched

X-parameter model parameter sweep. The only reason why we do not inject an extraction tone at the fundamental frequency is because we want to keep both $|a_{11}|$ and Γ_L constant for each extraction tone injection.

The parameter sweep described above will result in $33 \times 32 \times 2 \times 4 \times 8 = 67584$ different harmonic balance simulations. For each of these simulations the current and voltage at DC and the frequencies of interested are extracted and indexed by their swept parameters. These measurements will be used to extract the Γ_L-dependent X-parameter model.

5.2.3 Simulated 2-variable Cardiff Model Measurement

For the extraction of the 2-variable (a_{11} and a_{21}) Cardiff model in simulation, the following parameters are fixed:

1. The DC gate and drain bias voltages (v_{10} and v_{20}) are fixed to $-1V$ and $20V$ respectively (for class A power amplifier operation).

2. The impedances at the source and load side are set to 50Ω at all frequencies (to get a reflection coefficient of zero for a 50Ω referenced system). The variation of the fundamental load reflection coefficient will be the result of the active tone injected at the load.

The variable sweep required for this extraction is performed in the following way:

1. Sweep the input fundamental frequency incident power-wave ($|a_{11}|$). For the purpose of this comparison, the input power is swept from $0W$ to $62W$ linearly with steps of $2W$, which results in 32 different power levels.

2. For each fundamental frequency incident power-wave magnitude, sweep the magnitude of the output fundamental frequency incident power-wave ($|a_{21}|$). For the purpose of this comparison, the load fundamental power is swept from $0W$ to $16W$ linearly with steps of $0.5W$, which results in 33 different power levels.

3. For each load fundamental power magnitude, sweep the load fundamental power phase ($\angle a_{21}$). Since the reflected power-waves at all ports and harmonic indices b_{ph} vary periodically with the variation of $\angle a_{21}$ (for any fixed $|a_{11}|$ and $|a_{21}|$ combination), we can extract the Fourier series coefficients of this variation by performing a discrete Fourier transform on the simulated measurements over the sweep of this variable. For the purpose of this comparison, 21 different phases (spaced equally within $360°$) are swept.

The parameter sweep described above will result in $32 \times 33 \times 21 = 21176$ different harmonic balance simulations. For each of these simulations the current and voltage at DC and the frequencies of interested are extracted and indexed by their swept parameters. These measurements will be used to extract the 2-variable Cardiff model.

5.3 PHD Model Extraction From NVNA Measurement Data

Whether the measurements indexed by the swept parameters required by each PHD model discussed are extracted from a simulated measured (described in sections 5.2.1 through 5.2.3) or if they are extracted from an NVNA (or LSNA) on the lab bench, the model parameters will need to be extracted from each measurement set before we can implement them as a behavioural model in a simulator. Sections 5.3.1 and 5.3.2 will describe the process of extracting the X-parameter and Cardiff models respectively from appropriately swept NVNA measurement data of the power transistor periodic voltage and current behaviour.

5.3.1 Parameter Extraction of the X-parameter Models

For each swept value of the LSOP variables ($|a_{11}|$ for the 50Ω-matched X-parameter model; $|a_{11}|$, $|\Gamma_L|$ and $\angle\Gamma_L$ for the Γ_L-dependent X-parameter model), group the NVNA measurements together. These measurements will include the variation of the voltage and current at both ports and all frequencies of interest due to the injections of varying extraction tones.

A simple way to extract the X-parameter model parameters for each LSOP condition is to use a linear least squared error (LSE) fit of the NVNA measurements to find the X-parameter formulation coefficients of equation 3.35 (for 50Ω-matched X-parameters) or equation 3.43 (for Γ_L-dependent X-parameters). We can use the LSE algorithm to extract the parameters of the X-parameter formulation since it describes each reflection power-wave b_{ph} as a linear combination of the a_{ph} and a_{ph}^* terms. The coefficients of this linear combination are the X-parameter model coefficients. We will use the complex variable version of the LSE which uses the definition of the Wirtinger derivative in its formulation [20].

If the matrix X is defined such that each row reflects an NVNA measurement of the injection of a single state of the extraction tone (of the k different extraction tone injection states) as follows:

$$X = \begin{bmatrix} 1 & a_{21_1} & a^*_{21_1} & a_{12_1} & a^*_{12_1} & a_{22_1} & a^*_{22_1} & \dots \\ 1 & a_{21_2} & a^*_{21_2} & a_{12_2} & a^*_{12_2} & a_{22_2} & a^*_{22_2} & \dots \\ \vdots & \vdots & \vdots & \vdots & \vdots & \vdots & \vdots & \dots \\ 1 & a_{21_k} & a^*_{21_k} & a_{12_k} & a^*_{12_k} & a_{22_k} & a^*_{22_k} & \dots \end{bmatrix} \tag{5.2}$$

and the vector y of length k is defined to include the variation of a single one of the reflected power-waves b_{ph} as follows:

$$y = \begin{bmatrix} b_{ph_1} \\ b_{ph_2} \\ \vdots \\ b_{ph_k} \end{bmatrix} \tag{5.3}$$

then following relationship give us the linear LSE fit to the X-parameter formulation of equation 3.35:

$$\hat{\beta} = (X^T X)^{-1} X^T y \tag{5.4}$$

where the vector $\hat{\beta}$ will contain the relevant X-parameters that describe the behaviour of b_{ph} as a variation of the small signal variation of incident power-waves a_{qi} as follows:

$$\hat{\beta} = \begin{bmatrix} X^{(F)}_{ph} \\ X^{(S)}_{ph,21} \\ X^{(T)}_{ph,21} \\ X^{(S)}_{ph,12} \\ X^{(T)}_{ph,12} \\ X^{(S)}_{ph,22} \\ X^{(T)}_{ph,22} \\ \vdots \end{bmatrix} \tag{5.5}$$

The main difference between the extraction of the 50Ω-matched X-parameter and Γ_L-dependent X-parameters here is that the X matrix of equation 5.2 will not include the second and third columns that look at the variation with respect to an extraction tone injection at a_{21} since there will be no injection at this port and harmonic index (since injecting an extraction tone here will vary Γ_L).

All the X-parameter coefficients extracted using the above method are listed in a text file indexed by the LSOP parameters to be linearly interpolated in the simulation component.

5.3.2 Parameter Extraction of the Cardiff Models

To extract the 2-variable Cardiff model from the simulated measurement procedure described in section 5.2.3, we need to group the NVNA measurements for each combination of $|a_{11}|$ and $|a_{21}|$. For each of these input power magnitudes there will be $k = 21$ different NVNA measurements (one for each swept phase $\angle a_{21}$).

To extract each of the $G_{ph,n}(|a_{11}|, |a_{21}|)$ parameters of the Cardiff model formulation of equation 3.46, for each fixed $|a_{11}|$ and $|a_{21}|$ we use a discrete Fourier transform (DFT) to find the following k coefficients:

$$b_{ph} = \sum_{n=-10}^{10} G_{ph,n}(|a_{11}|, |a_{21}|) e^{j(n\angle a_{21})} \tag{5.6}$$

Since there are 21 swept $\angle a_{21}$ phases, we will have 21 $G_{ph,n}(|a_{11}|, |a_{21}|)$ DFT coefficients. The lower frequency DFT components will give a good approximation of the variation of the b_{ph} reflected power-wave as a function of the variation of the relative phase of the second large signal variable with respect to the first large signal variable ($\angle a_{21}$). For the purpose of this comparison we will limit the parameters of the Cardiff model to the 9th order (covering $n = -4$ to 4). Thus our 2-variable Cardiff model will be described by the following equation:

$$b_{ph} = \sum_{n=-4}^{4} G_{ph,n}(|a_{11}|, |a_{21}|) e^{j(n\angle a_{21})} \tag{5.7}$$

For each of the DFT coefficients $G_{ph,n}(|a_{11}|, |a_{21}|)$, we will fit a 7^{th}-order polynomial to its $|a_{21}|$ variation as follows:

$$G_{ph,n}(|a_{11}|, |a_{21}|) = \sum_{m=0}^{7} |a_{21}|^m \alpha_{ph,n,m}(|a_{11}|) \tag{5.8}$$

To find the polynomial parameters of equation 5.8 we can use the same linear LSE fit algorithm that was used to extract the X-parameters in section 5.3.1 as follows. Define for $r = 33$ different $|a_{21}|$ levels:

$$X := \begin{bmatrix} 1 & |a_{21}|_1 & |a_{21}|_1^2 & \dots & |a_{21}|_1^7 \\ 1 & |a_{21}|_2 & |a_{21}|_2^2 & \dots & |a_{21}|_2^7 \\ \vdots & \vdots & \vdots & & \vdots \\ 1 & |a_{21}|_r & |a_{21}|_r^2 & \cdots & |a_{21}|_r^7 \end{bmatrix} \tag{5.9}$$

$$y := \begin{bmatrix} G_{ph,n}(|a_{11}|, |a_{21}|_1) \\ G_{ph,n}(|a_{11}|, |a_{21}|_2) \\ \vdots \\ G_{ph,n}(|a_{11}|, |a_{21}|_r) \end{bmatrix} \tag{5.10}$$

we have through the LSE fit algorithm of equation 5.4:

$$\hat{\beta} = \begin{bmatrix} \alpha_{ph,n,0}(|a_{11}|) \\ \alpha_{ph,n,1}(|a_{11}|) \\ \alpha_{ph,n,2}(|a_{11}|) \\ \vdots \\ \alpha_{ph,n,7}(|a_{11}|) \end{bmatrix} \tag{5.11}$$

Using the above method to extract the polynomial coefficients that fit the Fourier series parameters $G_{ph,n}(|a_{11}|, |a_{21}|)$, we have the following 2-variable Cardiff model formulation:

$$b_{ph} = \sum_{n=-4}^{4} \sum_{m=0}^{7} |a_{21}|^m \alpha_{ph,n,m}(|a_{11}|) e^{j(n\angle a_{21})}$$

The $\alpha_{ph,n,m}(|a_{11}|)$ parameters are extracted and listed in a text file indexed by $|a_{11}|$ to be linearly interpolated in the simulation component.

5.4 Implementation of PHD Models in a Harmonic Balance Simulator

We will use the commercial harmonic balance simulator of the Agilent ADS software suite [26] to implement each of our PHD models and compare their results with the simulation performance of the compact model that was used to extract these models. Agilent ADS provides a frequency domain equation-based non-linear component called the Frequency Defined Device (FDD) that is very suitable for harmonic balance simulation and the implementation of PHD models. The 2-port FDD component as available in Agilent ADS allows one to define the current at each of the two ports and harmonic frequencies as a function of the voltages at both ports and all the harmonic frequencies of interest. This means that we can implement the voltage-current formulations of the PHD model 3.13 as simply as writing out their constitutive relations within the simulator.

However the PHD models that we will be comparing here are described using the power-wave input and output variables (as described in section 3.3.1.1). This means that we can't

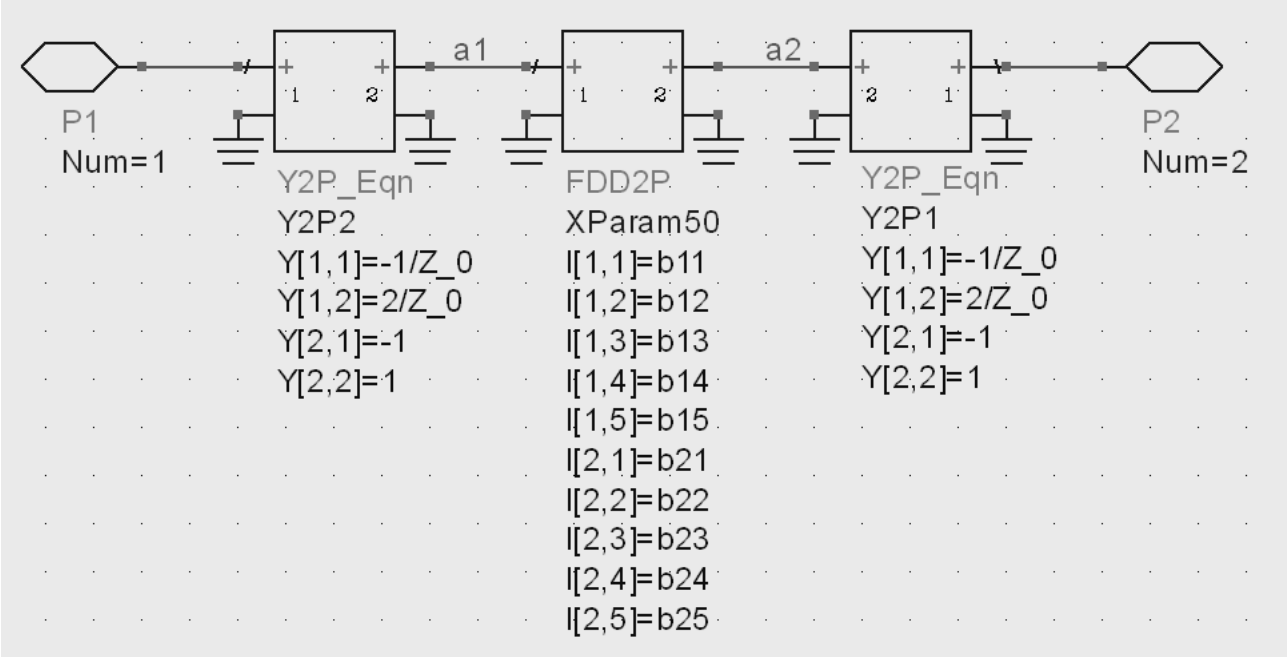

Figure 5.3: Implementation of a power-wave-defined PHD model using an FDD component in Agilent ADS

use the FDD component directly to implement the X-parameter and Cardiff models that were extracted in section 5.3 since the harmonic balance simulator as implemented by Agilent ADS solves for the voltages at each node of the circuit (not the reflected power-waves). The equivalence of power-wave-defined and voltage-current PHD models allows us to use a mathematical trick to implement the power-wave defined PHD model using the voltage-current defined FDD component.

Figure 5.3 shows this mathematical trick. Here two 2-port Y-parameter blocks are used to transform the incident and reflected power-waves at the interface of the power transistor behavioural model into voltages and currents at the interface of the FDD component. Note that these Y-parameter blocks do not actually physically exist. They are only there to implement the power-wave relations of equations 3.16 and 3.17. For each of these 2-port Y-parameter blocks we have:

$$\begin{bmatrix} I_1 \\ I_2 \end{bmatrix} = \begin{bmatrix} Y_{11} & Y_{12} \\ Y_{21} & Y_{22} \end{bmatrix} \begin{bmatrix} V_1 \\ V_2 \end{bmatrix} \tag{5.12}$$

For the values of $Y_{11} = -\frac{1}{Z_0}$, $Y_{12} = \frac{2}{Z_0}$, $Y_{21} = -1$ and $Y_{22} = 1$ implemented at the source side of the FDD component (where we have $I_1 = i_1$, $I_2 = b_1$, $V_1 = v_1$ and $V_2 = a_1$), we have the relations:

$$i_1 = -\frac{v_1}{Z_0} + 2\frac{a_1}{Z_0} \tag{5.13}$$

$$b_1 = -v_1 + a_1 \tag{5.14}$$

The relations of equations 5.13 and 5.14 are equivalent to equations 3.16 and 3.18 respectively through simple algebra. The same transformation holds for the load side of the power transistor.

All three model equations are implemented in the equation editor of Agilent ADS and the model parameters are read from the text files generated by the methods described in section 5.3. The Data Access Component (DAC) of this commercial simulator was used to linearly interpolate the parameters of each model from the respective text files so they can be used within the simulator. This interpolation is performed based on the LSOP variables for each of the X-parameter models and it is done based on the fundamental input power-wave magnitude ($|a_{11}|$) for the Cardiff PHD model.

5.5 Comparison of PHD Models

To compare the three PHD behavioural models described in this thesis, we implemented each model in Agilent ADS's harmonic balance simulator using the method described in section 5.4. These three behavioural models will be compared to each other and to the manufacturer compact model that was used to extract these behavioural models. The comparison will be performed using the following strategy:

1. Fix a set of passive reflection coefficients seen by the transistor at both sides of the transistor up to the fifth harmonic except the fundamental input reflection coefficient which we fix to 50Ω for maximum pseudo-power-wave transfer to the device model from the fundamental input power source. This means that we fix values for Γ_{12}, Γ_{13}, Γ_{14}, Γ_{15}, Γ_{21}, Γ_{22}, Γ_{23}, Γ_{24} and Γ_{25} for each comparison test case.

2. For each of the four models (the three PHD behavioural models and the compact model), we will sweep the fundamental input power of the 50Ω power source from $0W$ to $62W$ in small increments of $0.1W$. This is the same power range that the behavioural models were extracted using but with a much finer linear sweep.

3. Perform harmonic balance simulations of each of the models for every power level and plot the magnitude and phase of the variation of the reflected power-waves at both ports and the harmonic frequencies up to the third order. This means we will

be looking at the variation of b_{11}, b_{12}, b_{13}, b_{21}, b_{22} and b_{23} versus the power available from the source (P_{avs}) for each comparison test case. This will show how well each PHD model is modeling the harmonic interactions resulted by the non-linearity of the power amplifier.

We will now explore some test cases of interest that will highlight the differences in the modeling capabilities of each PHD behavioural model.

5.5.1 Case A: Power Sweep in a 50Ω-matched Network

In this test case, all the 50Ω-referenced reflection coefficients are set to zero. That is:

$$\Gamma_{12} = \Gamma_{13} = \Gamma_{14} = \Gamma_{15} = \Gamma_{21} = \Gamma_{22} = \Gamma_{23} = \Gamma_{24} = \Gamma_{25} = 0 \tag{5.15}$$

Figures 5.4 through 5.6 show the variation of the reflected power-waves versus a fundamental power sweep up to the third harmonic. For this case we see that all of the PHD models track the behaviour of the compact model well. This result is expected for all of these PHD models since the matching condition described by equation 5.15 does not result in the usage of the partial derivative X-parameter model terms (the $X^{(S)}$ and $X^{(T)}$ parameters). The X-parameter models are basically linearly interpolating the $X^{(F)}$ terms in the simulator. The Cardiff PHD model under this matched network also collapses to a simple interpolation of values in a look-up table.

5.5.2 Case B: Power Sweep in a Mildly Unmatched Network

Here the reflection coefficients will be randomly generated to have a magnitude in the $(0, 0.4)$ interval with a random phase from the interval $[0°, 360)$. Three different random sets of reflection coefficients were generated and the fundamental input power was swept to see whether there is any trend in the prediction capabilities of the implemented PHD behavioural models.

Tables 5.1 and 5.2 show the three randomly generated mildly unmatched test conditions used.

Figures 5.7 through 5.15 show the variation of the reflected power-waves versus a fundamental power sweep for each of the cases represented in tables 5.1 and 5.2. From these plots it can be seen that all of the extracted behavioural models show good prediction of the compact model behaviour. The X-parameter models seem to have an advantage here. This is mainly to do the fact that the two-variable Cardiff model generates the reflected power-waves b_{ph} only as a function of $|a_{11}|$, $|a_{21}|$ and $\angle a_{21}$. This means that the

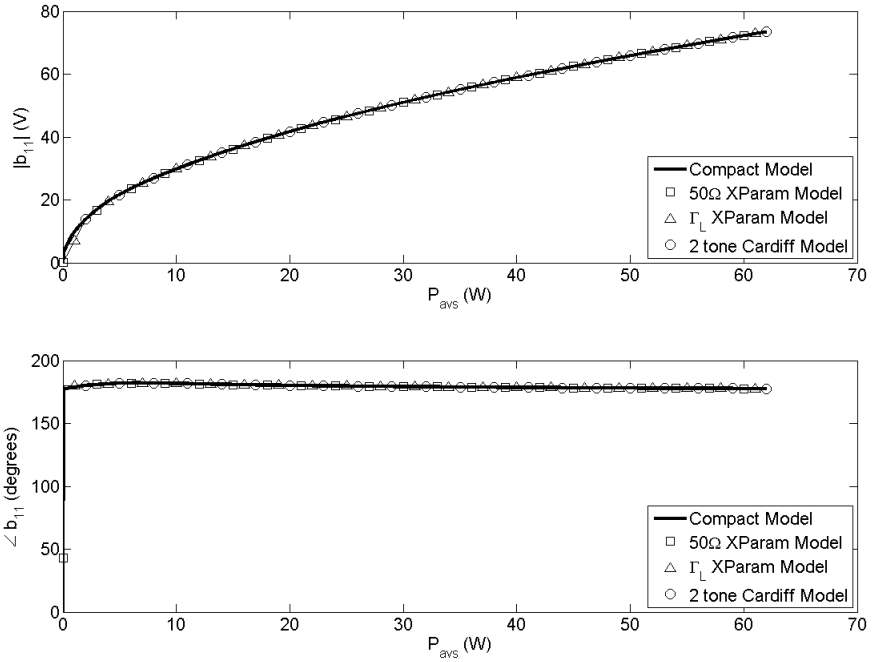

(a) b_{11} vs. P_{avs}

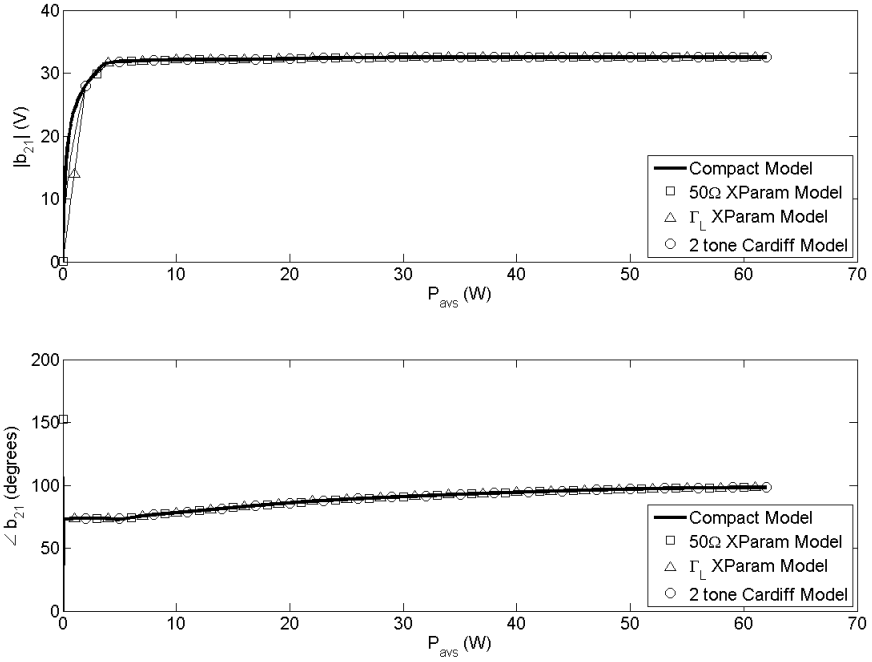

(b) b_{21} vs. P_{avs}

Figure 5.4: Case A: First harmonic reflected power-wave variations versus P_{avs}

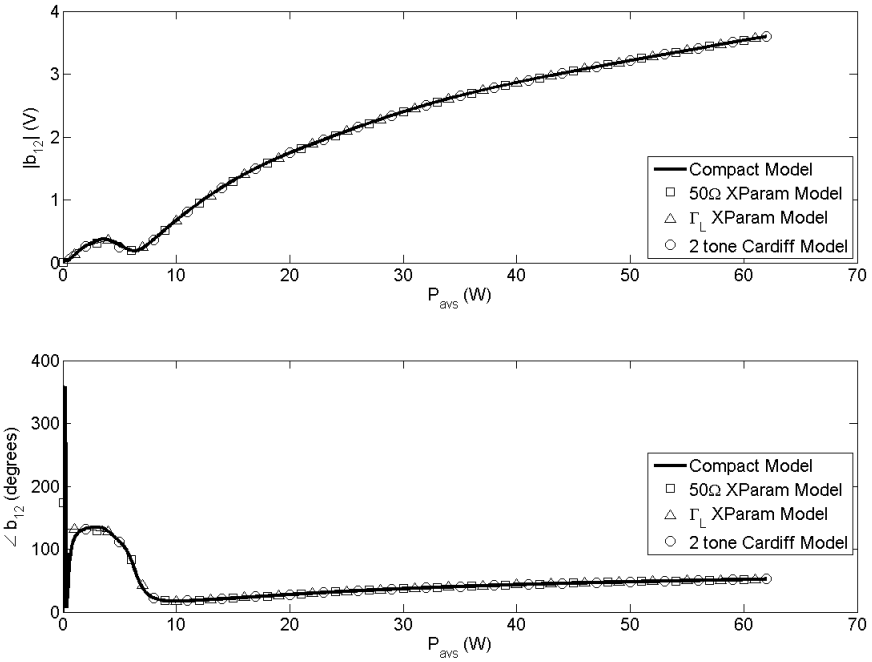

(a) b_{12} vs. P_{avs}

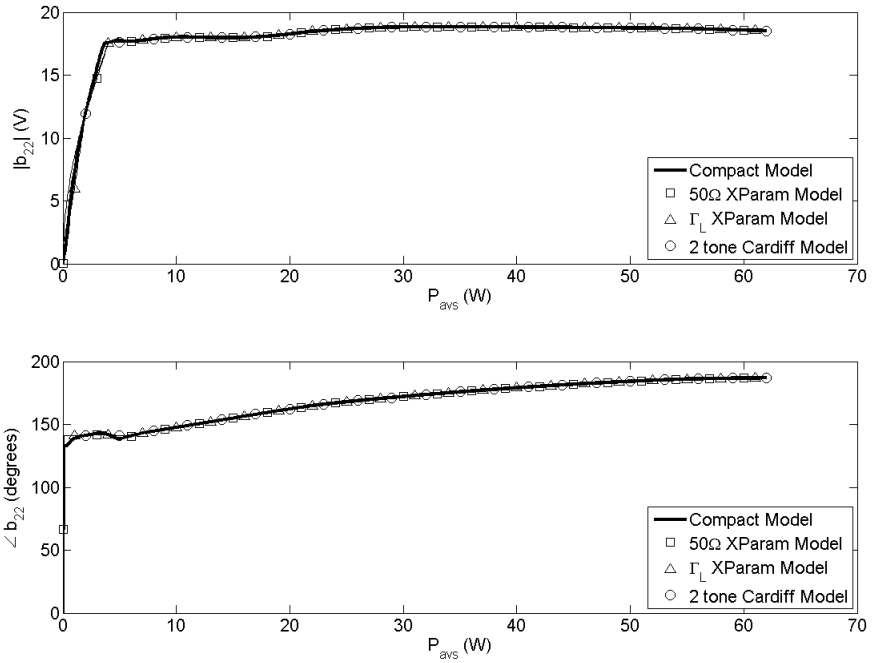

(b) b_{22} vs. P_{avs}

Figure 5.5: Case A: Second harmonic reflected power-wave variations versus P_{avs}

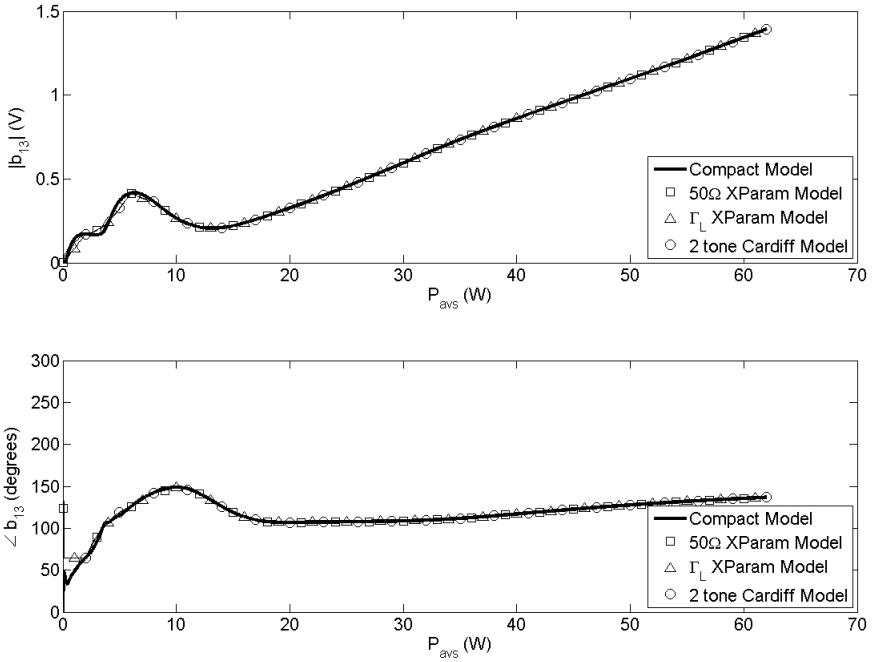

(a) b_{13} vs. P_{avs}

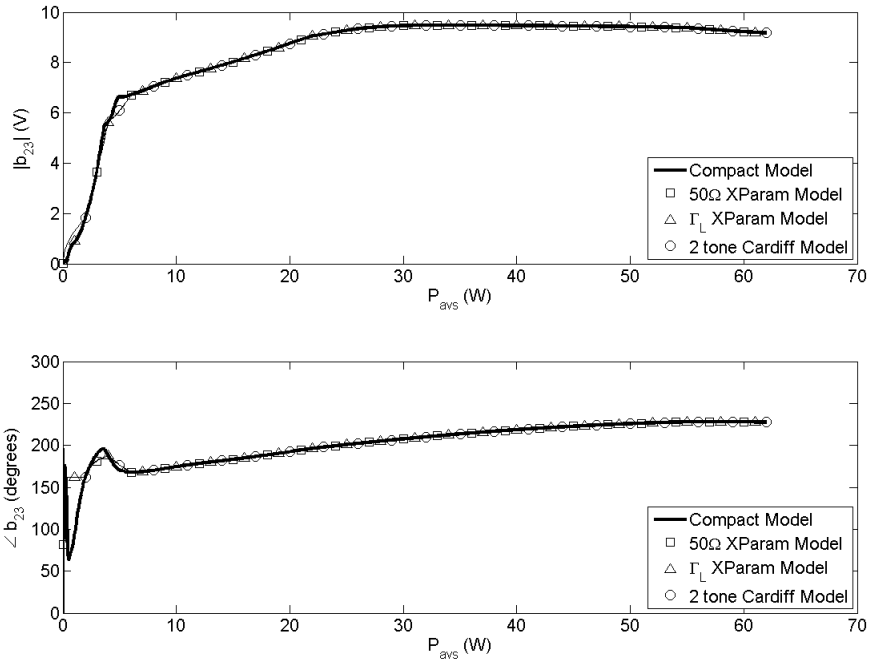

(b) b_{23} vs. P_{avs}

Figure 5.6: Case A: Third harmonic reflected power-wave variations versus P_{avs}

Table 5.1: Case B: Source side reflection coefficients

Test Case ID	Γ_{12}	Γ_{13}	Γ_{14}	Γ_{15}
B1	$0.218\angle 236°$	$0.383\angle 12°$	$0.194\angle 305°$	$0.320\angle 336°$
B2	$0.068\angle 99°$	$0.282\angle 244°$	$0.013\angle 235°$	$0.111\angle 58°$
B3	$0.175\angle 42°$	$0.153\angle 179°$	$0.306\angle 345°$	$0.318\angle 122°$

Table 5.2: Case B: Load side reflection coefficients

Test Case ID	Γ_{21}	Γ_{22}	Γ_{23}	Γ_{24}	Γ_{25}
B1	$0.056\angle 244°$	$0.169\angle 272°$	$0.366\angle 267°$	$0.317\angle 141°$	$0.383\angle 235°$
B2	$0.329\angle 210°$	$0.278\angle 80°$	$0.127\angle 270°$	$0.380\angle 91°$	$0.014\angle 182°$
B3	$0.196\angle 345°$	$0.178\angle 196°$	$0.258\angle 49°$	$0.284\angle 53°$	$0.302\angle 92°$

two-variable Cardiff model is invariant to the harmonic reflection coefficient terminations while the X-parameter models have the linear partial derivative modeling of the effect of the harmonic terminations.

5.5.3 Case C: Power Sweep with Highly Unmatched Γ_{21} and Mildly Unmatched Network

Here the reflection coefficients will be randomly generated to have a magnitude in the $(0, 0.4)$ interval with a random phase from the interval $[0°, 360)$, except for Γ_{21} which will have a random magnitude in the (0.7,1) interval. Three different random sets of reflection coefficients were generated and the fundamental input power was swept to see whether there is any trend in the prediction capabilities of the implemented PHD behavioural models.

Tables 5.3 and 5.4 show the three randomly generated mildly unmatched test conditions used.

Figures 5.16 through 5.24 show the variation of the reflected power-waves versus a fundamental power sweep for each of the cases represented in tables 5.3 and 5.4.

Here the case C1 and C3 cases had great performance from all of the behavioural models extracted (see figures 5.16 through 5.18). However the random set of impedances of case C2, resulted in worst performance from the Γ_L-dependent X-parameter model (see figures 5.19 through 5.21). This is most likely an artifact of the interpolation used in this model. In extracting the Γ_L-dependent X-parameter model (see section 5.2.2), we used a polar sweep of Γ_{21} and a separate X-parameter model was extracted for each Γ_{21} value. In simulation, when we used the Γ_L-dependent X-parameter model for a point that is not one of the points used in the Γ_L sweep, the simulator will linearly interpolate the X-parameters (in polar coordinates) and use the interpolated parameters for the model. Case C2 is at

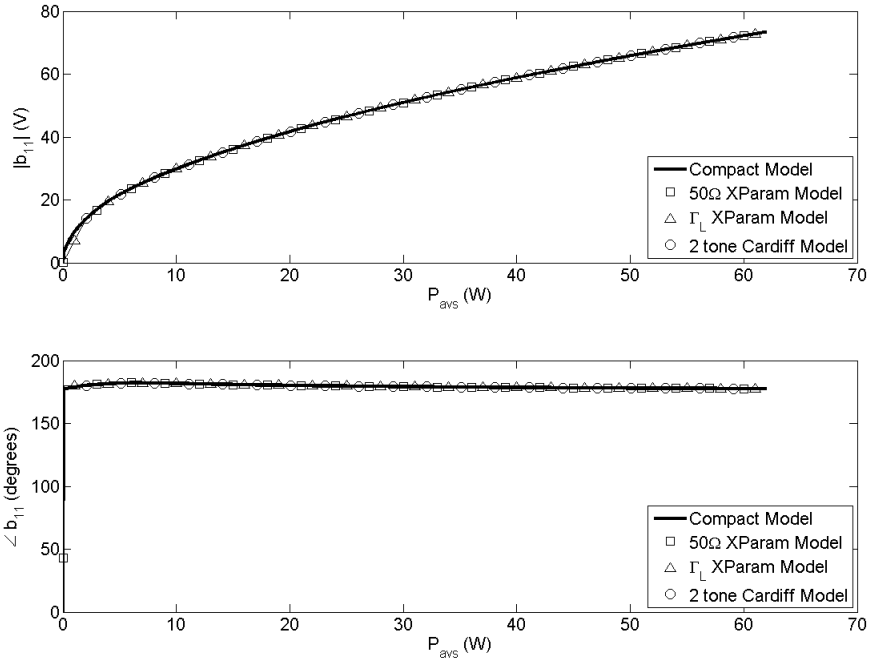

(a) b_{11} vs. P_{avs}

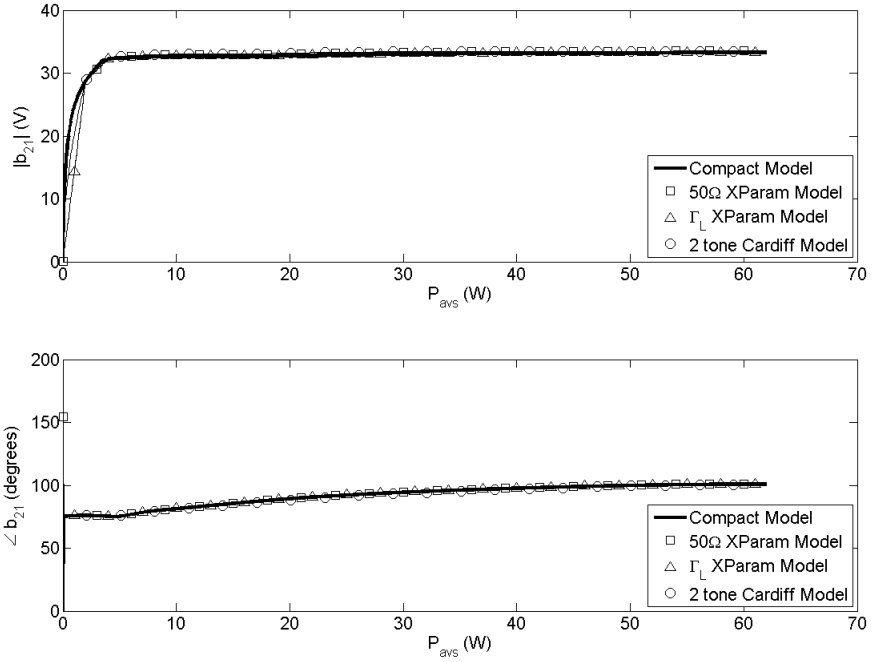

(b) b_{21} vs. P_{avs}

Figure 5.7: Case B1: First harmonic reflected power-wave variations versus P_{avs}

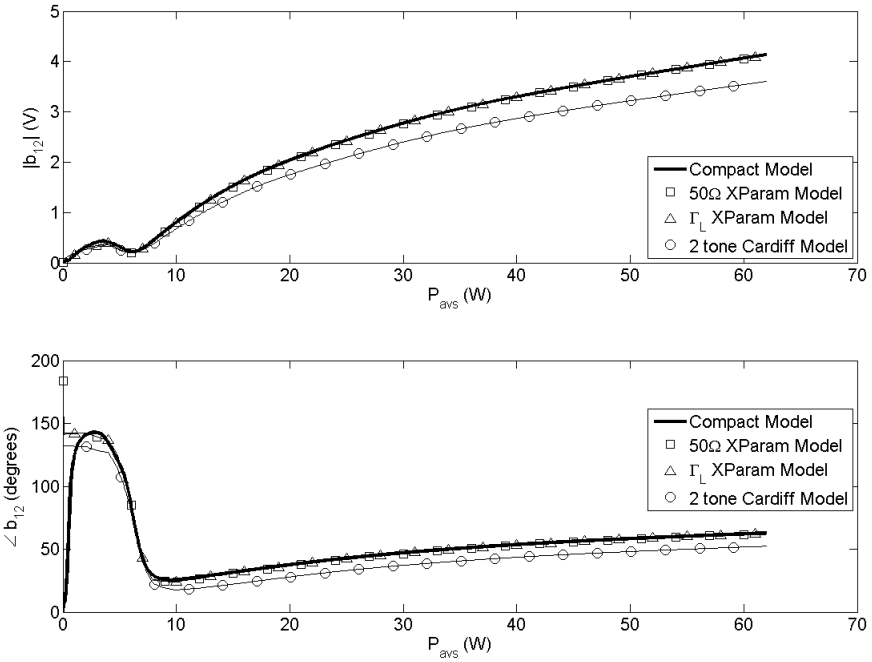

(a) b_{12} vs. P_{avs}

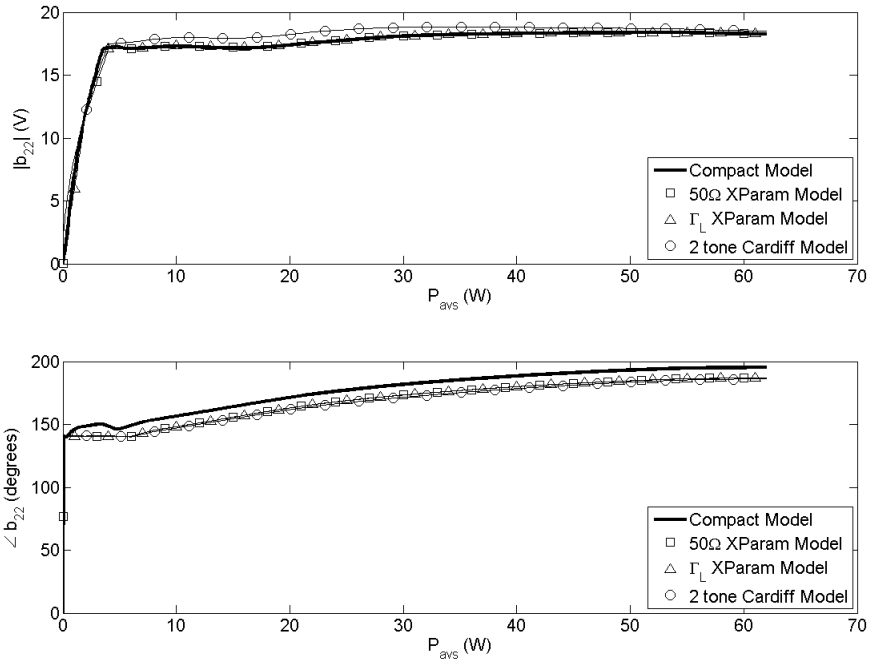

(b) b_{22} vs. P_{avs}

Figure 5.8: Case B1: Second harmonic reflected power-wave variations versus P_{avs}

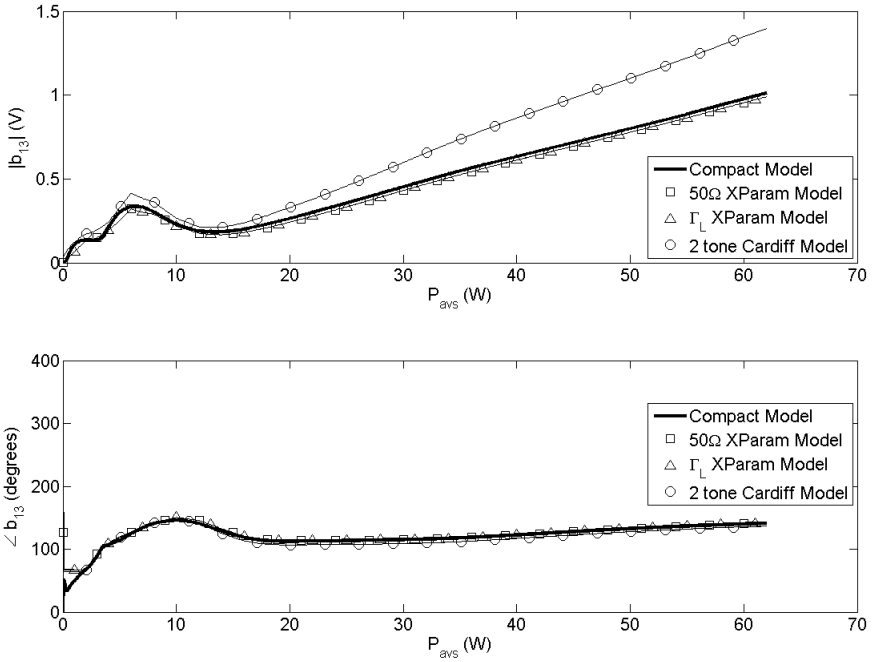

(a) b_{13} vs. P_{avs}

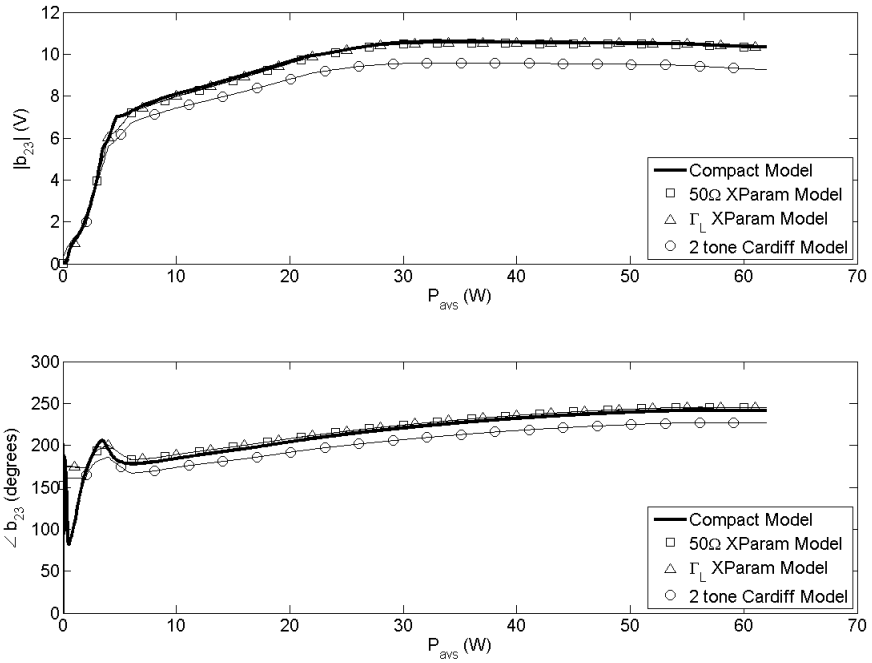

(b) b_{23} vs. P_{avs}

Figure 5.9: Case B1: Third harmonic reflected power-wave variations versus P_{avs}

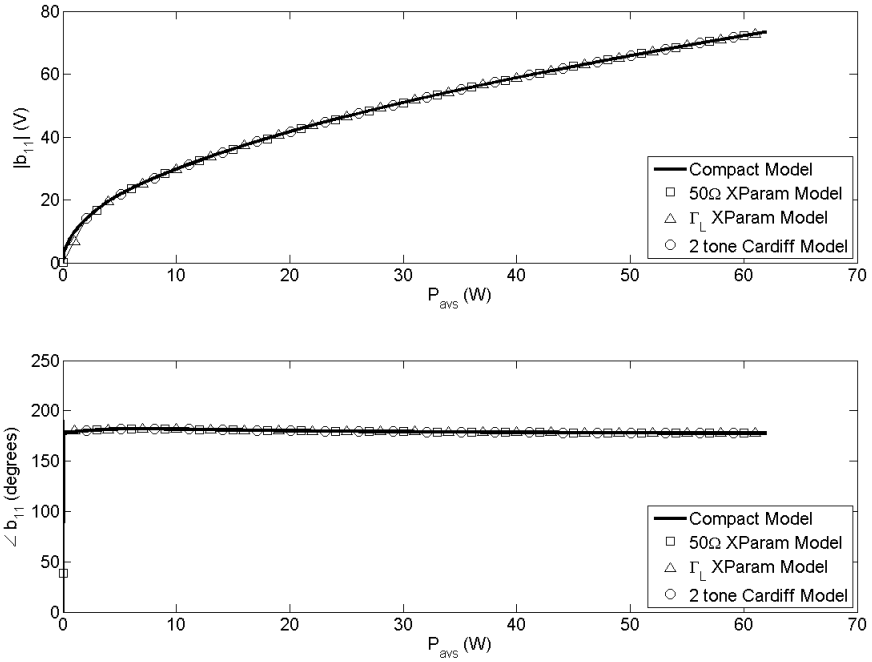

(a) b_{11} vs. P_{avs}

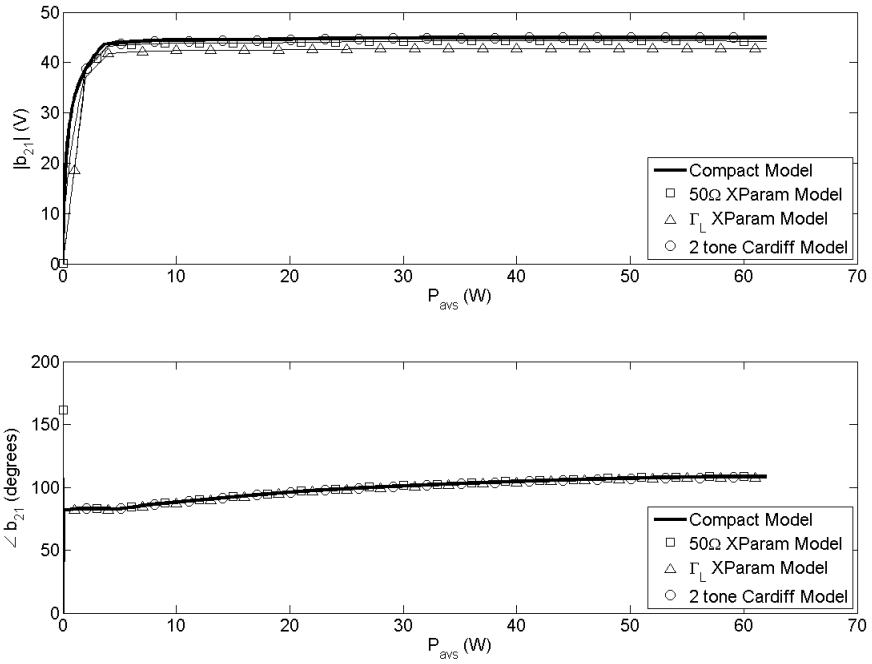

(b) b_{21} vs. P_{avs}

Figure 5.10: Case B2: First harmonic reflected power-wave variations versus P_{avs}

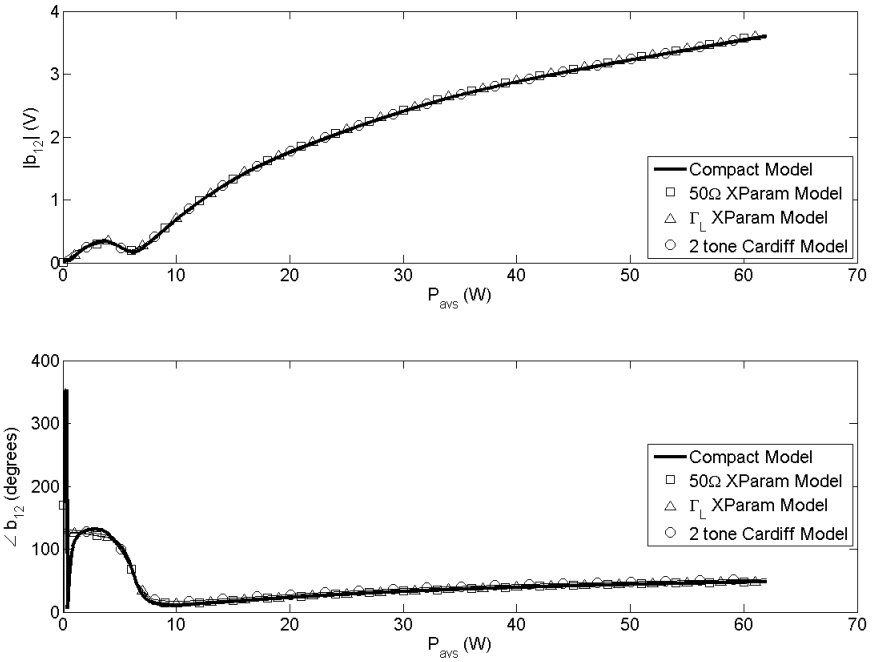

(a) b_{12} vs. P_{avs}

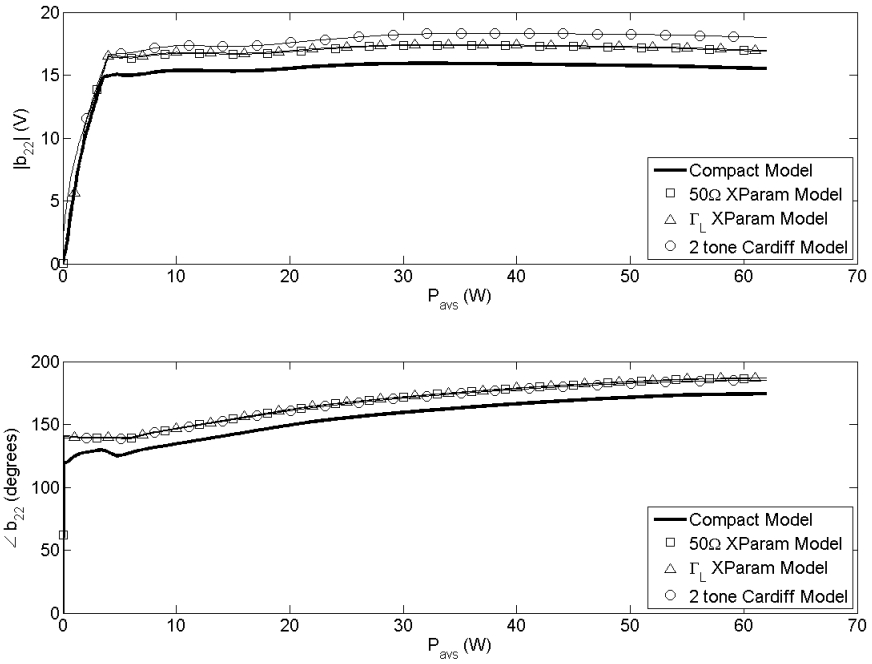

(b) b_{22} vs. P_{avs}

Figure 5.11: Case B2: Second harmonic reflected power-wave variations versus P_{avs}

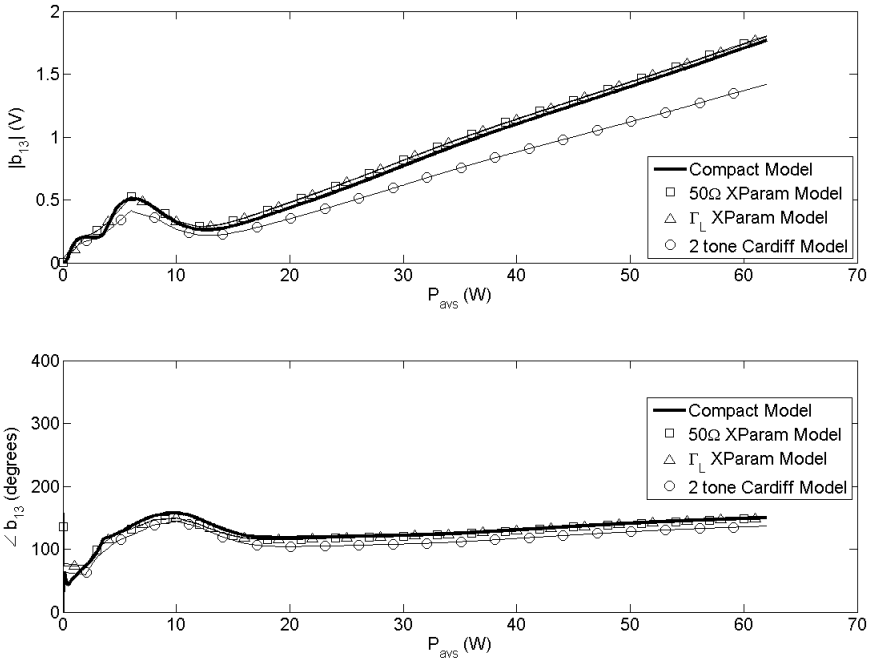

(a) b_{13} vs. P_{avs}

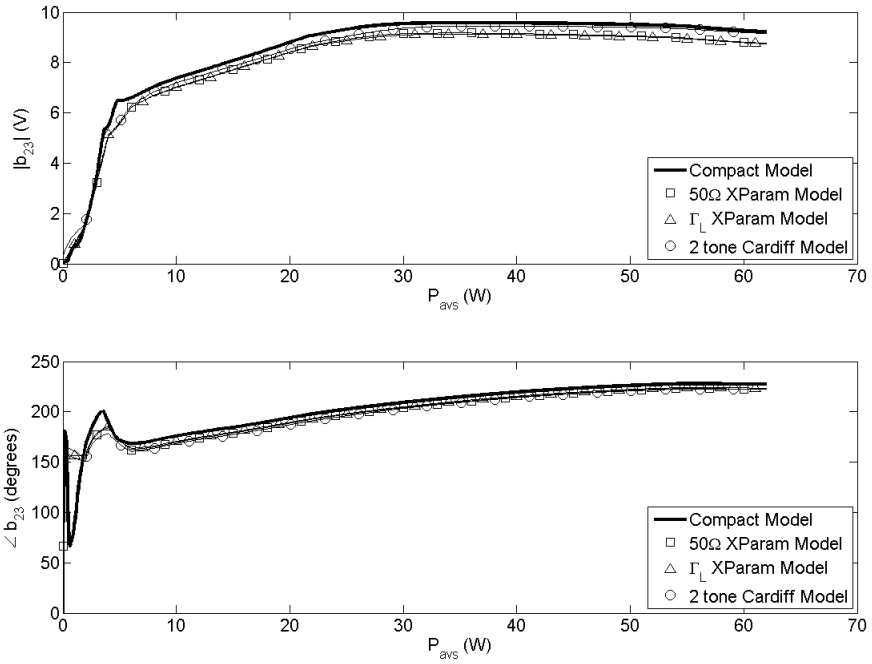

(b) b_{23} vs. P_{avs}

Figure 5.12: Case B2: Third harmonic reflected power-wave variations versus P_{avs}

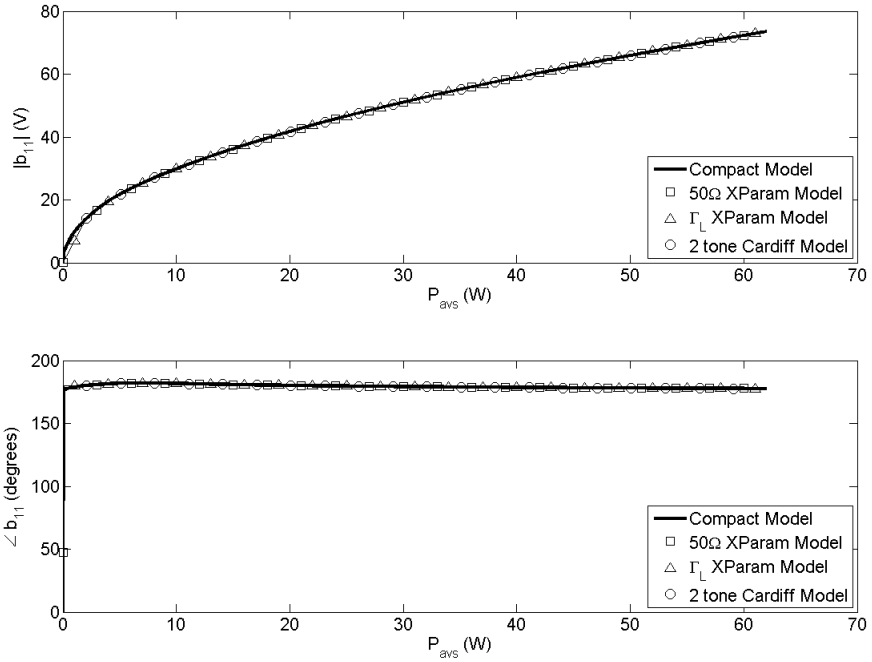

(a) b_{11} vs. P_{avs}

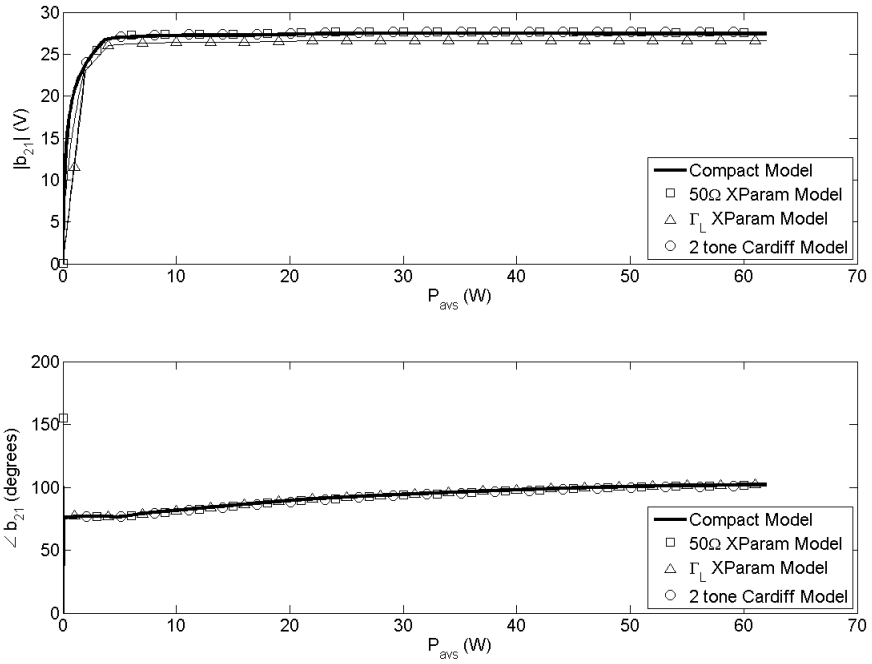

(b) b_{21} vs. P_{avs}

Figure 5.13: Case B3: First harmonic reflected power-wave variations versus P_{avs}

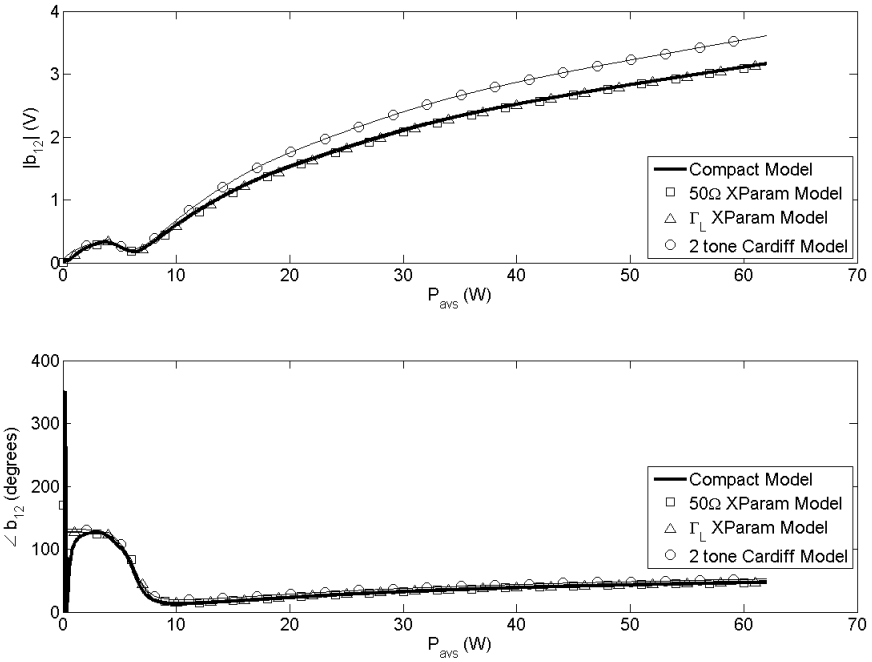

(a) b_{12} vs. P_{avs}

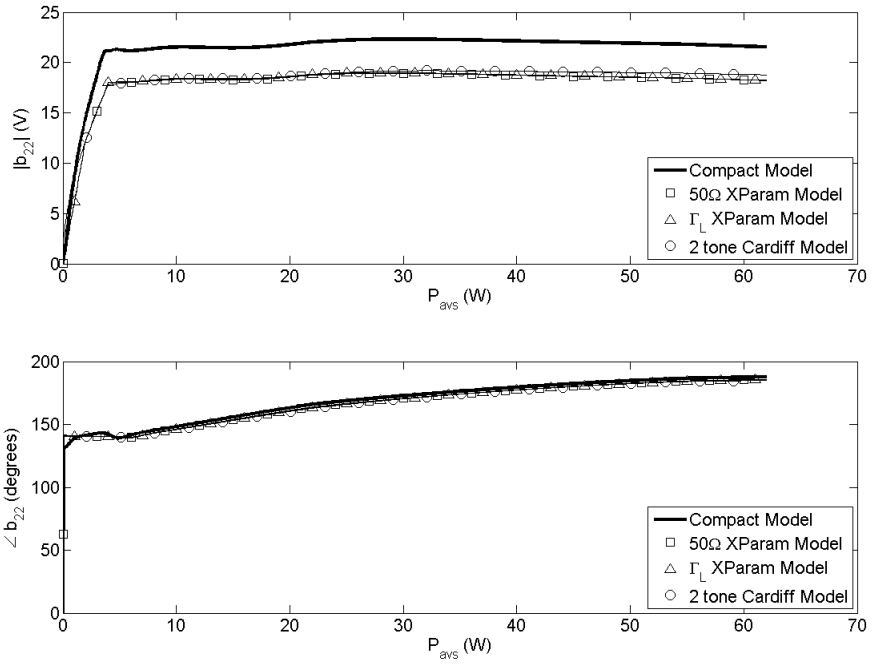

(b) b_{22} vs. P_{avs}

Figure 5.14: Case B3: Second harmonic reflected power-wave variations versus P_{avs}

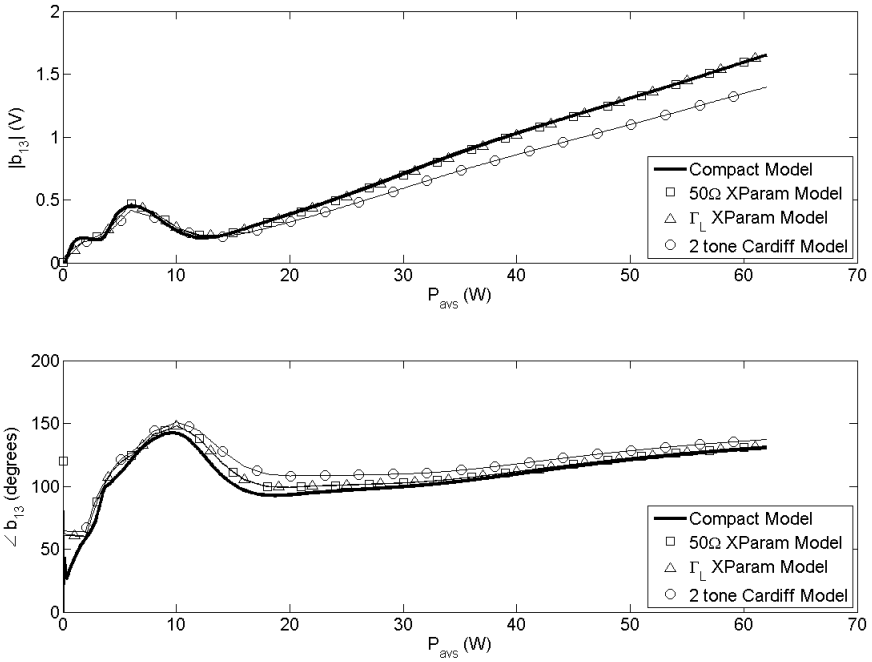

(a) b_{13} vs. P_{avs}

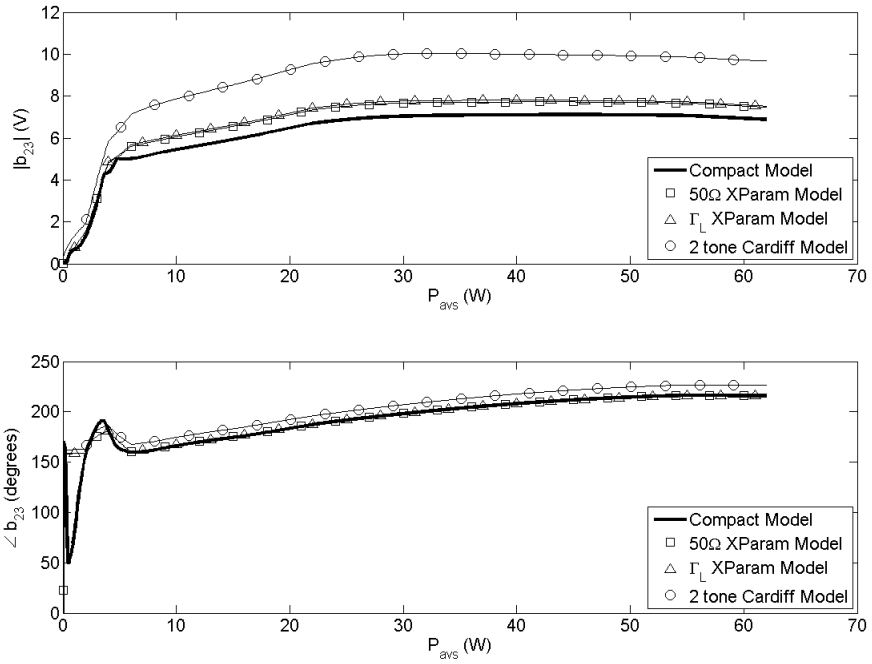

(b) b_{23} vs. P_{avs}

Figure 5.15: Case B3: Third harmonic reflected power-wave variations versus P_{avs}

Table 5.3: Case C: Source side reflection coefficients

Test Case ID	Γ_{12}	Γ_{13}	Γ_{14}	Γ_{15}
C1	$0.303\angle 112°$	$0.079\angle 190°$	$0.100\angle 59°$	$0.246\angle 216°$
C2	$0.152\angle 94°$	$0.189\angle 235°$	$0.141\angle 248°$	$0.332\angle 269°$
C3	$0.227\angle 162°$	$0.220\angle 30°$	$0.367\angle 82°$	$0.114\angle 328°$

Table 5.4: Case C: Load side reflection coefficients

Test Case ID	Γ_{21}	Γ_{22}	Γ_{23}	Γ_{24}	Γ_{25}
C1	$0.952\angle 54°$	$0.030\angle 297°$	$0.022\angle 193°$	$0.212\angle 358°$	$0.312\angle 28°$
C2	$0.776\angle 159°$	$0.374\angle 38°$	$0.052\angle 346°$	$0.227\angle 1°$	$0.188\angle 278°$
C3	$0.805\angle 294°$	$0.005\angle 312°$	$0.135\angle 30°$	$0.065\angle 143°$	$0.318\angle 93°$

least one example that shows that this interpolation of parameters could lead into a worse model than a standard 50Ω model that does not interpolate parameters. The fact that the interpolation is open to arbitrary implementation decisions (using a polar grid versus a rectangular grid, using a linear sweep in the 50Ω Smith chart versus some other arbitrarily chosen reference impedance or simply interpolating the real and imaginary parts of the load impedance Z_L) should cause one to be very cautious of the region of validity of interpolated X-parameter models.

5.5.4 Case D: Power Sweep with Highly Unmatched Network

Here all the reflection coefficients will be randomly generated to have a magnitude in the $(0.7, 1)$ interval with a random phase from the interval $[0°, 360)$. This case will try to push the power transistor into very non-linear regions. Three different random sets of reflection coefficients were generated and the fundamental input power was swept to see whether there is any trend in the prediction capabilities of the implemented PHD behavioural models.

Tables 5.5 and 5.6 show the three randomly generated mildly unmatched test conditions used.

Figures 5.25 through 5.33 show the variation of the reflected power-waves versus a fundamental power sweep for each of the cases represented in tables 5.5 and 5.6.

The major trend here is that all the PHD behavioural models implemented for this thesis degrade in their harmonic prediction under highly unmatched conditions. The two-variable Cardiff model obviously is only sensitive to the fundamental incident power-wave components and so it is quite understandable why it had trouble predicting the harmonic content under these highly unmatched test cases. The X-parameter models being that they are first-order Taylor series approximations start degrading in performance when the

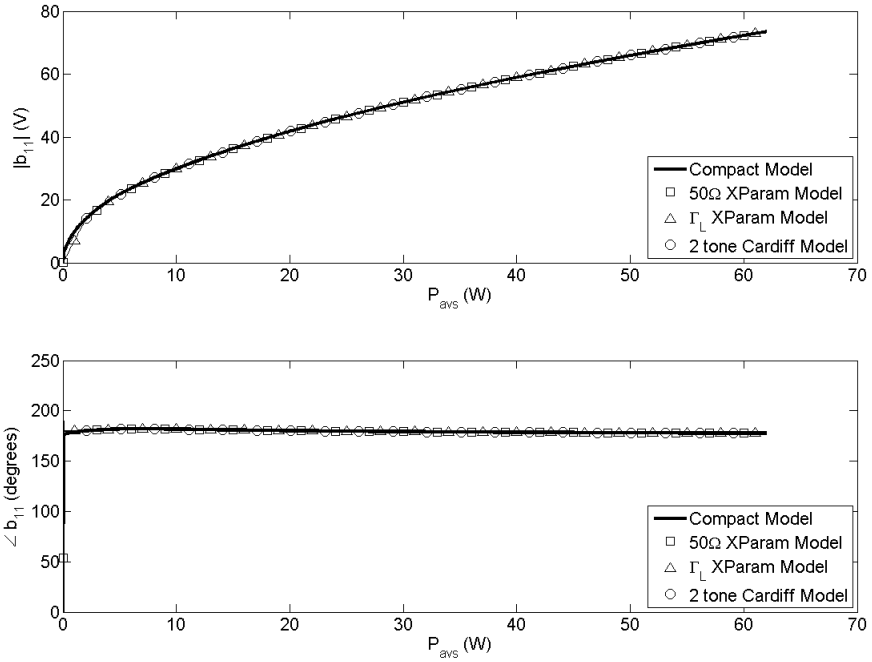

(a) b_{11} vs. P_{avs}

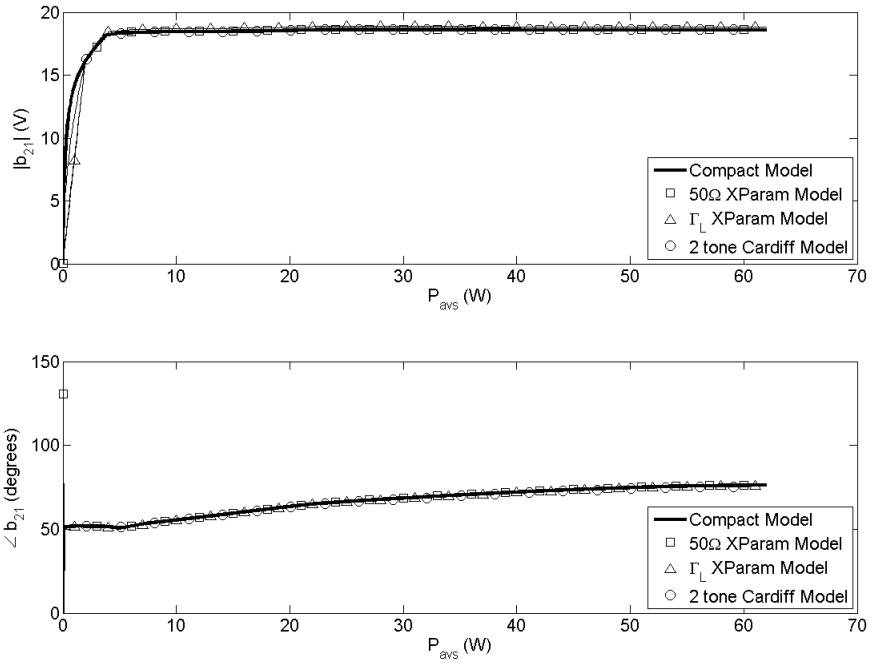

(b) b_{21} vs. P_{avs}

Figure 5.16: Case C1: First harmonic reflected power-wave variations versus P_{avs}

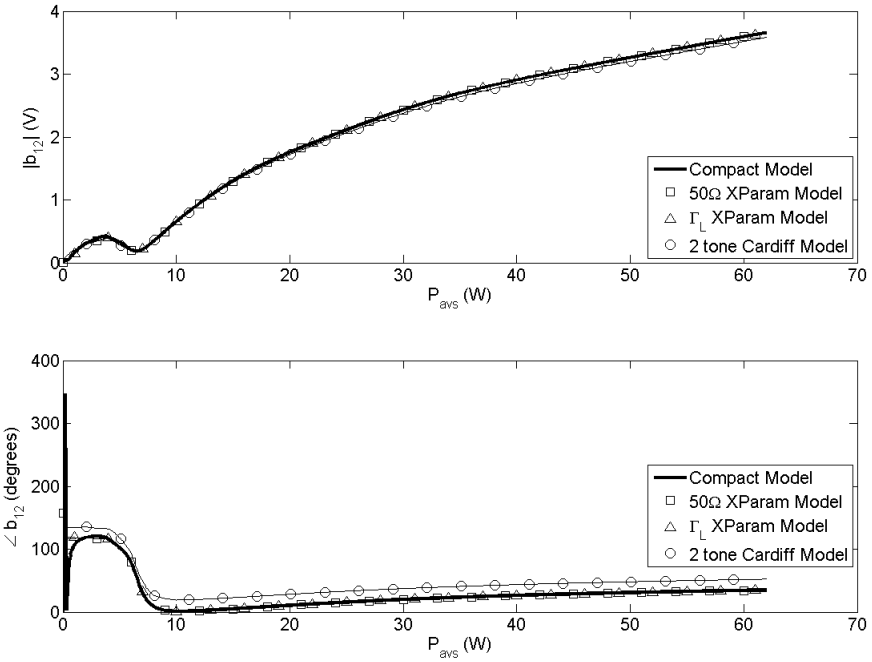

(a) b_{12} vs. P_{avs}

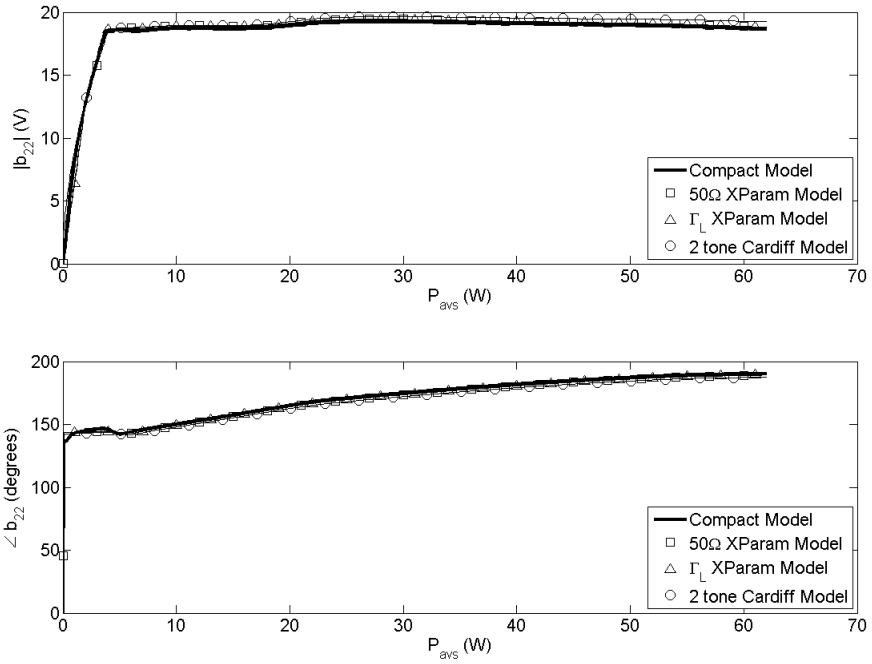

(b) b_{22} vs. P_{avs}

Figure 5.17: Case C1: Second harmonic reflected power-wave variations versus P_{avs}

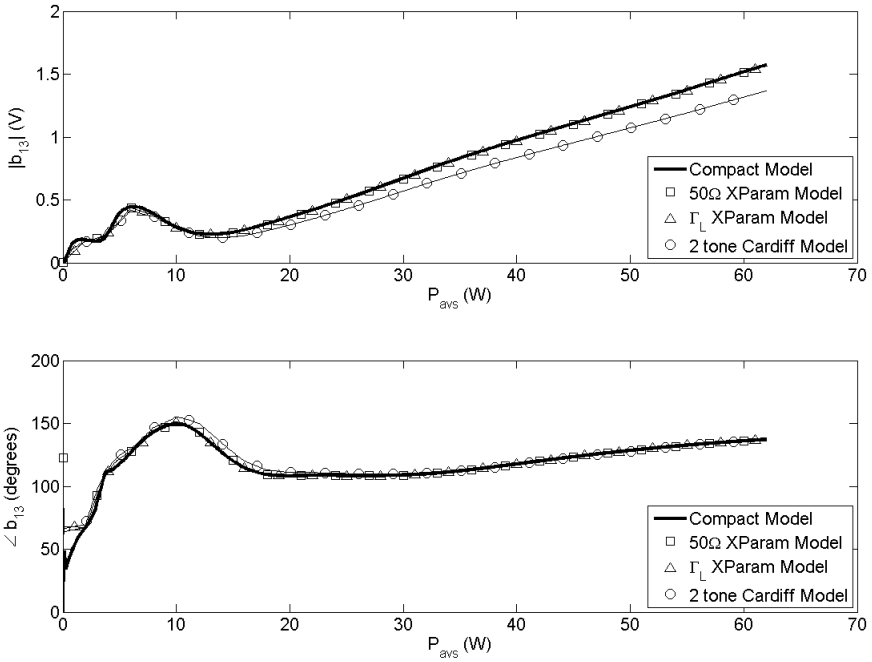

(a) b_{13} vs. P_{avs}

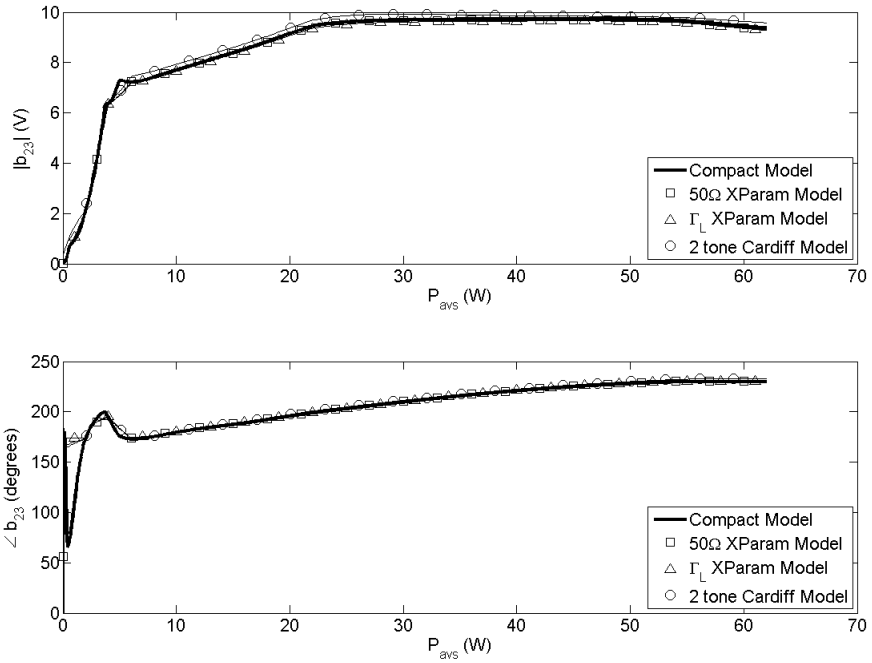

(b) b_{23} vs. P_{avs}

Figure 5.18: Case C1: Third harmonic reflected power-wave variations versus P_{avs}

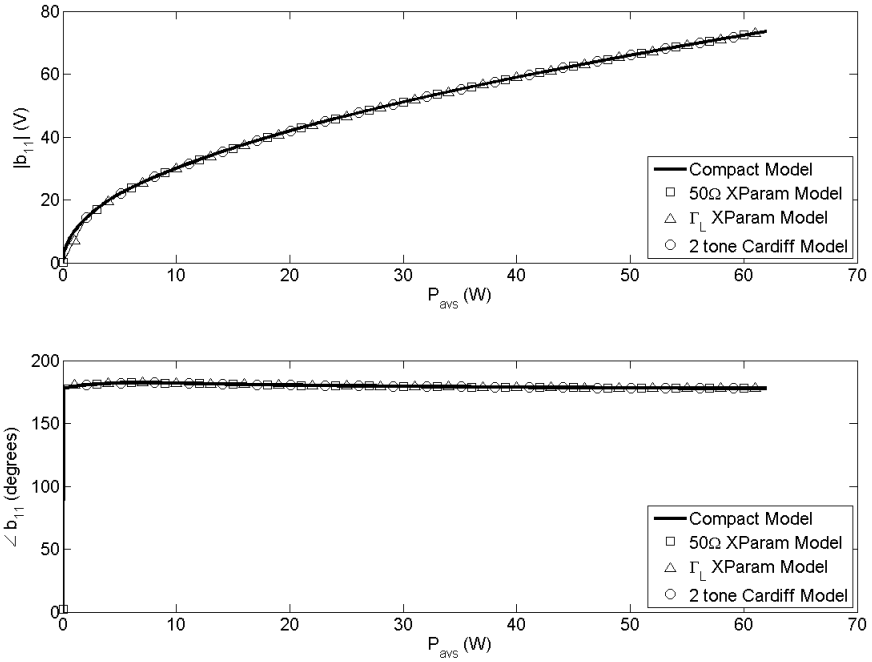

(a) b_{11} vs. P_{avs}

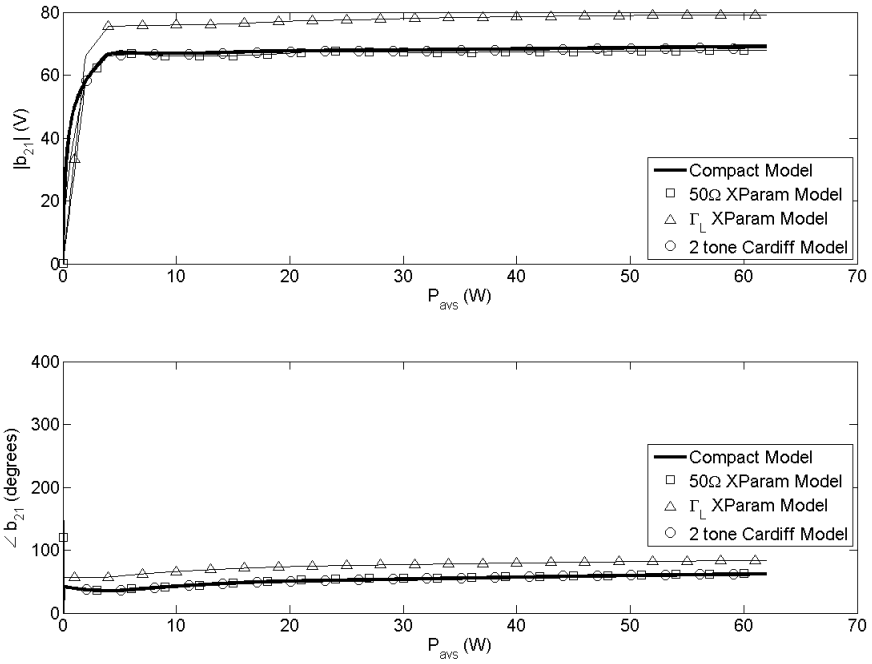

(b) b_{21} vs. P_{avs}

Figure 5.19: Case C2: First harmonic reflected power-wave variations versus P_{avs}

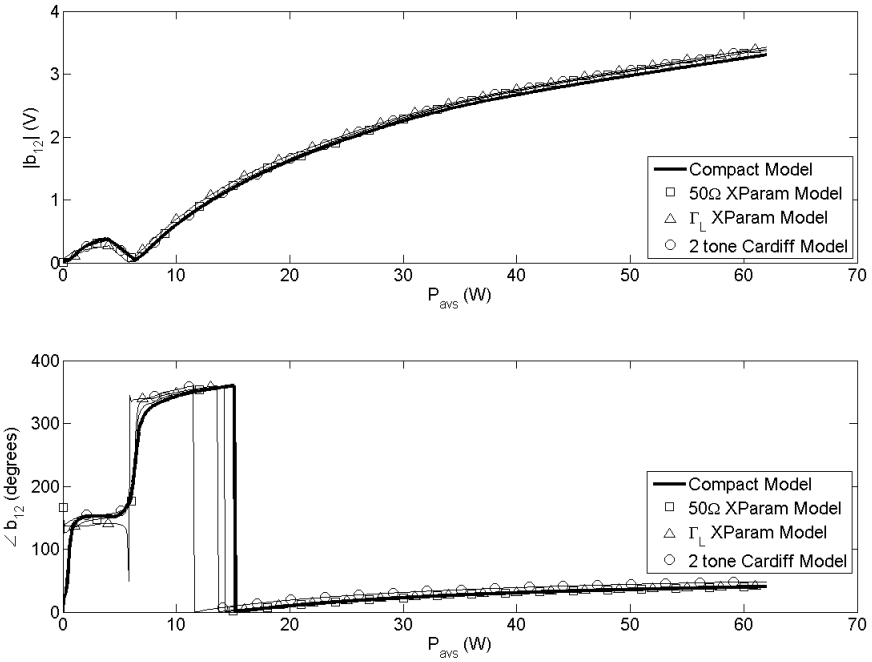

(a) b_{12} vs. P_{avs}

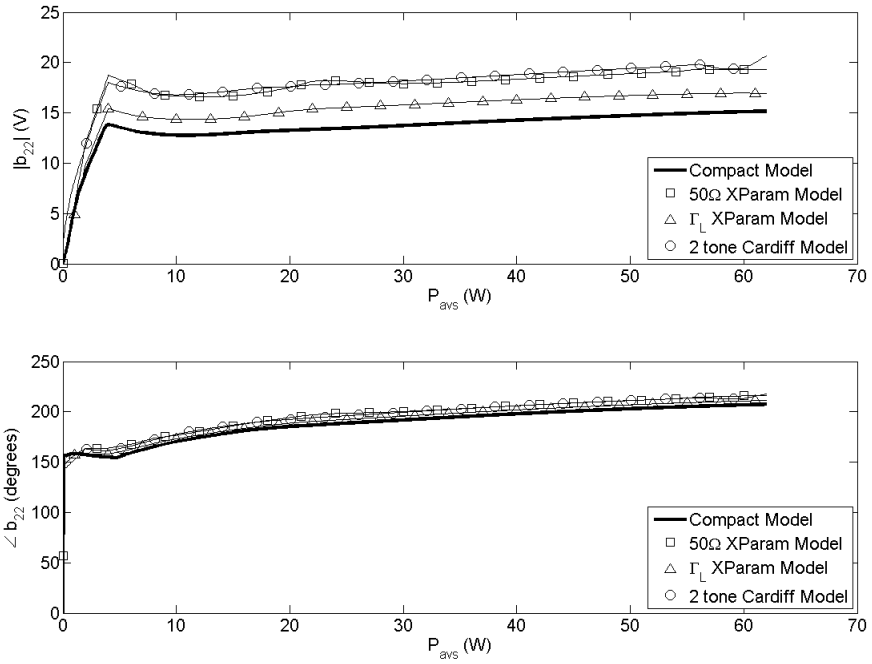

(b) b_{22} vs. P_{avs}

Figure 5.20: Case C2: Second harmonic reflected power-wave variations versus P_{avs}

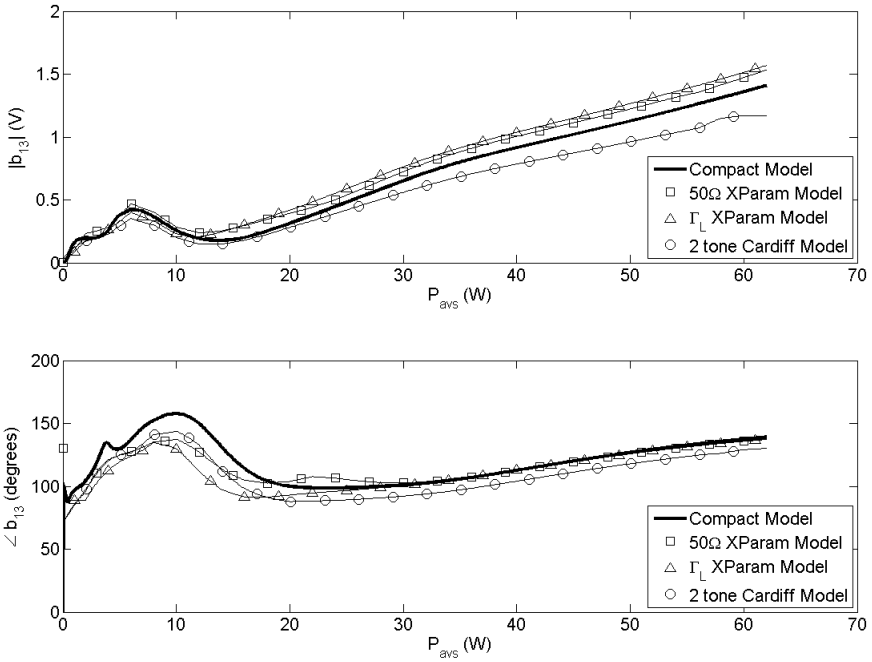

(a) b_{13} vs. P_{avs}

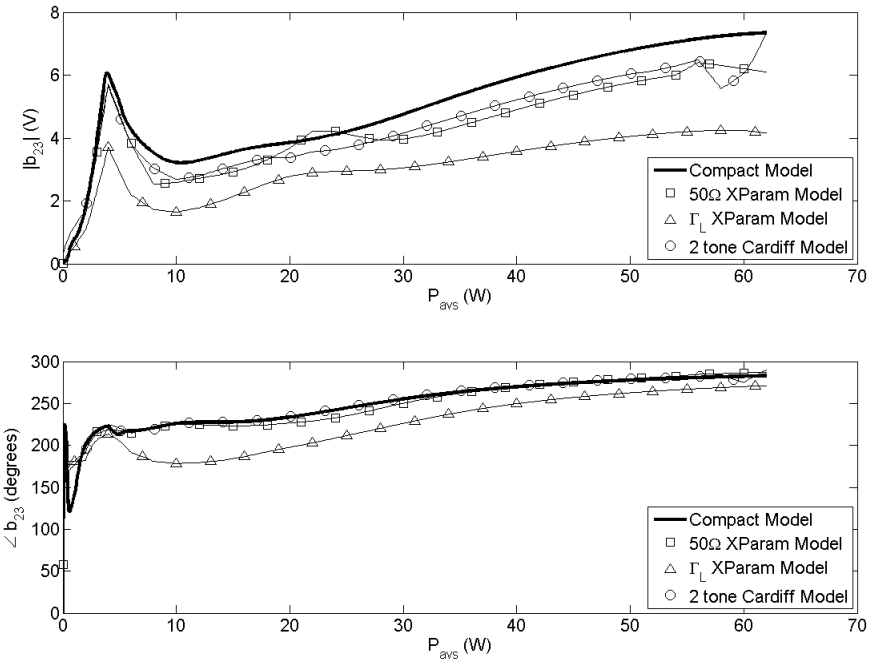

(b) b_{23} vs. P_{avs}

Figure 5.21: Case C2: Third harmonic reflected power-wave variations versus P_{avs}

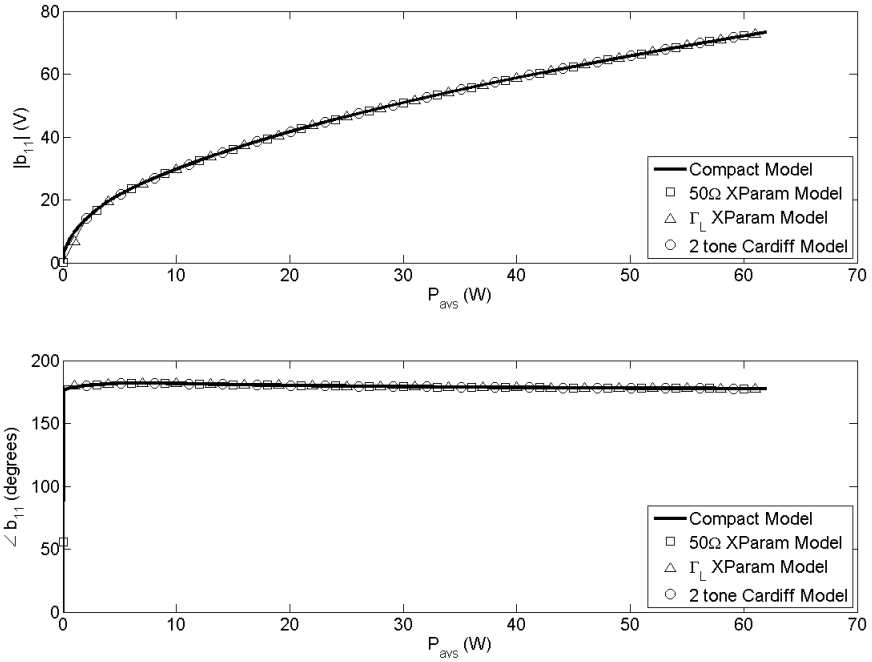

(a) b_{11} vs. P_{avs}

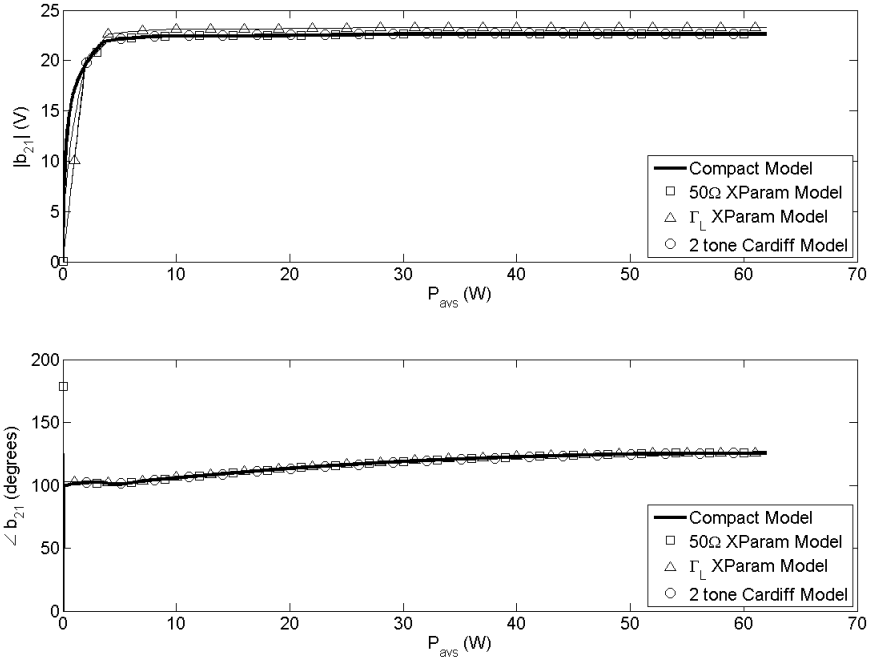

(b) b_{21} vs. P_{avs}

Figure 5.22: Case C3: First harmonic reflected power-wave variations versus P_{avs}

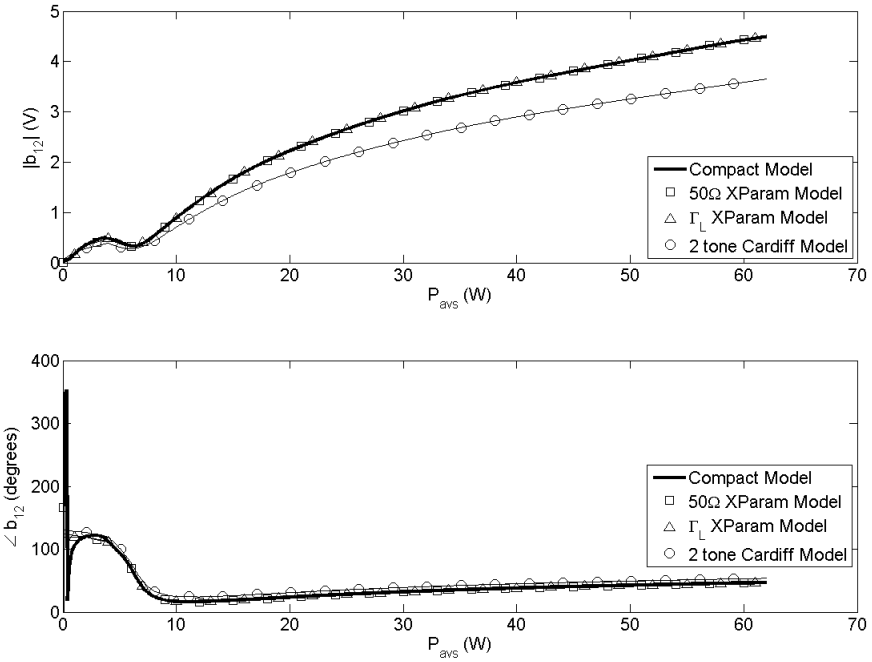

(a) b_{12} vs. P_{avs}

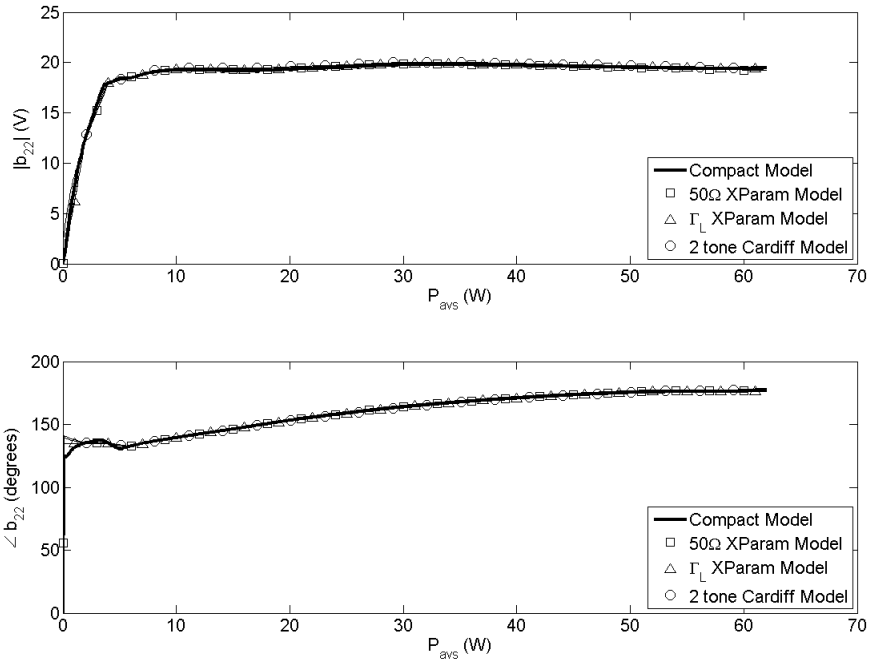

(b) b_{22} vs. P_{avs}

Figure 5.23: Case C3: Second harmonic reflected power-wave variations versus P_{avs}

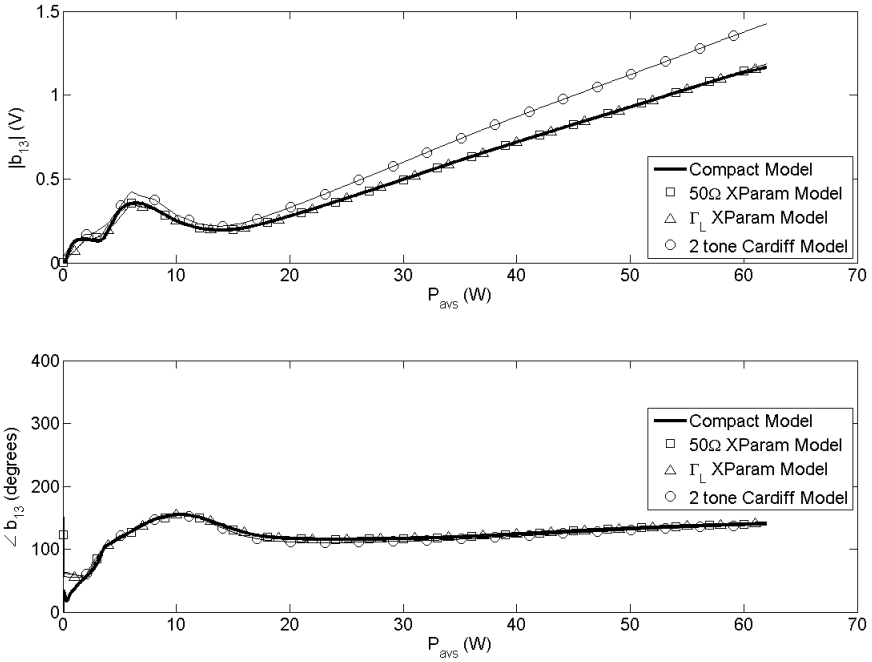

(a) b_{13} vs. P_{avs}

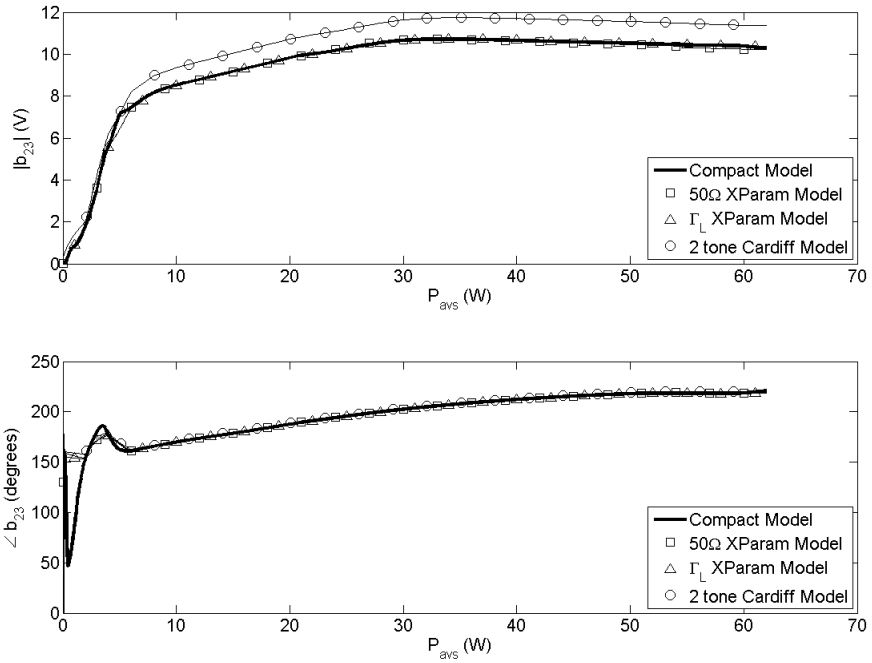

(b) b_{23} vs. P_{avs}

Figure 5.24: Case C3: Third harmonic reflected power-wave variations versus P_{avs}

Table 5.5: Case D: Source side reflection coefficients

Test Case ID	Γ_{12}	Γ_{13}	Γ_{14}	Γ_{15}
D1	0.970∠288°	0.811∠155°	0.733∠327°	0.934∠65°
D2	0.817∠94°	0.772∠52°	0.821∠48°	0.729∠312°
D3	0.740∠208°	0.983∠197°	0.987∠52°	0.873∠307°

Table 5.6: Case D: Load side reflection coefficients

Test Case ID	Γ_{21}	Γ_{22}	Γ_{23}	Γ_{24}	Γ_{25}
D1	0.718∠223°	0.770∠126°	0.806∠184°	0.946∠144°	0.705∠27°
D2	0.713∠86°	0.751∠44°	0.895∠66°	0.920∠86°	0.894∠150°
D3	0.835∠17°	0.864∠324°	0.789∠340°	0.923∠176°	0.757∠176°

simulation is far away from the LSOP condition. Even the Γ_L-dependent X-parameter model didn't manage to do much better at harmonic content prediction.

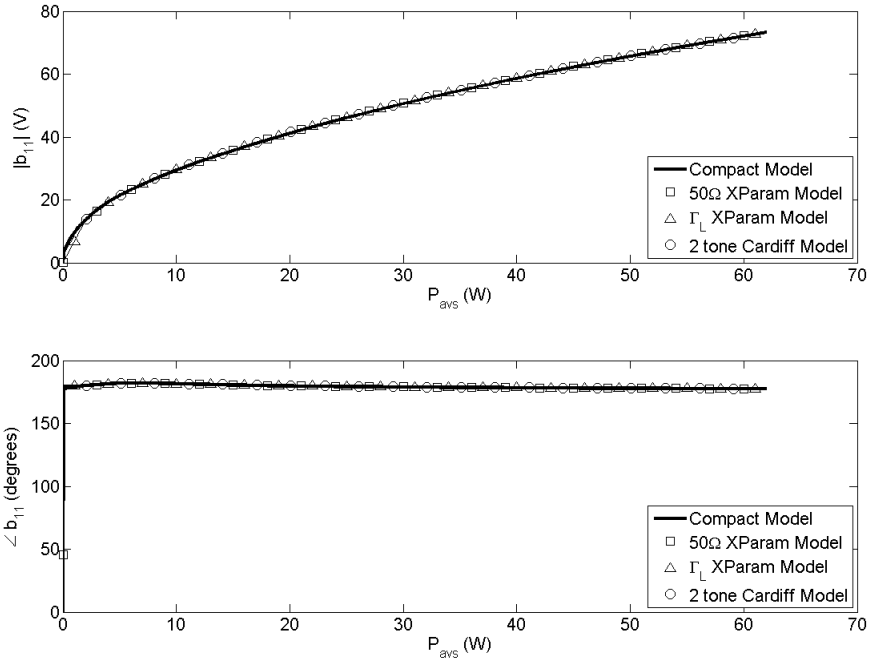

(a) b_{11} vs. P_{avs}

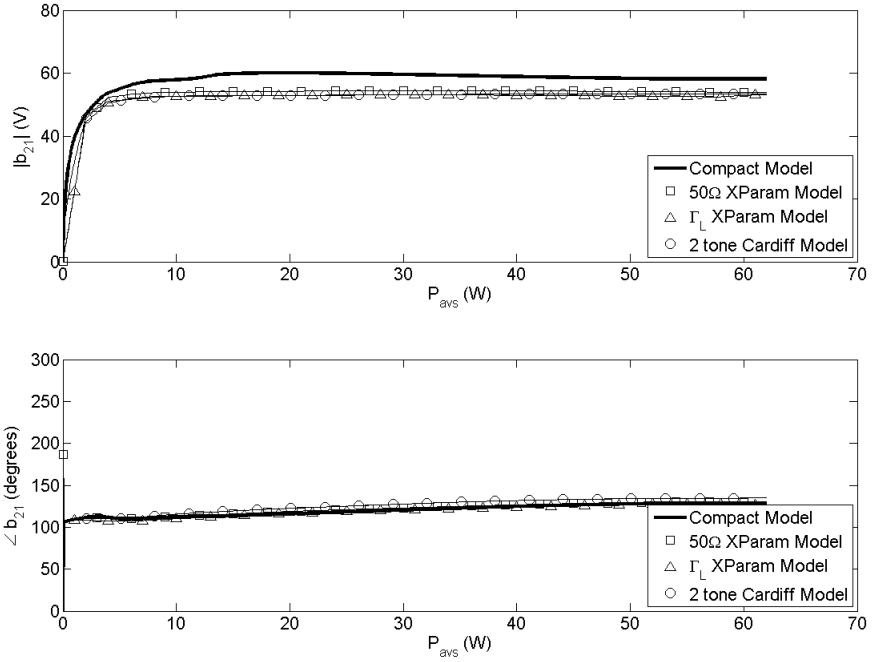

(b) b_{21} vs. P_{avs}

Figure 5.25: Case D1: First harmonic reflected power-wave variations versus P_{avs}

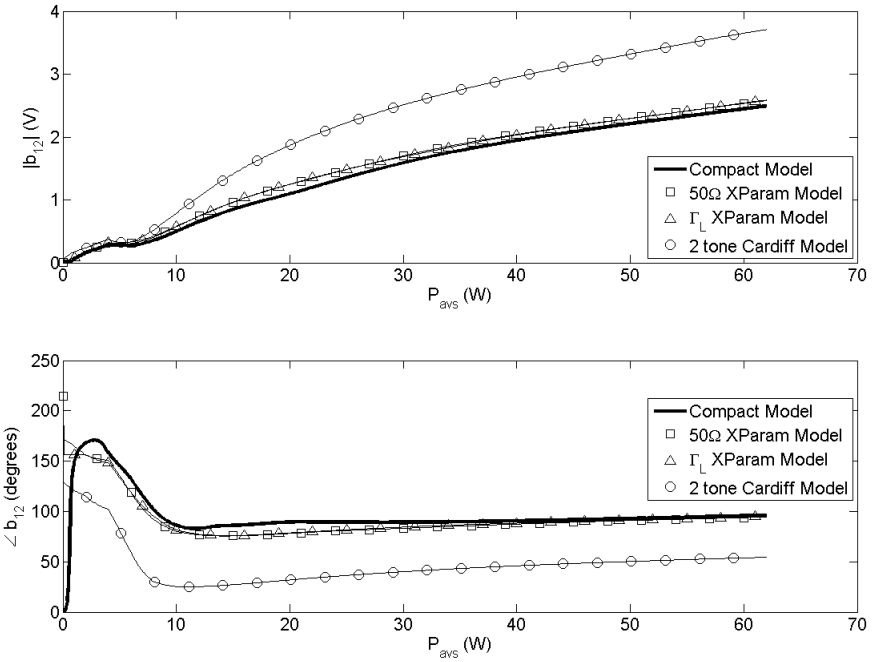

(a) b_{12} vs. P_{avs}

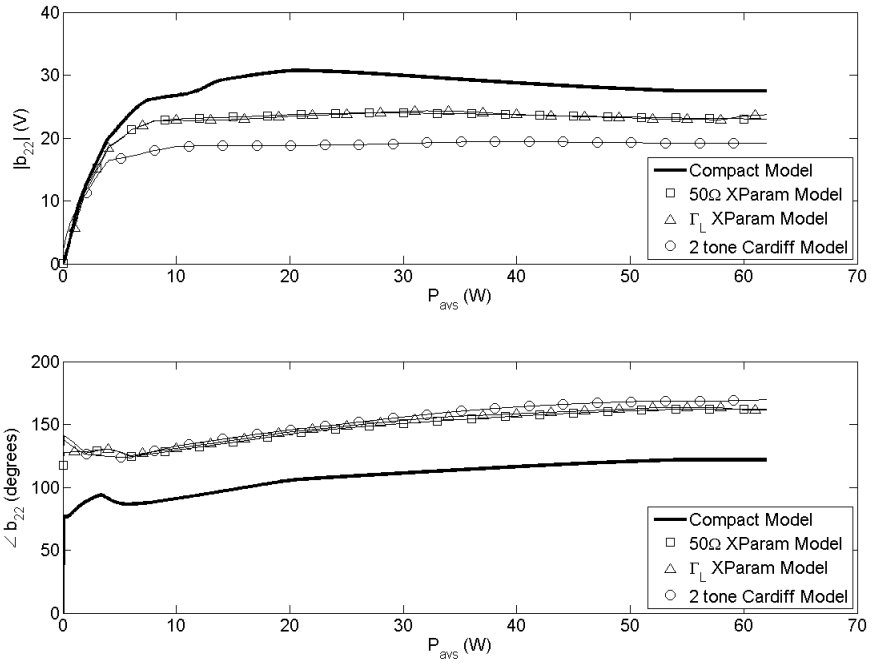

(b) b_{22} vs. P_{avs}

Figure 5.26: Case D1: Second harmonic reflected power-wave variations versus P_{avs}

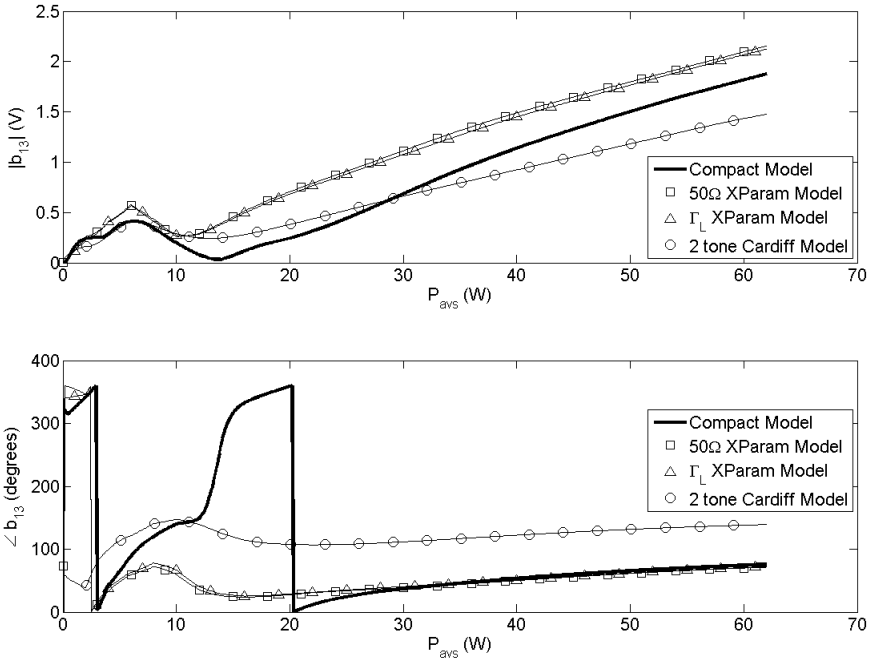

(a) b_{13} vs. P_{avs}

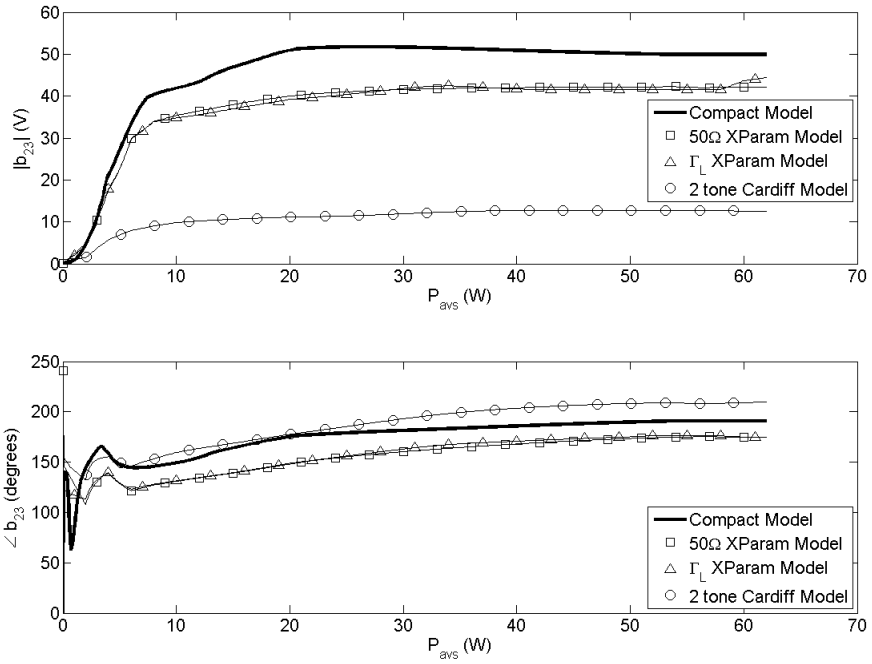

(b) b_{23} vs. P_{avs}

Figure 5.27: Case D1: Third harmonic reflected power-wave variations versus P_{avs}

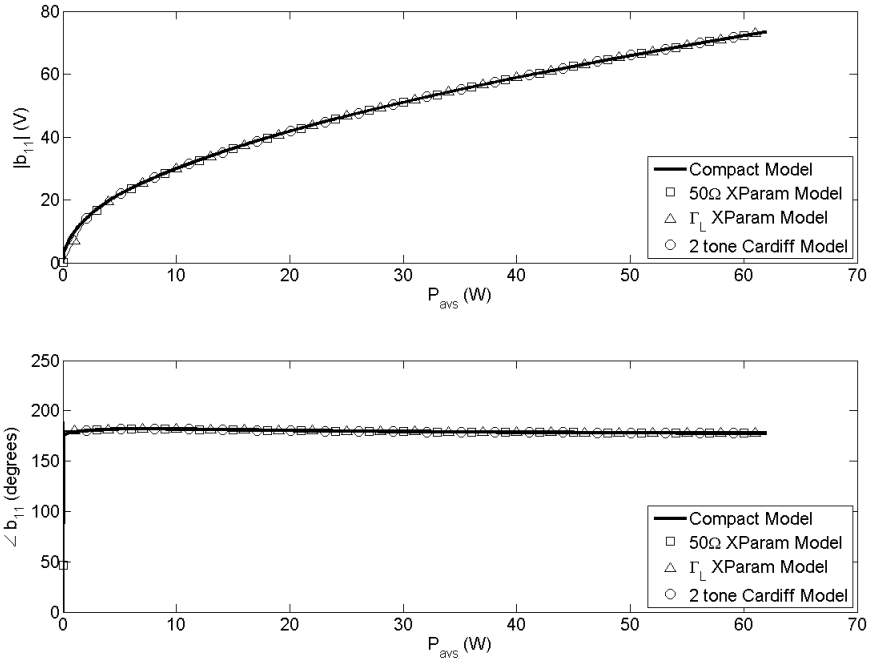

(a) b_{11} vs. P_{avs}

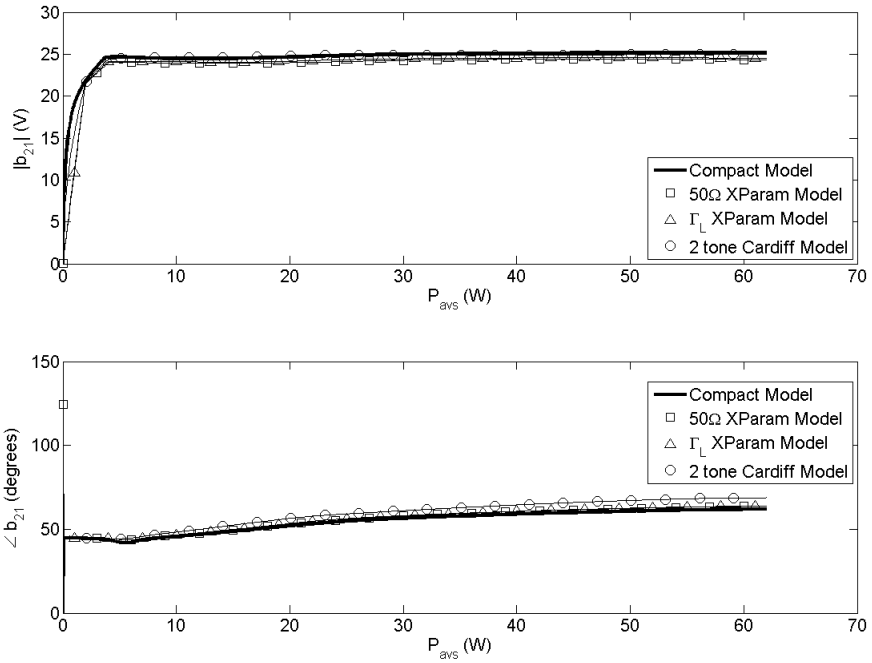

(b) b_{21} vs. P_{avs}

Figure 5.28: Case D2: First harmonic reflected power-wave variations versus P_{avs}

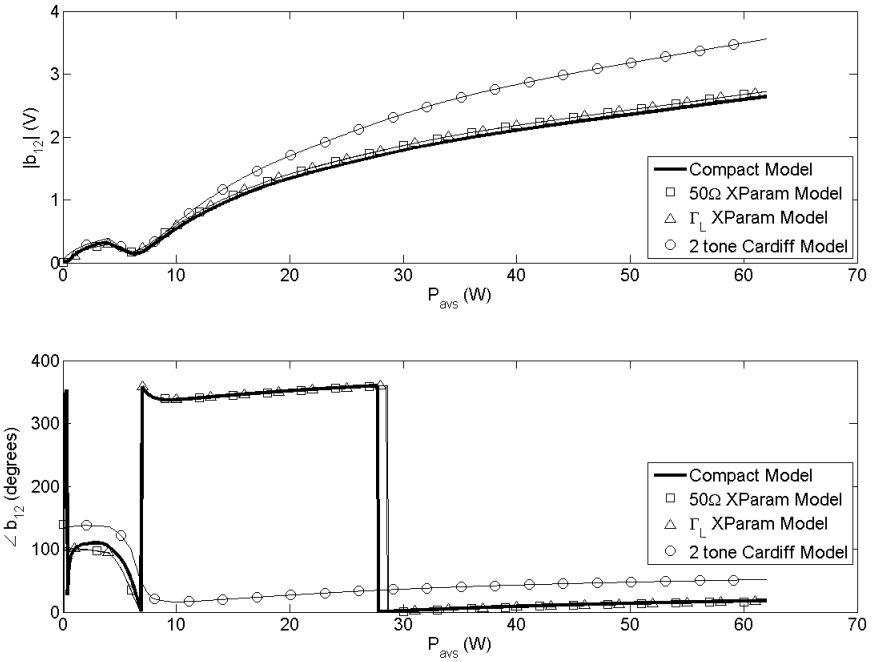

(a) b_{12} vs. P_{avs}

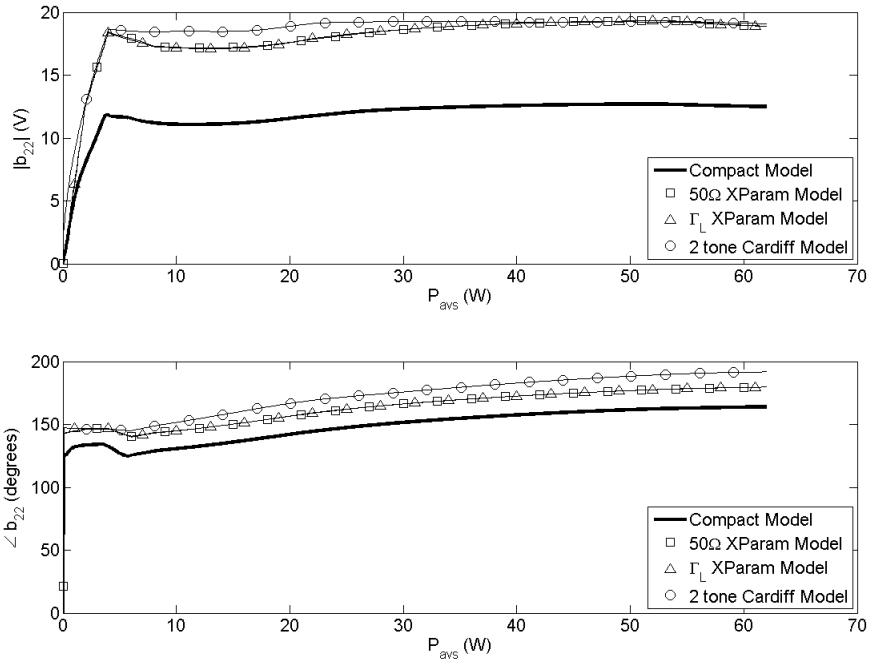

(b) b_{22} vs. P_{avs}

Figure 5.29: Case D2: Second harmonic reflected power-wave variations versus P_{avs}

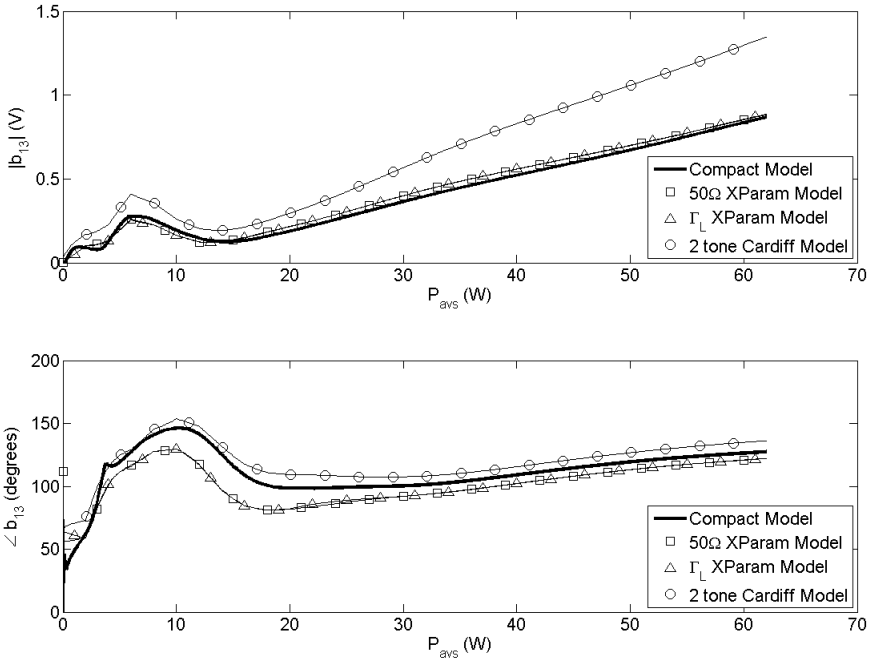

(a) b_{13} vs. P_{avs}

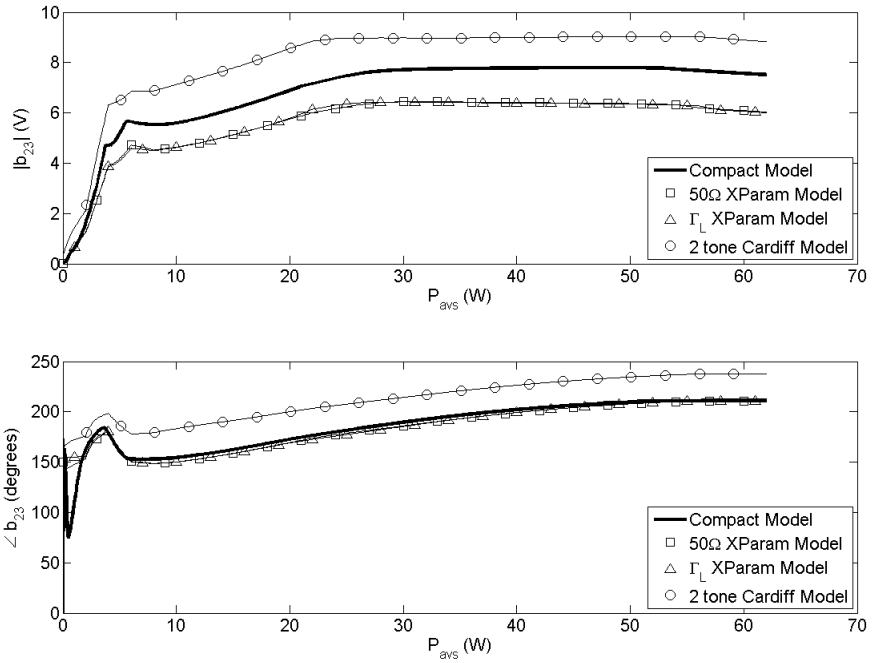

(b) b_{23} vs. P_{avs}

Figure 5.30: Case D2: Third harmonic reflected power-wave variations versus P_{avs}

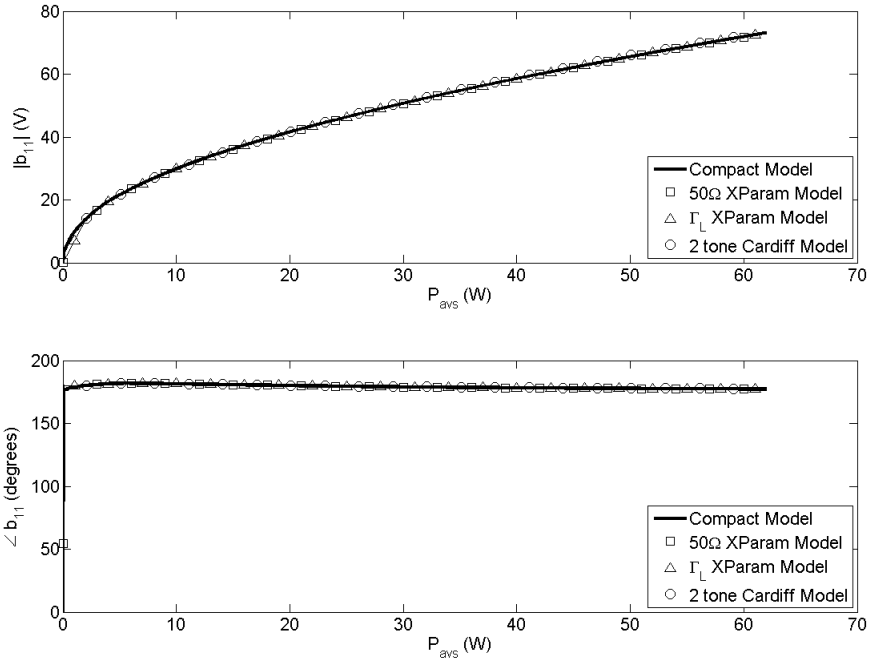

(a) b_{11} vs. P_{avs}

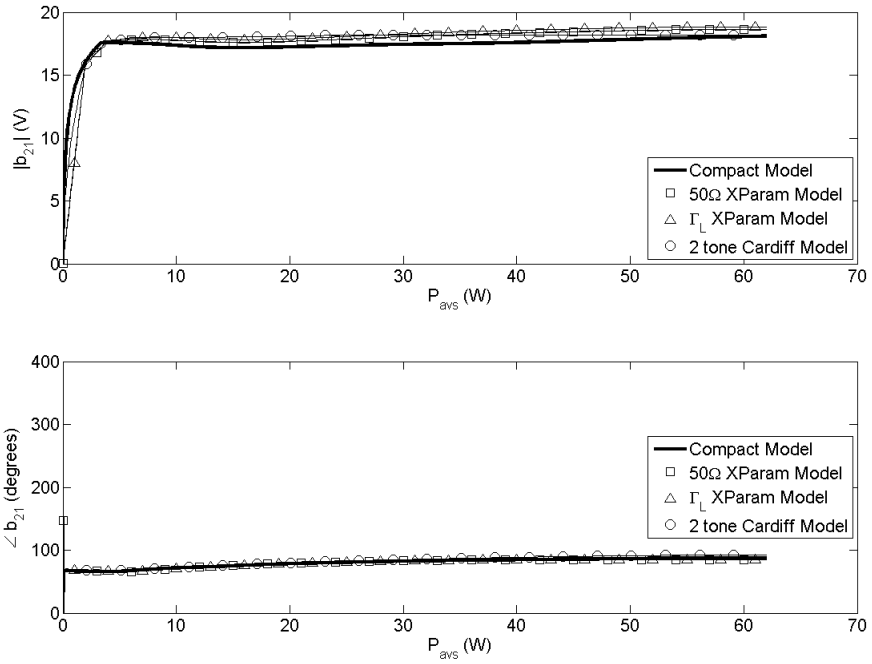

(b) b_{21} vs. P_{avs}

Figure 5.31: Case D3: First harmonic reflected power-wave variations versus P_{avs}

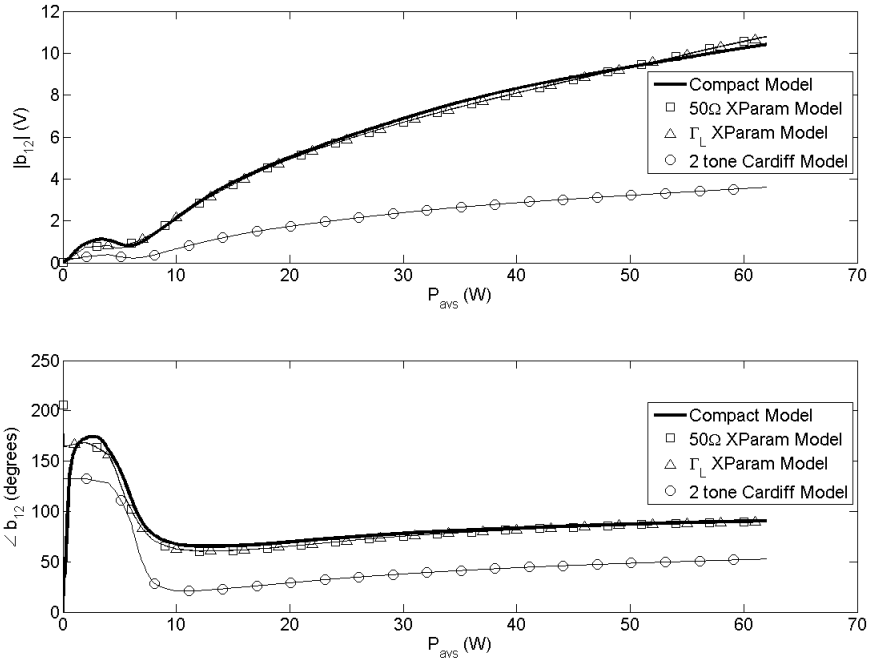

(a) b_{12} vs. P_{avs}

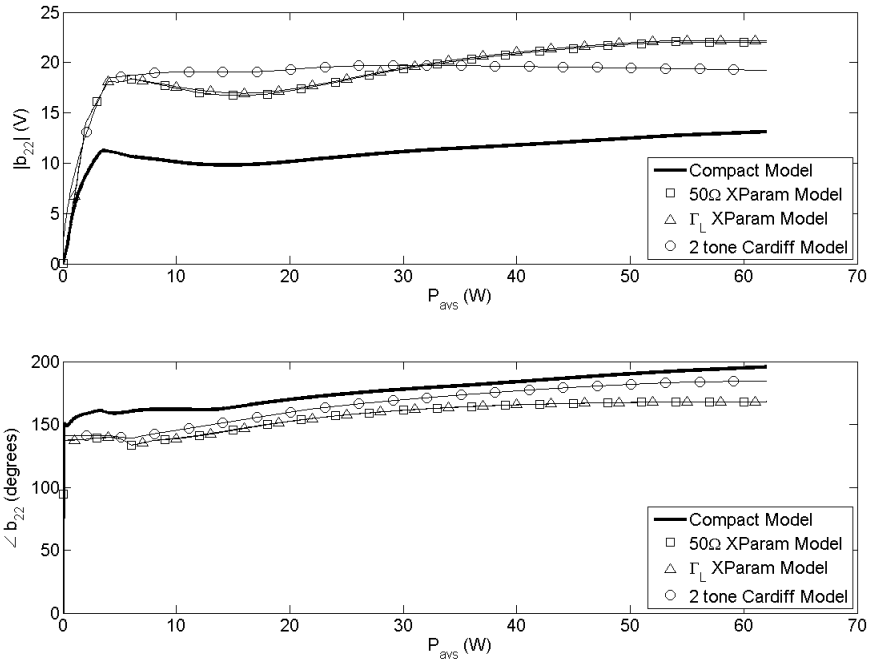

(b) b_{22} vs. P_{avs}

Figure 5.32: Case D3: Second harmonic reflected power-wave variations versus P_{avs}

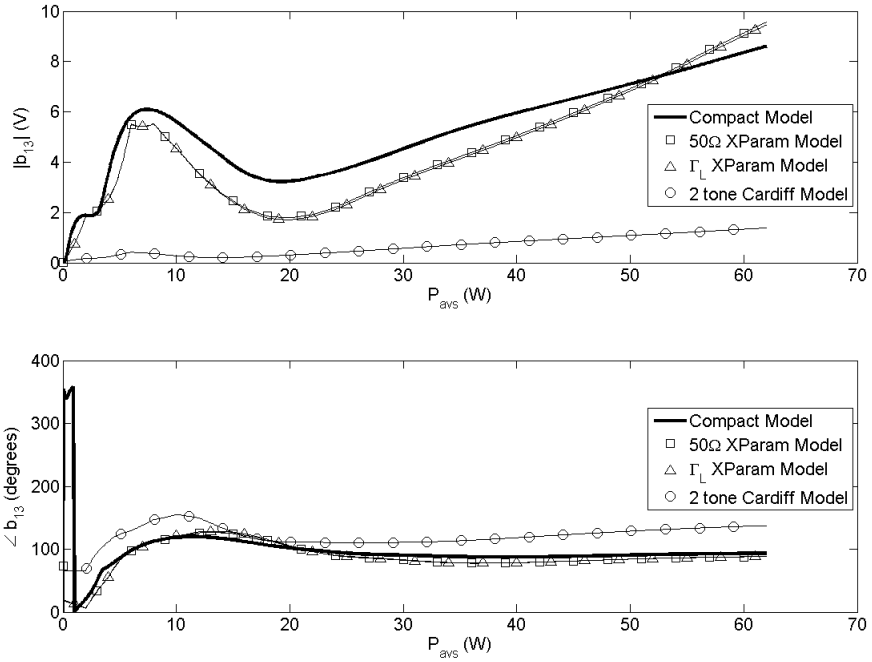

(a) b_{13} vs. P_{avs}

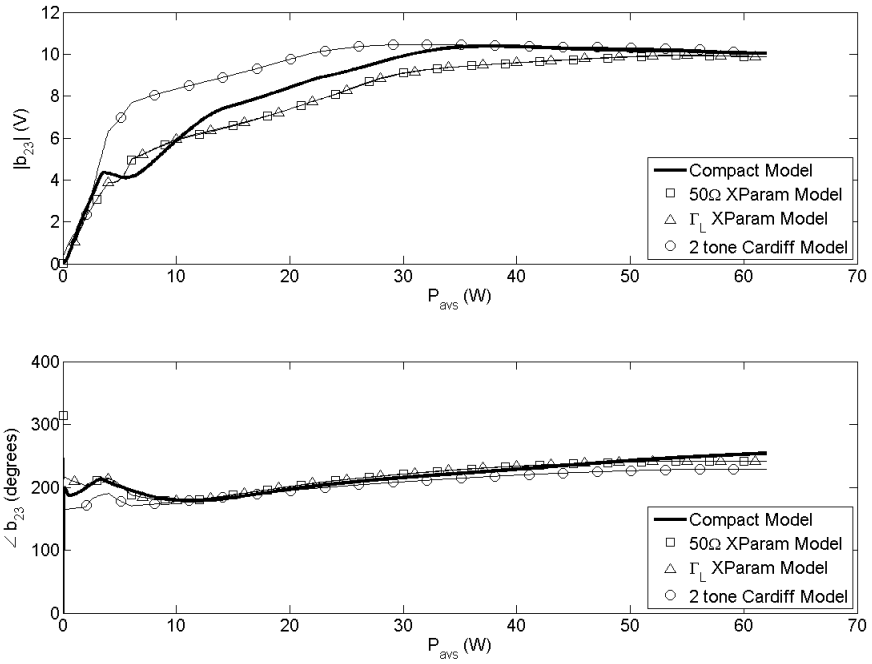

(b) b_{23} vs. P_{avs}

Figure 5.33: Case D3: Third harmonic reflected power-wave variations versus P_{avs}

Chapter 6

Conclusions and Future Work

In this chapter the conclusions of the thesis will be restated regarding the applicability of the PHD modeling framework and the specific implementations of PHD models extracted in this thesis. Also, possible future research work based on improvements to the PHD model application are discussed here. The work presented in this thesis is the analysis and comparison of the major implementations of behavioural modeling techniques that are mainly suitable for the design of narrow-band power amplifiers.

6.1 Conclusions

From the analysis in chapter 3 and validation of models in chapter 5, we can conclude that:

1. The Poly-Harmonic Distortion behavioural modeling framework as applied to power transistor devices is derived from the assumption that the power transistor is a Volterra system and it is embedded within a stable circuit under the stimulus of periodic inputs. Since narrow-band communication signal approach the behaviour of periodic signals (they are almost-periodic signals), the PHD modeling framework is theoretically capable of providing a black-box power transistor model that can be used to design power amplifiers.

2. The X-parameter models, being that they are first-order Taylor series approximations of the PHD framework describing functions, are mainly useful for modeling the power transistor behaviour under mildly unmatched conditions. Under highly unmatched conditions the first-order approximation used in the model breaks down and the models degrades in performance.

3. Using an LSOP expansion of an X-parameter model should be performed with caution

as the choice of interpolation used can potentially degrade the predictive capability of the model. Increasing the LSOP variables further than what was performed in this thesis would result in a very highly dimensional model that will take exponentially longer to extract, implement and simulate. There is no guarantee that LSOP expansion will result in better performance under highly unmatched conditions.

4. The Cardiff model fits the measurement where it is extracted really well. However it breaks down quicker than the normal X-parameter models when there is significant harmonic content that is outside the model. Increasing the dimension of the Cardiff model to account for further harmonic content should improve this model's capability but it comes at the cost of the same complexities that come with the LSOP expansion of the X-parameter models.

6.2 Future Work

Other models can be potentially implemented within the PHD modeling framework. A few ideas for further research work are:

1. The implementation of the describing functions used in the PHD modeling framework can be done by using artificial neural networks (ANNs). This might prove to be a lot easier to extract and implement in simulation for measurement conditions that are not on a grid. The complexity of the ANNs that are capable of fitting the PHD describing function could be a topic of further research.

2. Multi-variate complex polynomials can be used instead of a Taylor series approximation to model the describing functions of the PHD modeling framework. These polynomials can be designed with regards to the Volterra framework that the PHD framework is based on.

Bibliography

[1] J. Wood, P. Aaen, D. Bridges, D. Lamey, M. Guyonnet, D. Chan, and N. Monsauret, "A nonlinear electro-thermal scalable model for high-power rf ldmos transistors," *Microwave Theory and Techniques, IEEE Transactions on*, vol. 57, no. 2, pp. 282 –292, feb. 2009.

[2] C. Pettey, "Gartner says worldwide mobile connections will reach 5.6 billion in 2011 as mobile data services revenue totals $314.7 billion," August 2011. [Online]. Available: http://www.gartner.com/it/page.jsp?id=1759714

[3] S. C. Cripps, *RF Power Amplifiers For Wireless Communications*. Artech House, 2006.

[4] J. Verspecht and D. E. Root, "Polyharmonic distortion modeling," *IEEE Microwave Magazine*, vol. 7, pp. 44–57, 2006.

[5] N. N. Taleb, *The Black Swan: The Impact of the Highly Improbable*. Random House, 2007.

[6] S. Vitanov, "Simulation of high electron mobility transistors," Ph.D. dissertation, Technischen Universität Wien, 1981.

[7] J. W. Peter Aaen, Jaime A. Plá, *Modeling and Characterization of RF and Microwave Power FETs*. Cambridge University Press, 2007.

[8] J. Xu, J. Horn, M. Iwamoto, and D. Root, "Large-signal fet model with multiple time scale dynamics from nonlinear vector network analyzer data," in *Microwave Symposium Digest (MTT), 2010 IEEE MTT-S International*, may 2010, pp. 417 –420.

[9] G. L. F. Giannini, *Nonlinear Microwave Circuit Design*. Wiley, 2004.

[10] S. A. Maas, *Nonlinear Microwave and RF Circuits, 2nd Edition*. Artech House, 2003.

[11] E. Ngoya and R. Larcheveque, "Envelop transient analysis: a new method for the transient and steady state analysis of microwave communication circuits and systems," in *Microwave Symposium Digest, 1996., IEEE MTT-S International*, vol. 3, jun 1996, pp. 1365 –1368 vol.3.

[12] A. I. Umran S. Inan, *Engineering Electromagnetics*. Prentice Hall, 1998.

[13] M. R. Fréchet, "Sur les fonctionnelles continues." *Annales Scientifiques de l'Ecole Normal Superieure*, vol. 27, pp. 193–219, 1910.

[14] J. Barrett, "The use of functionals in the analysis of nonlinear physical systems," *J. Elect. Control.*, vol. 15, pp. 567–615, 1963.

[15] ——, "Functional series representation of nonlinear systems–some theoretical comments," in *IFAC Symp. Ident. Sys. Param. Est*, 1982.

[16] V. Volterra, *Theory of functionals and of integral and integro-differential equations.* Dover Publications, 2005.

[17] K. Knopp, *Theory of Functions, Parts I and II.* Dover Publications, 1996.

[18] D. M. Pozar, *Microwave Engineering.* Wiley, 2005.

[19] R. Marks and D. Williams, "A general waveguide circuit theory," *J. Res. Nat. Inst. Standards. Technol.*, vol. 97, pp. 533–562, 1992.

[20] S. H. Tülay Adali, *Adaptive Signal Processing: Next Generation Solutions.* Wiley-IEEE Press, 2010.

[21] S. P. Woodington, R. S. Saini, D. Willams, J. Lees, J. Benedikt, and P. J. Tasker, "Behavioral model analysis of active harmonic load-pull measurements," in *Microwave Symposium Digest (MTT), 2010 IEEE MTT-S International*, may 2010, p. 1.

[22] W. Van Moer and L. Gomme, "Nvna versus lsna: enemies or friends?" *Microwave Magazine, IEEE*, vol. 11, no. 1, pp. 97 –103, feb. 2010.

[23] M. Kahrs, "50 years of rf and microwave sampling," *Microwave Theory and Techniques, IEEE Transactions on*, vol. 51, no. 6, pp. 1787 – 1805, june 2003.

[24] P. Blockley, D. Gunyan, and J. Scott, "Mixer-based, vector-corrected, vector signal/network analyzer offering 300khz-20ghz bandwidth and traceable phase response," in *Microwave Symposium Digest, 2005 IEEE MTT-S International*, june 2005, p. 4 pp.

[25] G. Simpson, "Hybrid active tuning load pull," in *Microwave Measurement Conference (ARFTG), 2011 77th ARFTG*, june 2011, pp. 1 –4.

[26] A. Technologies, "Harmonic balance simulator." [Online]. Available: http://www.home.agilent.com/agilent/editorial.jspx?cc=CA&lc=eng&ckey=2061503&nid=-34333.804586&id=2061503